UNIVERSITY OF CAPE TOWN
DEPARTMENT OF MECHANICAL ENGINEERING
RONDEBOSCH, CAPE TOWN, SOUTH AFRICA

ELECTRONIC SPECKLE PATTERN INTERFEROMETRY (ESPI) NDE OF CRACKS IN PRESSURE VESSELS WITH FEA MODELLING

by
J.R. MYLES

supervisor: Professor J. Gryzagoridis

May 1997

Submitted as partial fulfilment of the requirements for the degree of
Master of Science in Engineering

DECLARATION

This is to certify that the work presented in this thesis is essentially my own, and that it has not been submitted for a degree at any other university.

J.R. Myles

April 1997

Acknowledgements

I would like to thank the following people for their help and advice.

Professor Jasson Gryzagoridis, Department of Mechanical Engineering, for his help with the ESPI work and general guidance as my supervisor.

Mr Dirk Findeis, Department of Mechanical Engineering, for help and guidance with the ESPI work.

Dr Greg Mitchell and Mr Hellmut Bowles, CERECAM, for their advice on and help with the Finite Element modelling.

Mr Mike Eastman for help with UNIX.

Terms of Reference

Electronic Speckle Pattern Interferometry is an established interferometric measurement technique capable of providing qualitative data about a wide variety of flaw types that may be present in a specimen. Work, however, is still required to allow quantification of the flaw size and depth from the fringe patterns obtained. By establishing a reliable method of simulating the fringe patterns by finite element methods it is hoped that the finite element model may be used to obtain a better understanding of how the various fringe parameters affect the experimental fringe patterns. The simulation method could also be used to build up a comprehensive reference source, without resorting to time-consuming and expensive controlled experiments, to aid in the interpretation of unknown flaws.

This thesis will investigate the procedure of modelling the fringe patterns and verification of the model.

The specific brief was:

1. To simulate the fringe patterns for an unflawed cylinder using finite element methods.
2. To calibrate this numerical model with the actual fringe patterns obtained by interferometry.
3. To simulate the fringe patterns for various thumbnail crack geometries.
4. To compare these simulations with the actual patterns obtained from the interferometry process.

Synopsis

This dissertation describes the results of an attempt to simulate the Electronic Speckle Pattern Interferometric fringe patterns observed around a crack or combination of cracks in a pressure vessel by finite element methods.

Electronic Speckle Pattern Interferometry (ESPI) is a coherent optical measurement technique that produces a contour map of the surface displacement of an object when it is stressed. The sensitivity of the techniques is of the order of half the wavelength of light.

The objective of the study was to determine a procedure for the modelling of interferometric fringes by finite elements. The finite element model may then be used to study the effects of crack geometry on fringe patterns and produce a library of reference fringe patterns for comparison with experimental fringe patterns found for unknown flaws.

The approach to the problem was to simulate the fringe patterns for a crack free cylinder and compare these with those observed experimentally. The FE model modulus of elasticity was then to be calibrated to minimise uncertainty in the exact value of the elastic modulus. Once the model was calibrated, various cracks and combinations of cracks were introduced into both the physical cylinders and the FE model and fringe patterns obtained were compared. The experimental results for the cracks and combinations of cracks were compared with the finite element predictions at a range of loads.

The cylinders were simulated using simple shell elements for the cylinder walls and line spring elements to model the cracks. This combination gave acceptable accuracy

combined with economical computer use and provided a simple method of altering crack geometry.

Satisfactory correlation was observed between prediction and experiment with a mean error of 10% between the two. The worst correlation was observed for the internal crack.

The major conclusions that were drawn from the findings were:

1. FEM is a viable method of simulating fringe patterns of surface displacement and the approach used in this study is a viable procedure for their simulation and study. The modelling is, however limited to controlled conditions.
2. The correlation is limited to areas where the stress distribution is unaffected by complex factors such as end closures. Modelling of complex effects such as threads would dramatically increase computer usage.
3. Stability constraints for the object under observation may prove to be the limiting factor in the usefulness of the FE model in determining crack size from experimental fringe patterns.
4. The model could be used to predict the smallest observable flaw for a given load.

The recommendations include:

1. The line spring model should be evaluated further for use in simulating internal crack systems.
2. A reliable system of securing specimens for observation should be developed.

3. The model should be tested with actual cracks which are grown in a controlled environment.

Table of Contents

List of Illustrations

APPENDIX A

APPENDIX C

Nomenclature

element	A finite element model is made up of a series of discrete 'pieces' simulating the physical geometry, the geometry of which are defined by *nodes*.
ESPI	Electronic Speckle Pattern Interferometry
FEM	Finite Element Methods
FEA	Finite Element Analysis
mesh	The term used to describe a finite element model
node	Points used in the definition of model geometry
e	natural log base (approx. 2.7183)
λ	Wavelength of light
$\Delta\phi$	Change in phase introduced by the surface displacement
θ_c	Angle between surface normal and camera viewing angle
θ_i	Angle between surface normal and illumination direction
ΔP	Total change in path length introduced by the surface displacement
d	Surface displacement vector
l_c	Path length change in scattered light
l_i	Path length change in illumination beam
n	Number of interference fringes
psi	pound per square inch. 1 psi = 6895Pa

1. Introduction

Non-destructive evaluation tools capable of reliably detecting and quantifying flaws in industrial equipment and manufactured products are of considerable importance. Such tools are useful in enhancing existing quality control methods and aid in accurate residual life prediction in pressure vessels and piping. Residual life prediction allows for more effective use of equipment by ensuring that components are not replaced before the end of their useful life. Equipment is also removed from service if failure is imminent which reduces down time and injuries.

Electronic Speckle Pattern Interferometry (ESPI) is an interferometric measurement technique used in non-destructive evaluation (NDE). The technique is capable of detecting displacements of the order of 0.3 μm, producing a 'contour map' of the surface displacement across the whole field of view. It can be used to measure both static and dynamic variables such as strain, shape, vibration, and, most commonly, displacement. When measuring static displacement two interference patterns are produced by illuminating the specimen with laser light, one before and one after the displacement has been introduced. These are subtracted from or added to one another to produce an interference fringe pattern which is a contour map of the displacement that was introduced between the two images.

If the specimen has a flaw in it, the structure will be weaker at the flaw site, and thus the surface displacement characteristics around the flaw will differ from those of the rest of the structure as illustrated in Figure 1-1. The localised displacement will introduce a localised fringe pattern around the flaw site which is distinct from the general pattern across the surface. The technique can thus be used to reliably detect the location of a wide variety of flaws in objects such as surface and sub-surface cracks, debonds, delaminations and corrosion. The location of the flaw can be quantified, but the size of the flaw can only be assessed qualitatively. Data such as the length and depth of the flaw is at present not obtainable from interferograms. If this data were available ESPI would be an extremely attractive NDE tool as it allows the inspection of an entire surface at once unlike most other NDE methods.

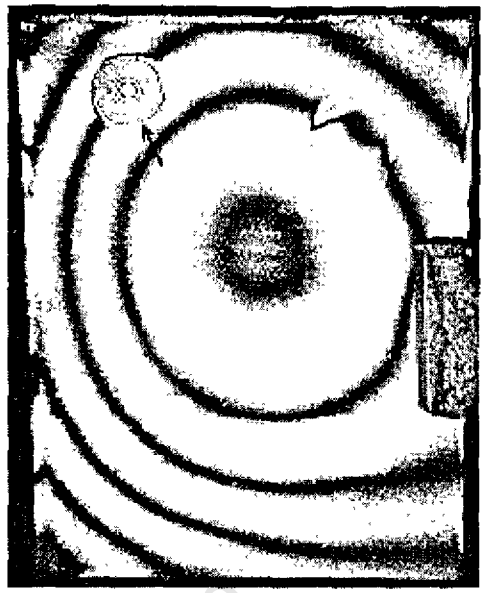

Figure 1-1 Distinct localised fringe pattern around a flaw indicated by arrow. From ASM Handbook vol.17, p. 422

The aim of this study is to establish a reliable method of simulating the interferometric fringe patterns using finite element methods. The finite element model is intended to provide a quick and inexpensive method of investigating the effects of the flaw configuration on the fringe patterns and to provide an inexpensive reference source to aid in the interpretation of fringe patterns without resorting to time-consuming controlled physical experiments.

This thesis investigates the use of Finite Element Methods (FEM) in the evaluation of ESPI interferograms. Computer generated fringe patterns produced from FE models of

flawed pressure vessels are compared to interferograms of the actual flawed component to verify the accuracy of the FE model.

This thesis will first lay out the relevant theory regarding ESPI, it will then review the relevant literature and describe the finite element modelling and experimental procedure. The results of the experiments will be compared with the finite element predictions and the comparisons discussed.

2. Electronic Speckle Pattern Interferometry

Electronic Speckle Pattern Interferometry is a powerful non-contact measurement technique capable of measuring both static and dynamic variables, such as displacement, strain, shape and vibration. The technique supplies the information over the full field of view, as opposed to conventional measurement techniques which measure point by point. ESPI produces an image of the object with interferometric fringes across it. The fringes indicate lines of constant value of the variable that is being measured.

The most common uses of this technique are shape measurement, design evaluation and non-destructive flaw detection, both in quality control and residual life studies. Areas that are flawed in a structure will be weaker than surrounding areas and therefore less stiff, allowing greater surface displacement or a discontinuity in surface displacement under load. The localised displacement pattern results in either a higher fringe density or a fringe discontinuity around the flaw. The fringe patterns will thus change in areas where there is uneven load distribution or there are strain concentrations. These characteristics allow the detection of flaws or areas in an experimental design that may require strengthening or redesign.

The technique is capable of detecting extremely small displacements, of the order of 0.3 μm without any special processing. The sensitivity can be improved with the use of special processing techniques such as phase stepping, which is theoretically capable of a 100-fold improvement, although 30 times is more readily obtainable. Heterodyning is another technique used to improve sensitivity, theoretically capable of

a 1000-fold improvement. It is also possible to reduce the sensitivity of the system up to a point if larger displacements need to be measured.

A major advantage of this method is that it is not limited to a particular material type, it has been used successfully on metals, plastics, composites and concrete, among others. The only preparation which may be required is a coat of matt paint to prevent excessively bright reflections from the surface.

One major disadvantage of ESPI as a non-destructive evaluation tool is the lack of quantitative information about the flaws. According to the ASM Handbook (vol. 17, 1989, p406):

> *"Although* [ESPI] *is capable of accurately locating a flaw within the surface area of the test object being inspected, the cross-sectional size of the flaw can only be approximately determined, and the information concerning the depth of the flaw, when obtainable at all, is qualitative in nature."*

2.1 Principles of Electronic Speckle Pattern Interferometry

This investigation used only the static displacement measuring capabilities of ESPI. It is possible to measure in-plane or out-of-plane displacement using Electronic Speckle Pattern Interferometry, or the first or second derivatives of these displacements. However, only the measurement of out-of-plane displacement was required by the investigation. For this reason only out-of-plane displacement and some background to the technique will be dealt with here. A more extensive treatment of the subject may be found in Jones and Wykes (1989).

2.1.1 Laser light

ESPI relies on the unique properties of laser (Light Amplification by Stimulated Emission of Radiation) light for its operation. The properties of importance are:

1. The light is monochromatic, so it is of a single wavelength. The wavelength is dependant on the lasing material. (For Helium-Neon it is 632.8 nm)

2. It is coherent within the particular laser's coherence length, i.e. all the 'peaks' and 'troughs' of the waves are in step. The coherence length is generally defined as the distance in which interference fringe visibility falls to $1/e^2$, where e is the natural log base (approximately 2.7183). The coherence length varies from laser to laser as it is a function of the properties of the laser chamber.

2.1.2 Laser Speckle

Laser speckle is the grainy effect observed when an object is illuminated with coherent light. It only occurs when the object is optically rough, i.e. the surface height variation is of the order of or greater than the wavelength of the illuminating light. When laser light strikes an optically rough surface, the tiny peaks and troughs scatter the light randomly.

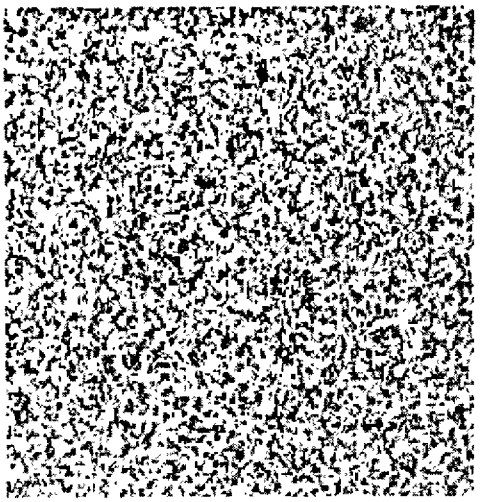

Figure 2-1 Typical laser speckle pattern. From ASM Handbook, vol. 17.

At any point in space the intensity of the light will be due to the complex addition of the random scatterings off the active surface. The path lengths of the beams arriving at the point vary and the resultant phase of the complex addition varies randomly from

point to point. This results in a random intensity distribution which produces a grainy effect. The speckle pattern is unique for given object surface, illumination and viewing conditions. A typical speckle pattern is shown in Figure 2-1.

2.1.3 Simple Michelson-type Speckle Pattern Interferometer

The interferometer shown in Figure 2-2 is sensitive to out-of-plane displacement. It is similar in design to the standard Michelson interferometer, but the two mirrors have been replaced by non-specular surfaces.

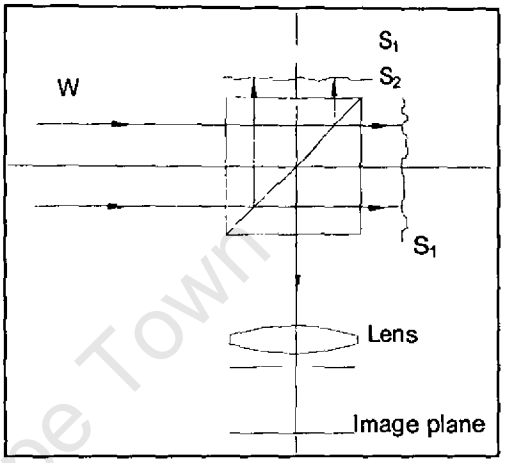

Figure 2-2 The Michelson type out-of-plane interferometer. Adapted from Jones & Wykes (1983)

The plane wavefront W is split into two equal parts by the beamsplitter. The two wavefronts then recombine after being scattered by the two optically rough surfaces S_1 and S_2. An image of the interference pattern formed by the interference of the image plane speckle patterns of the surfaces S_1 and S_2 is formed at the image plane. The intensity of any point on the image is given by:

$$I_1 = A_1^2 + A_2^2 + 2\sqrt{A_1^2 A_2^2}\cos(\Phi_1 - \Phi_2) \qquad (2\text{-}1)$$

where A_1 and A_2 are the complex amplitudes of the two wavefronts respectively, and $(\Phi_1\text{-}\Phi_2)$ is the phase difference between the two wavefronts at the point of interest.

If one of the surfaces, say S_1, is moved a small distance d parallel to the surface normal, the path length of the one wavefront will change by the distance 2d. This change introduces an additional phase difference. So the intensity of any point on the image when S_1 has moved is given by:

$$I_2 = A_1^2 + A_2^2 + 2\sqrt{A_1^2 A_2^2}\cos\left((\Phi_1 - \Phi_2) + \Delta\phi\right) \qquad (2\text{-}2)$$

If these two expressions are subtracted from or added to one another, an expression which is a function of the phase change introduced by the surface displacement. The system used in this investigation used the subtraction process, which results in an image with an intensity distribution given by:

$$I_r = I_1 - I_2 = 4\sqrt{A_1^2 A_2^2}\sin\left((\Phi_1 - \Phi_2) + \tfrac{1}{2}\Delta\phi\right)\sin\left(\tfrac{1}{2}\Delta\phi\right) \qquad (2\text{-}3)$$

If the correlation coefficient of this expression is calculated it is shown (Jones & Wykes 1989) that maximum correlation between the two images occurs at points where the phase difference introduced by the surface displacement is given by:

$$\Delta\phi = 2n\pi \qquad (2\text{-}4)$$

The magnitude of the phase change introduced by the displacement d can be calculated if the wavelength of the illuminating light is known:

$$\Delta\phi = \frac{4\pi \cdot d}{\lambda} \qquad (2\text{-}5)$$

Where λ is the wavelength of the light.

Equating these equations and solving for the displacement gives:

$$d = \frac{n \cdot \lambda}{2} \qquad (2\text{-}6)$$

Thus lines of maximum correlation indicate contours of constant surface displacement.

2.1.4 Practical ESPI System

The interferometer described in the previous section demonstrates the principle of ESPI, but is not practical for experimental work. This section will describe the general process of an ESPI experiment to measure out-of-plane displacement, and then derive slightly modified equations that take the differing geometry of the practical set-up into account.

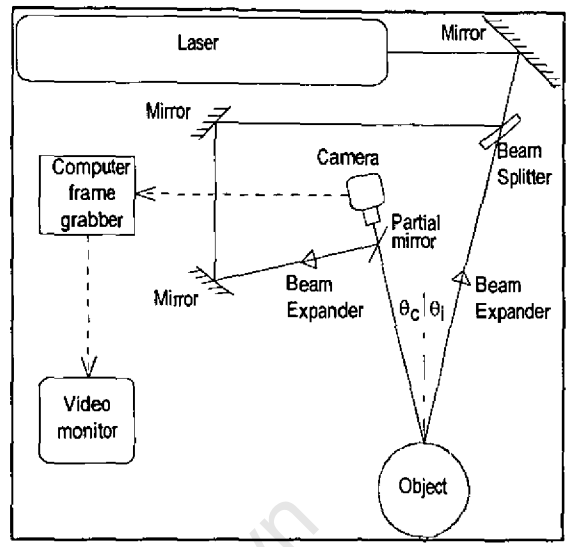

Figure 2-3 Practical ESPI set-up

A typical set-up used to measure out-of-plane displacement is shown in Figure 2-3. The laser beam is split into two by the beamsplitter; the one which passes through the splitter forms the object beam which is expanded to illuminate the test specimen. The other beam, known as the reference beam, is led, via the two mirrors, to a second beam expander which illuminates the partial mirror. The partial mirror recombines the reference and object beams before they are imaged on the CCD. The camera images are processed by the frame grabber and computer and the results displayed on the monitor.

The image recorded by the camera is thus an image of the speckled interference pattern formed by the interference of the speckled object and smooth reference beams. The speckled interference pattern recorded in this way is unique and is a function of the object's position in space.

The process of making an electronic speckle interferogram is as follows:

An image of the speckle pattern associated with the object in its undisturbed state is recorded and stored digitally in the computer, with an intensity distribution as given in equation (2-1).

The object is then stressed. This is achieved by either mechanical, vibration or pressure loading.

A second image of the speckle pattern is then recorded with the object in it's deformed state. Any object surface deflection will alter the object beam path length between object and camera. A new random phased speckle pattern will form at the CCD image plane which is related to the original (undeformed) speckle pattern by the magnitude of the change in beam path length, and has an intensity distribution given by equation (2-2).

These two images are then subtracted from one another by the image processing software to produce the interferogram with an intensity distribution given by equation (2-3). The two speckled images were captured using the same reference beam, so any intensity variations between image I and II are caused by a change in the object beam path length and associated phase distribution. By subtracting the two images one effectively subtracts out the reference beam, leaving only the object beam distribution. Areas of correlation will be visible as dark areas, and areas of decorrelation will be visible as bright areas. These bright and dark areas form bands known as fringes. The two images of the object are equally bright, so the subtraction process removes the object image by subtracting the two equal images from one another. All that remains is an interferogram which depicts areas of correlation and decorrelation.

2.1.5 Ray Geometry and Practical Equations

The beam geometry in the practical set-up deviates from that shown in Figure 2-3 - the beams are no longer parallel to the surface normal. This causes the interferometer to be sensitive to in-plane as well as slightly less sensitive to out-of plane displacement. For small deviations from the surface normal these effects may be ignored. This section derives the governing equations which take these deviations into account.

Any surface displacement of the object shown in Figure 2-3 may be broken up into three components, an in-plane component perpendicular to the dotted surface normal, an out-of plane component parallel to the surface normal and a vertical component, out of the plane of the page. In Figure 2-3 θ_c is the angle of the camera axis to the surface normal of the object and θ_i is the angle of the illumination direction to the surface normal. The surface displacements are assumed to be much smaller than the distance from source to surface, therefore the rays from source to P (I_1) and source to P' (I_2) can be assumed parallel. The same applies to the rays from surface to camera,

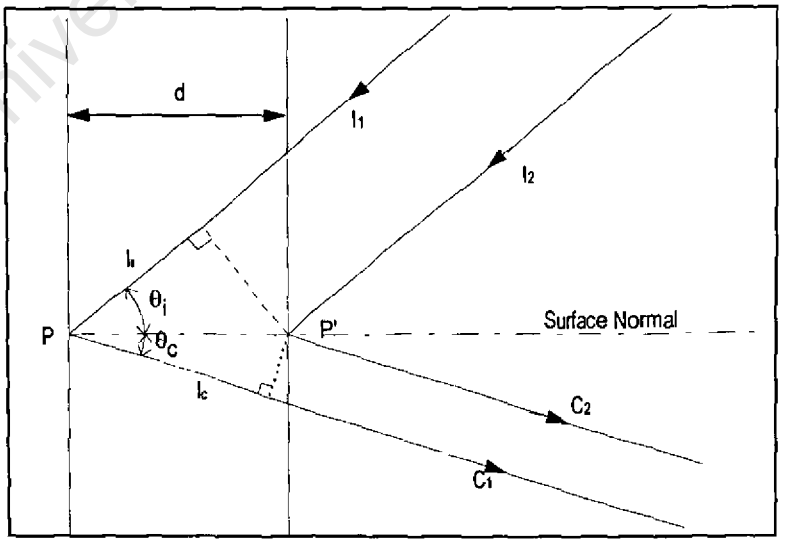

Figure 2-4 Ray geometry for out-of-plane displacement

C_1 and C_2. For pure out of plane displacement, Figure 2-4, the change in path length of the illuminating ray I_1 is given by

$$l_i = d \cdot \cos\theta_i \tag{2-7}$$

similarly the change in path of the scattered ray is given by

$$l_c = d \cdot \cos\theta_c \tag{2-8}$$

Thus the total change in path length of the ray is

$$\Delta P = d \cdot (\cos\theta_i + \cos\theta_c) \tag{2-9}$$

which results in a phase change of

$$\Delta\phi = \frac{2 \cdot \pi}{\lambda} \cdot d \cdot (\cos\theta_i + \cos\theta_c) \tag{2-10}$$

where λ is the wavelength.

Interference will occur where there is a phase difference of 2π radians (360°), thus the number of fringes n is given by

$$n = \frac{\Delta\phi}{2 \cdot \pi} \tag{2-11}$$

Substituting this into the above equation and solving for the displacement d gives

$$d = \frac{n \cdot \lambda}{(\cos\theta_i + \cos\theta_c)} \tag{2-12}$$

For small angles of θ_i and θ_c the cosine terms approach unity. In many cases, where the in-plane component of displacement does not need to be minimised, the camera

axis can be placed normal to the object surface reducing θ_c to zero. For most practical purposes equation (2-12) can be simplified to

$$d = \frac{n \cdot \lambda}{2} \qquad (2\text{-}13)$$

Figure 2-5 shows the ray geometry for an in-plane displacement.

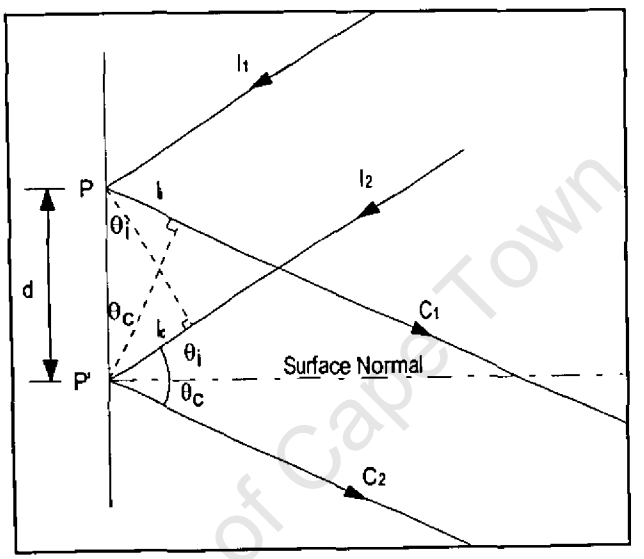

Figure 2-5 Ray geometry for an in-plane displacement

The change in path of the illuminating and reflected rays are given by

$$l_i = d \cdot \sin\theta_c \qquad (2\text{-}14)$$

and

$$l_c = -d \cdot \sin\theta_i \qquad (2\text{-}15)$$

resulting in a total path length change of

$$\Delta P = d \cdot (\sin\theta_i - \sin\theta_c) \qquad (2\text{-}16)$$

For small angles sinθ tends to zero, so for most practical set-ups for measurement of out-of-plane displacement the effect of an in-plane component can be ignored. If θ_i equals θ_c the path change according to equation (2-16) is exactly zero. In-plane displacement sensitivity can therefore be minimised by placing the camera and illumination axes at equal angles on either side of the surface normal.

The path change due to a vertical component is also a sine term, and can therefore also be ignored with little loss of accuracy.

The displacement of a point on the surface can thus be calculated using equation (2-13) for cases where the angles θ_i and θ_c are small.

2.1.6 Advantages and Limitations of ESPI

This section covers some of the relevant advantages and limitations of ESPI.

The most important advantages of ESPI are the ability to investigate an entire surface at one time and the ability to view the results in real time, unlike the alternative methods such as Photographic Speckle Pattern Interferometry and Holographic Interferometry, both of which require photographic processing before the results can be viewed.

The resolution of ESPI is limited by the speckle size, which is a function of both the surface under inspection and the imaging system used. Figure 2-6 shows an example of an ESP Interferogram demonstrating the graininess due to speckle. The use of a small aperture in the video camera also makes

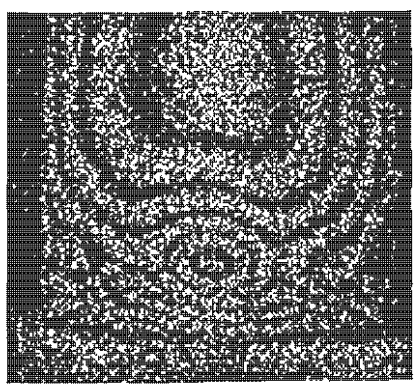

Figure 2-6 Speckle interferogram demonstrating the grainy effect of speckle.

ESPI less efficient in terms of light usage than other systems. The low resolution of ESPI compared to Holographic Interferometry and its inefficient light usage is, however, outweighed in many instances by the convenience of the method. The fringe formation can be observed in real time and easily recorded on video tape, which is extremely difficult with alternative techniques. The results are also available immediately and can be further manipulated by image processing software, allowing automatic fringe analysis and enhancement.

The maximum object size that can be inspected is largely limited by the laser power available, and the sensitivity of the camera. The object must, however, not be subject to rigid body movements of more than a fraction of a wavelength between exposures. This factor also affects the size of the object that can be inspected. The 'exposure time' of the video camera is about 1/25 sec, which may be reduced by using pulsed lasers, which lessens the stability requirements substantially.

The range of displacement measurable by ESP interferometry is limited because decorrelation occurs between the images. The interference pattern at any point on the image plane is a function of the particular surface topology of the area that is imaged at that point. If the area that is imaged moves sufficiently it will be imaged at a different point, so the difference in phase observed between the two images will be the result of two different areas being imaged and not due to the displacement of the point of interest. The result is a random phase difference at any point that is unrelated to the surface displacement, therefore no fringe pattern will be observed. It is possible to make an interferometric layout less sensitive, extending the possible range of measurement.

If a small area is being inspected, a relatively large deforming force may be required which could introduce rigid body motions, which in turn causes either spurious fringes to form or decorrelation between the images.

3. Literature Review

This section reviews the relevant work by other researchers in modelling cracks using finite element methods or modelling ESPI or Holographic Interferometry by finite element methods.

Most of the work carried out in crack modelling using finite element methods has been aimed at studying the crack tip area and crack propagation. The emphasis has been on the accurate modelling of the crack tip area so that accurate estimates of the crack tip stress value, stress intensity factors or crack opening displacement can be obtained. Work aimed at studying the crack propagation has also concentrated on the crack tip region. Crack propagation studies are also generally dynamic analyses, or consist of a series of static analyses with remeshing in between to account for the propagation of the crack.

Despite the importance of verifying numerical models, there are very few works in the literature that evaluate numerical models experimentally.

The work in this investigation involves static analyses, and the general effects of the crack on surface displacement behaviour are of interest, not the localised crack tip effects.

3.1 Crack Simulation by Finite Element Methods

A number of methods of simulating cracks in components by finite element methods have been published. All have been shown to give satisfactorily accurate predictions of various crack variables.

This section will first deal very briefly with the necessary fracture mechanics concepts and terminology and then with the most common simulation methods individually with a view to the most suitable method for this application. Simulation of cracks in non-isotropic and non-homogeneous materials such as composites have not been investigated here.

3.1.1 Effects and Behaviour of Cracks in metals

The primary effect of a crack is to weaken the structure in which it exists. This occurs because the crack introduces a local stress concentration at the crack tip, thus altering the effective stiffness of the structure. One of the fundamental equations of linear elastic fracture mechanics (Ewalds and Wanhill, 1989) is

$$\sigma_{ij} = \frac{K}{\sqrt{2\pi r}} \cdot f_{ij}(\theta) + \ldots \qquad (3\text{-}1)$$

where σ is the stress at a distance r from the crack tip at an angle θ to the axis of the crack and K is a constant stress intensity factor giving the magnitude of the elastic stress field. This equation shows that, when r is zero, i.e. at the crack tip the stress tends to infinity. Therefore there will always be a small plastic zone at the crack tip, however, the extent of the plastic zone varies.

The other terminology relevant here is the J integral, the Crack Opening Displacement (COD) and the three modes of loading.

The J integral is a measure of the energy release rate as a crack propagates in a specimen. If the energy released is sufficient it will cause the crack to propagate, leading to failure. Thus the J integral is a measure of the stability of a crack.

Crack Opening Displacement methods of analysis assume that fracture occurs when the crack tip strain reaches a critical value. The strain is characterised by the displacement of the crack flanks very close to the crack tip, hence the name.

The three modes of loading are shown in Figure 3-1. The first mode is tension while the other two are shear modes.

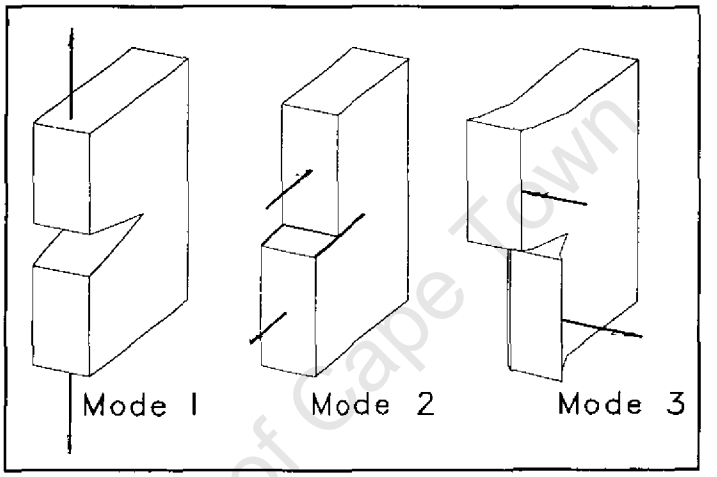

Figure 3-1 The three modes of loading.
(from Ewalds and Wanhill 1989)

3.1.2 Three Dimensional Crack Models

Three dimensional models generally employ either eight noded linear or twenty noded quadratic brick elements to model the areas surrounding the crack site. The quadratic elements, which have a node at the mid-point of each edge of the brick, allow curved surfaces to be modelled using fewer elements than would be required if linear elements were used to approximate the curve. The mesh is then refined around the crack site. The crack itself is modelled using singular elements of various types to simulate the stress singularity found at the crack tip as predicted by equation (3-1) above. An example of a three dimensional mesh is shown in Figure 3-2.

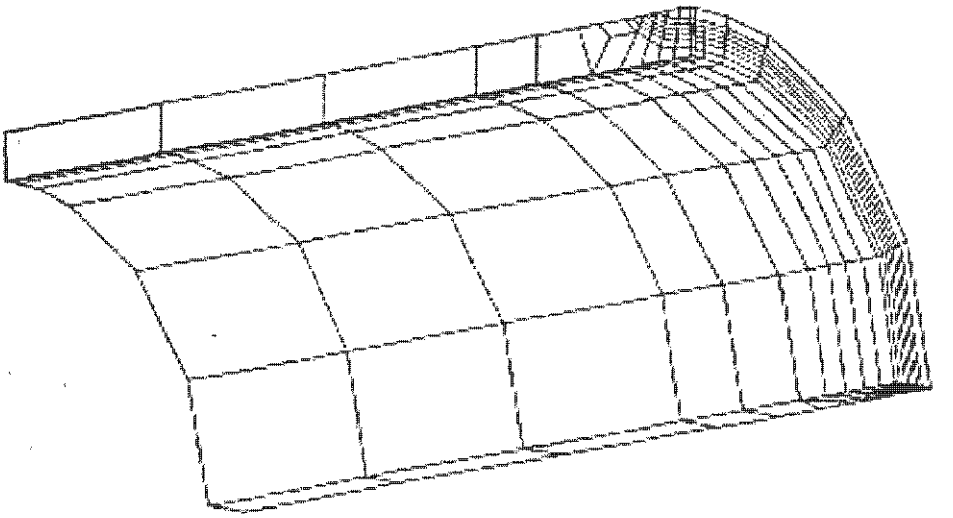

Figure 3-2 Fully 3-D finite element mesh around a crack. (from Kaufmann et al., 1987)

There are a number of ways of introducing the required singularity into the model. Gensheimer and Packman (1988) used elements with quarter point mid-side nodes to model a number of cracks with different aspect ratios in a flat plate under bending and tension. The quarter point nodes result in the same square root singularity predicted in the linear elastic fracture mechanics equation (3-1). The quarter point technique involves moving the mid-side node of a quadratic element to the quarter point to introduce the singularity.

Kaufmann et al., (1987), used collapsed singular elements to model the singularity for an analysis of a part circular crack in an internally pressurised cylindrical vessel. Kaufmann claims that collapsed singular elements are the best choice out of the three dimensional singular elements when modelling a crack, but his results show similar agreement with analytical and experimental data as Gensheimer and Packman.

Both systems demonstrated close agreement with the theoretical work of Raju and Newman (1982), a standard reference for comparing crack models with theory. They

also demonstrated satisfactory agreement with the limited experimental work carried out, although Gensheimer and Packman's work tended to overpredict the stress intensity factor that they obtained in their experimental work.

Maji and Shah (1990) also used quarter point nodes to model crack propagation in concrete. Their results showed that the FEM analysis results accurately predicted the direction of crack propagation but the crack opening displacements predicted did not agree with the displacements measured experimentally. The disagreement in this case may be due to the difficulties in accurately modelling the material behaviour of concrete, which in reality is not a homogeneous material. This investigation used the stepping technique to follow the crack propagation - the model was remeshed after each step to include the new section of crack in the direction that the previous step predicted.

3.1.3 Two Dimensional Crack Models

Two dimensional crack models are inherently limited in their application because they can only be applied where the crack is in a thin section that can be modelled as a thin plate or shell.

There are two common methods of simulating cracks in plates and shells, the damage zone model and the line-spring model. The damage zone model (Cordes et al., 1993) superimposes the cohesive stresses found around the crack tip, or damage zone, onto a linear elastic analysis. These cohesive stresses tend to close the damage zone faces. The superposition is achieved in two steps. First an elastic analysis is performed to determine at what load local failure occurs at the crack tip, then the model is altered to include the cohesive stresses calculated from the value of the load found in the first

step. This method requires extremely fine meshing around the crack zone and the crack itself is modelled as a 'slit' in the mesh, so this technique is limited to through cracks.

The line spring model on the other hand is limited to part-through cracks in plates and shells. The model, which has been extensively used, was first proposed by Rice and Levy (1972). The crack, shown in Figure 3-3a, is modelled as a through-crack in a plate or shell. The remaining material, of thickness t-a(x), causes forces and moments to be transmitted across the crack faces, thus the through crack model deviates from actual behaviour. This is overcome by modelling the stiffness of the remaining material as a series of one dimensional springs, or line springs connecting the two crack faces, as shown in Figure 3-3b. This allows the crack opening displacement and rotation to be extracted. The individual stiffness of these springs is assumed to be the same as that encountered in a single edge notched plane strain specimen with width t and notch depth a(x), as shown in Figure 3-3c, for which an exact expression for the additional compliance introduced by the notch may be obtained (Rice and Levy, 1972). Rice and Levy show in their analysis that the approximations become more accurate when the surface length of the crack is large compared to the material thickness. They also show that in pure bending or pure tension loading the line spring method predictions of stress intensity factors deviate from those predicted by an analytical solution, but are on the conservative side.

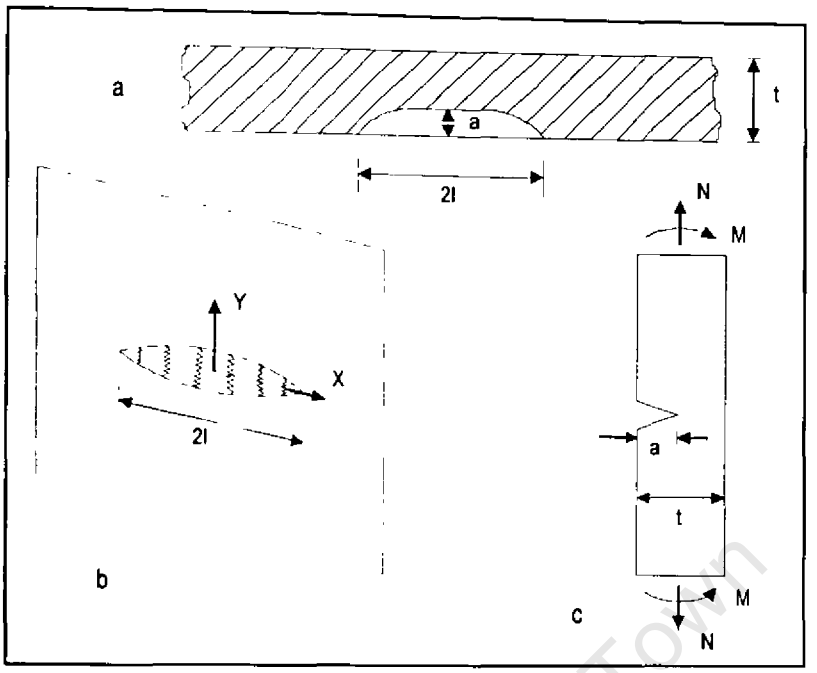

Figure 3-3 Schematic of line spring model concepts (from Kumar et al., 1985)

Kumar et al. (1985) used the line spring method to successfully model elastic surface cracks in cylinders. Their work investigated a wide range of cylinder to wall thickness ratio, flaw depth and crack aspect ratio. The model used 8 noded quadratic elements with 5 degrees of freedom at each node (2 rotational and 3 translational DOF) which take the effect of transverse shear into account. It is believed that transverse shear may have a significant effect on surface crack problems. They found that the results agreed well with those of a full three dimensional solution. The stress intensity factor predicted for an external crack was larger than for an internal crack of the same geometry, which is expected because an internal crack is somewhat constrained in bending when the cylinder is under internal pressure. Their results also showed that the line spring model is subject to some limitations near to the crack tip, but provides fairly accurate results along most of the crack front. This result gives confidence in the accuracy of the line spring model along the crack front and surrounding areas, which

is what the current study requires. It also gives some confidence in the predictions of J integral and Stress Intensity Factor along the crack front.

Parks and White (1982) extended the elastic line spring model to include elastic-plastic behaviour, thus allowing the prediction of the J integral in surface cracked plates and shells. They found that the results were reasonable but had yet to be validated to the same extent as the elastic model.

Miyoshi et al. (1986) also did work on the elastic-plastic line spring model, based partly on the work of White. They showed that the J integral for surface cracks in work-hardening plates and shells can be calculated with acceptable accuracy and short computing time.

3.2 Simulation of Holographic Interferometry and ESPI by FEM

Some work has been done with the specific aim of simulating interferometric fringe patterns by finite element methods. Some other work has been placed in this section where HI or ESPI has been used to verify finite element models because this work also compares finite element predictions with interferometric measurements.

Hulett and Penny (1992) and Penny and Gryzagoridis (1994) set out to simulate the fringe patterns obtained around surface cracks in cylindrical pressure vessels using finite element methods. They investigated a number of flaw geometries, including axial and circumferential thumbnail cracks and axial and circumferential grooves.

The finite element model adopted consisted of shell elements to model the test cylinders and line spring elements, mentioned above, to model the cracks. Their results showed good correlation between model and experiment. Contour patterns

were found to match well, but in the case of the axial thumbnail crack the finite element model predicted that one fringe would be further from the crack than indicated by the interferogram. These studies did not include any quantitative comparison of the experimental and numerical results.

In the work of Maji and Shah (1990), mentioned above, the crack extension in concrete was investigated. HI was used to measure the crack opening displacement which was found to disagree with the finite element model predictions, but it was found that the FE model can predict the propagation direction using the maximum hoop stress criterion, as mentioned above.

Miller et al. (1988) also used Holographic Interferometry to test a linear elastic fracture mechanics (LEFM) finite element model for concrete. They showed that the LEFM model was accurate at low load levels and with short crack lengths. At higher loads and with longer cracks large deviations between model and experiment were observed. One possible reason for this is the fact that concrete can behave as a brittle material. The current study involves only short crack lengths and low loads, so these problems should not be encountered.

Ratnam and Evans (1993) used HI to verify a finite element model of the thermal expansion of a piston. The aim was to asses the effects of various assumptions that were made in the generation of the finite element model. The holographic set-up was such that the deformation at the front and rear of the cylinder could be measured simultaneously so as to minimise any errors introduced by rigid body motion. The set-up was also capable of measuring both in-plane and out-of-plane displacement, allowing the calculation of radial displacement, which was then compared to the

predictions of the finite element model. The results of their investigation showed good correlation in areas where no assumptions were made in the FE model, and fair correlation in the areas where the assumptions were being investigated. When the assumptions were modified better correlation was observed, allowing a more accurate model to be obtained.

Kaufmann et al., mentioned above, used speckle photography and holographic interferometry to evaluate the accuracy of their 3D numerical model of a part-through crack in a pressure vessel. They found good agreement between the experimental and numerical results. 3D elements were used in this case because the cylinder being modelled was a thick cylinder, so any thin cylinder or 2D assumptions would introduce unacceptable errors.

4. Investigation Process

4.1 General Procedure

The investigation set out to determine if the fringe patterns observed around a number of different cracks and combinations of cracks located near one another could be accurately modelled by finite element methods.

This section briefly describes the general approach to the investigation and the following sections describe each part in more detail.

The investigation consisted of three major steps. Firstly the fringe patterns for the crack free cylinders under internal pressure load were simulated using the finite element package ABAQUS. These patterns were compared with the experimentally observed patterns. Secondly the finite element model was calibrated against the experimental results to obtain the best possible correlation between the two. The calibration principally involved adjustment of the elastic modulus used in the finite element model. The range of adjustment was limited to the range of accepted values for the particular aluminium alloy that was employed. Finally, once satisfactory correlation was obtained, various thumbnail cracks and combinations of cracks were introduced. The experimental and finite element results for each different crack configuration were compared, with no further adjustment of the material properties. The quantitative comparisons were made at the crack site, as this was the area of interest. The general fringe pattern was evaluated qualitatively.

This approach minimises errors before the cracks are introduced so that the accuracy of the crack model may be evaluated with as little influence from other sources of error as possible.

4.2 Cylinder Design and ESPI Experiments

One of the major applications of NDT lies in the testing and residual life prediction of pressure vessels and piping. The wall thickness to diameter ratio of this type of equipment allows it, for the most part, to be viewed as thin cylinders. For this reason it was felt that it would not be unrealistic or unduly limiting to use thin cylinders in this investigation.

The experimental work made use of a continuous wave laser ESPI system (the experimental system is described in detail later in this section). One of the problems associated with such an ESPI system is the stability requirement. The change of position between images of the specimen must be less than the wavelength of the laser light. This constraint introduces fairly stringent requirements for the clamping of the specimen. It must be held firmly enough so that the load source cannot move the specimen when the load is applied. The whole experimental set-up is mounted on a large vibration isolation table which can be tilted by external loads. The loading must also not introduce any detectable movement of the table between images. For these reasons it was desirable to keep the magnitude of the required loading at low levels as far as possible.

Two factors were the major design criteria for the cylinders: they should be thin cylinders and should require as small a load as possible to produce a surface displacement of sufficient magnitude to be easily detected by ESPI.

Perspex was investigated as a possible material, but proved ineffective. Aluminium cylinders were then investigated. One design was discarded, and a second design accepted. The three designs are discussed in the following sections, followed by a discussion of the ESPI experiments.

4.2.1 Perspex Cylinders

The proposed design of the perspex cylinder consisted of a section of tubing with two perspex end caps glued onto the ends. One of these caps was fitted with a pressure fitting so that the internal pressure load could be applied. The ends of the tube needed to be carefully prepared so that the tube would not crack when the perspex cement or chloroform was applied to glue the end cap on.

The only tubing available in the sizes required here is extruded tubing. It was noted before any ESPI tests were done that the wall thickness varied considerably around the circumference. This variation proved to be too large to allow consistent and regular fringe patterns to be observed. The interferograms showed fringe concentrations in a number of places on the cylinder. The fringe patterns were also not symmetrical, as they should have been if there were no material defects. The geometry of the optical system was carefully checked to ensure that this was not the cause of the asymmetry. It was shown that this was not the case, and a number of points were located on the cylinder where fringe concentrations were observed in the following manner. The fringe pattern is displayed on the monitor. The centre of the fringe concentration is then marked on the screen. The display is then switched to a 'live' view from the camera. A pointer or marker can then be used to mark the point on the cylinder surface

by matching the position of the marker with the mark on the screen. This system works because the camera and object are not moved after the interferogram is made.

Once the points had been marked the cylinder was cut open and the location of these fringe concentrations examined. The locations proved to be points where there was either thickening or thinning of the walls. The remaining tubing was examined and thickening and thinning of the walls of similar magnitude was observed in a number of places.

Based on this investigation it was decided that the available perspex tubing was of insufficient quality for the purposes of this investigation.

4.2.2 Aluminium Cylinders

A number of aluminium alloy cylinders of outside diameter 90 mm, wall thickness 4mm and length 340 mm were available. It was proposed that these cylinders be used in the investigation. Three possible methods of sealing the ends of the tubes were proposed:

1. An end cap which screws into the ends of the cylinder walls, the screws being parallel to the axis of the cylinder.
2. End caps that are clamped together by means of tie rods running either inside or outside the cylinder.
3. A simple threaded plug which screws into a thread cut on the inside of the cylinder.

The first proposal was not practical as the walls of the cylinder were too thin. The second was impractical because of the difficulty of ensuring that the same tension existed in each of the tie rods. Any mismatch in tension would result in an uneven pre-

load on the cylinder, and could possibly introduce some bending of the cylinder which could alter the fringe patterns. The most practical solution was thus the threaded plugs.

A photograph of the cylinder is shown in Figure 4-1.

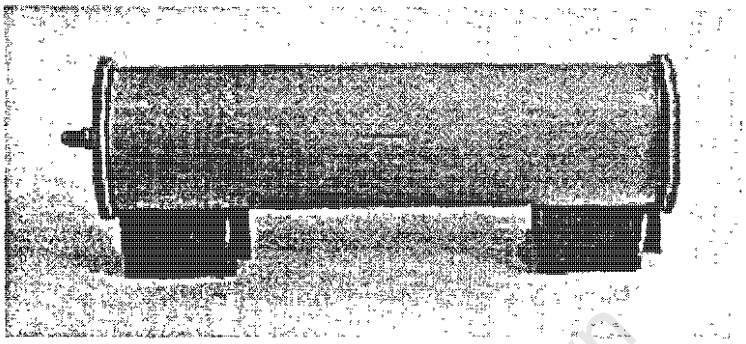

Figure 4-1 Aluminium alloy cylinder with screw-in caps.

The ESPI fringes produced by this cylinder under internal pressure load displayed substantial asymmetry. The expected pattern of fringe formation would be to observe the fringes forming at the middle of the tube, where the largest deformation is expected, and expanding towards the edges and end of the tube image. They would also be expected to be symmetrical about the axis of the cylinder, and nearly symmetrical about the middle of the cylinder. The fringes appeared to originate near the ends of the tube, which was unexpected. As the load increased the fringes expanded from the end slightly, and a second closed fringe began forming at the middle of the cylinder, where the initial fringe was expected to form. The fringe patterns at the ends were not symmetrical about the axis of the cylinder, which was also indicative of a flaw or other anomaly, nor were the fringes symmetrical about the middle of the cylinder.

The tube was held vertically by one end, and the asymmetry about the middle of the cylinder was suggestive of tilting or bending of the cylinder towards or away from the camera. To test this theory, the cylinder was shortened by 25%. If there was bending

or tilting, the fringe patterns would still have been asymmetrical, but to a much lesser degree because the maximum displacement of the end would be less, and the shorter tube would be more stable. No difference was observed in the fringe pattern, indicating that the asymmetry was caused by some other effect.

It was noted that the thread which had been cut on the inside of the cylinder extended beyond the end of the cap when it was fully screwed in. The cylinder had constant wall thickness along its length, so the area where the thread had been cut was thinner than the remaining wall, and therefore weaker. The first area to displace enough to produce a fringe thus appeared to be the weakened thread area, and then, as the load increased, the expected fringe pattern began to manifest itself, to produce an asymmetrical fringe pattern. This theory was confirmed when the ends of the tube were cut down slightly so that when the end cap was screwed tight the thread on the inside of the tube did not extend beyond the end of the cap. An immediate improvement in the fringe pattern was observed. The fringes were still, however, forming at the ends of the tube, although not to such a marked degree. The behaviour of the thread - end cap interaction could not be predicted, so the initial deformation at the end was still very likely to be the result of the weakening of the tube caused by the thread and the possible movement between the two mating parts. To overcome this problem the tube was skimmed along its length to reduce the wall thickness along most of the length. The tube was thus left with a 'waist', as shown in Figure 4-2.

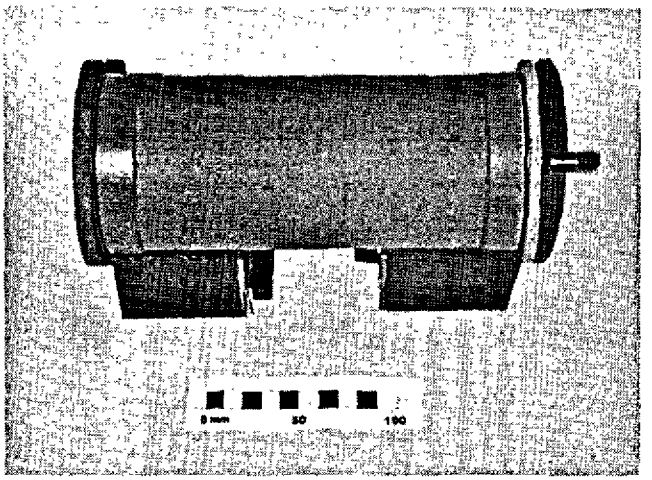

Figure 4-2Aluminium alloy cylinder with screw-in caps and thinner walls

This modified cylinder produced better results, with good symmetrical fringes forming at very low loads. At higher loads, however, the fringe pattern once again exhibited the characteristics of rigid body motion or bending. This behaviour suggested that the method of holding the cylinder for the experiments was unreliable. The various holding methods are discussed in a later section.

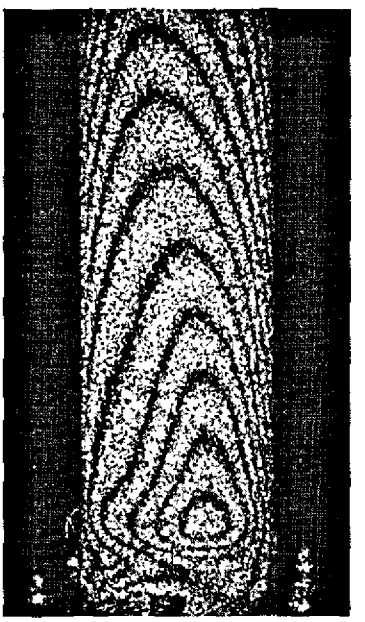

Figure 4-3Typical asymmetrical fringe pattern observed for cylinder held at one end.

The mounting for the cylinder was redesigned to be very sturdy and stable. With the tube mounted using this system (discussed below) the fringe patterns were repeatable, indicating that the cylinder was being held in a stable manner, but some permanent deformation was observed if the object was loaded and unloaded. The fringes were once again forming from the ends of the cylinder, specifically from the threaded area, which indicated that the thread was moving against the end cap under load. For this reason it was decided to redesign the cylinder and avoid using a threaded end cap.

The new cylinder was machined from solid Aluminium alloy, 6261 T6. The cylinder without end caps is shown in Figure 4-4, and the dimensions are shown in Figure 1 of Appendix A.

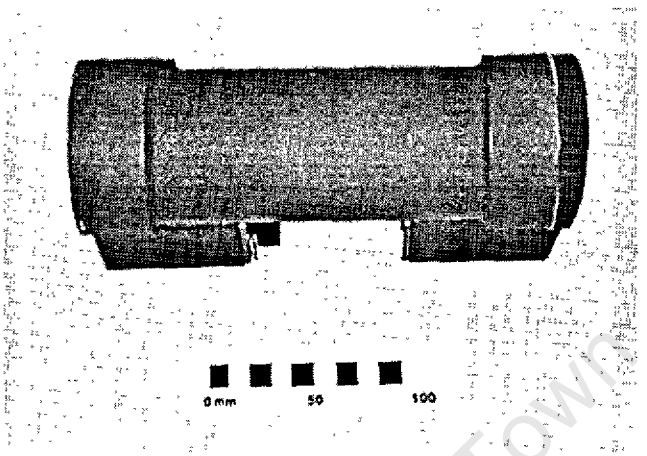

Figure 4-4 Final cylinder design without end caps

The method used to attach the end caps in this cylinder proved to be more satisfactory. The fringe patterns at the ends were more even, indicating that the screws into the ends of the walls did not cause as much weakening of the structure as observed in the previous cylinder. The initial ESPI results displayed the characteristics of rigid body motion, and were found to be caused by the mounting system which was initially used for the experiments, however once these problems had been overcome the cylinders proved to be very successful, with easily reproducible results. This cylinder design was used in the final experiments.

4.2.3 Jig and Mounting System for Experiments

The mounting system for the pressure vessel was designed to hold the cylinder firmly enough to satisfy the requirements for stability imposed by the continuous wave ESPI set-up, but also allow the cylinder to expand in the same manner as a vessel in industry might be expected to expand. Commonly, a vessel will be free-standing or fixed at the base, with the top end free. The initial design of the mounting system set

out to hold the cylinder in this manner - standing vertical on the table, with the base held firmly.

The major cause of rigid body motion or bending was expected to be the tube running from the hydraulic dead-weight tester to the vessel. As the pressure increases this tube tends to stiffen and exert a force on the points of attachment of the tube. To minimise this effect the pressure inlet was located at the base where the cylinder was most firmly held, so the possible leverage of the force exerted by the stiffening tube would be at a minimum. The initial design, used for the first aluminium cylinder, is shown in Figure 4-5

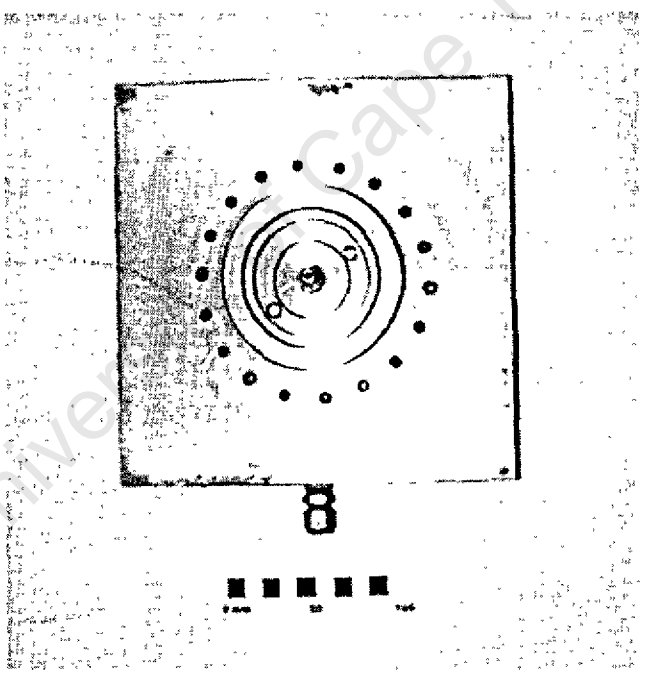

Figure 4-5 Steel base stabiliser ring and pressure inlet on the side and outlet in the centre.

The equipment consisted of the large square steel base (215 x 215 x 40 mm) The pressure tube was attached to the side of the base, as shown in Figure 4-5. The base had a hole drilled horizontally to the centre and a vertical hole drilled down from the centre to form a pipe from the edge to the centre of the plate. The tube was screwed

onto a fridge fitting which was in turn screwed into the vertical hole, as shown in the photograph. The steel stabiliser ring consisted of two parts. One was bolted to the base, and the other was threaded and screwed onto the first. This could then be screwed up against the end cap of the tube to stabilise it against any possible bending of the fridge fitting.

This arrangement proved ineffective due to instability. It proved impossible to ensure that the cylinder was perfectly vertical when mounted on the fridge fitting. Any variation from vertical caused the stabilising ring to be hard up against one side of the end cap and not the other, so the cylinder was not properly stabilised against bending. Removing the ring did not make the situation any worse, so it appears that the ring was serving no useful purpose.

The method of attaching the cylinder to the base was thus redesigned to overcome this problem. A new end cap was designed for one end which could be bolted directly to the steel base. An o-ring was used between the end cap and the base to seal the pressure inlet. This new end cap is shown in Figure 4-6.

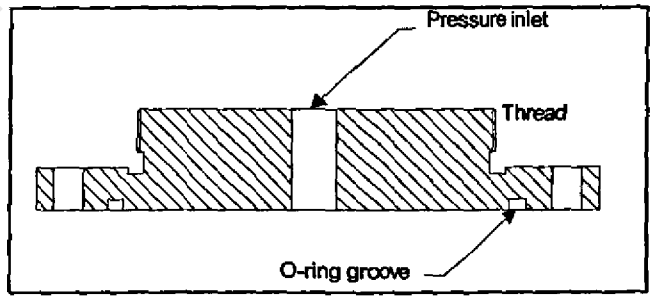

Figure 4-6 Cross section of redesigned end cap to be bolted to steel base

The movement of the thread as the load was applied which was discussed above was noted using this end cap.

It was decided to use this method of mounting the newly designed cylinders, which were discussed above. The end cap required modification to accommodate the new closure method of the new cylinder. The modified cap is shown in Figure 4-7.

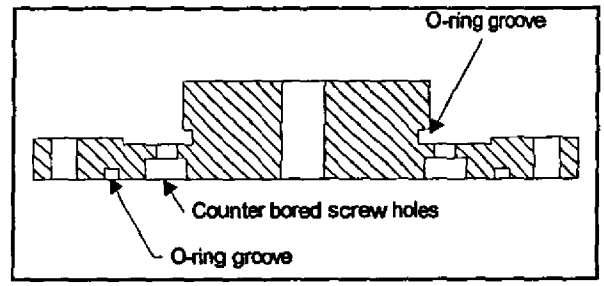

Figure 4-7End cap for newly designed cylinder.

The new cylinders did not exhibit the same movement of the end relative to the end caps. Nearly symmetrical fringe patterns were observed at very low loads, but the fringe patterns were indicative of rigid body motion or bending of the cylinder at slightly higher loads. Some asymmetry was expected about the centre of the cylinder due to the manner in which the cylinder expands under internal pressure when one end is built in, but the extent of the asymmetry was expected to be much smaller than that observed. An example is shown in Figure 4-8. A number of attempts were made to isolate the cause of this bending or movement, including re-orienting the whole system with the cylinder horizontal, increasing the number of bolts holding the end cap to the base and the cylinder to the end cap and replacing the rubber o-rings with non-compressible gaskets. The optical geometry was carefully checked and measured to ensure that this was not the cause of the problem. The

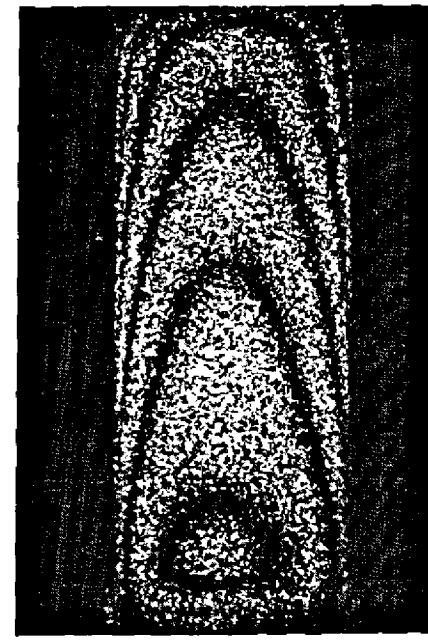

Figure 4-8 Asymmetrical fringe pattern observed with the new cylinder and end cap.

location of the cylinder and loading system was also moved around on the vibration isolation table to ensure that the loading was not tilting the table. Despite these attempts the cause of the movement could not be determined, and this mounting system was abandoned due to time constraints.

The end caps were then modified as shown in Figure 4-9 so that the end caps were the same diameter as the ends of the cylinder.

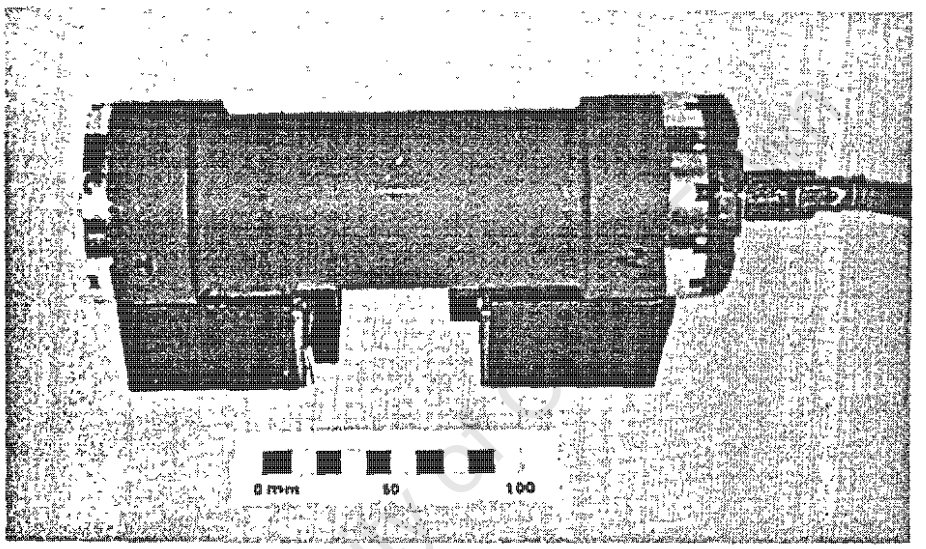

Figure 4-9 Final cylinder design with endcaps and pressure tube

A number of methods of mounting the tube were tried, including lying the cylinder on a pair of v-blocks with the pressure pipe entering at 90° to the viewing direction, clamping the pressure connection in a vice and standing it vertically on the table with the pressure pipe clamped by means of a retort stand. These all proved to be unstable arrangements. In some cases a symmetrical fringe pattern was observed once, but it was not repeatable. A magnet was then inserted into the one end cap to hold it firmly on the steel vibration isolation table. This arrangement improved matters, but the fringe patterns were still not repeatable despite numerous attempts to stabilise the pressure pipe, including replacing the flexible rubber pipe with a metal tube which

was led vertically from the dead weight tester, then horizontally, then vertically down into the top of the cylinder and clamped with two retort stands. The fringe patterns observed with this arrangement were still characteristic of rigid body tilting above a critical load. The characteristic tilt pattern could be eliminated by adjusting the clamps on the pipe after the load had been applied and before the final interferogram was captured. The number of fringes observed did not change as a result of the adjustment, just the general pattern. Adjustment in this manner was not, however, an acceptable solution because the amount of adjustment required could not be determined. A small amount of asymmetry was expected due to the way in which the cylinder expands when one end is fixed, but exactly how much could not be determined, so the correct amount of adjustment could not be determined.

Based on these results it was decided that the cylinder should be mounted in such a way that both ends were effectively built in to prevent any uncertainty in the shape of the fringe patterns. If both ends of the cylinder are built in then the fringe pattern should be symmetrical about the middle and the long axis.

The cylinder was mounted in the jig as shown in Figure 4-10. The two tie rods were carefully measured and cut so that the two ends of the jig were exactly parallel and were of a length such that the distance between the ends was the same as the length of the cylinder when tightly bolted. This set-up prevented an excessive preload being placed on the cylinder by tightening the jig. A repeatable preload could thus be introduced by placing a number of sheets of paper between the end of the cylinder and the jig. The preload was kept to a minimum to minimise its effect on the fringe patterns. The preload required to hold the cylinder firmly in this manner is

substantially smaller than that which would be required if tie rods were used to seal the cylinder.

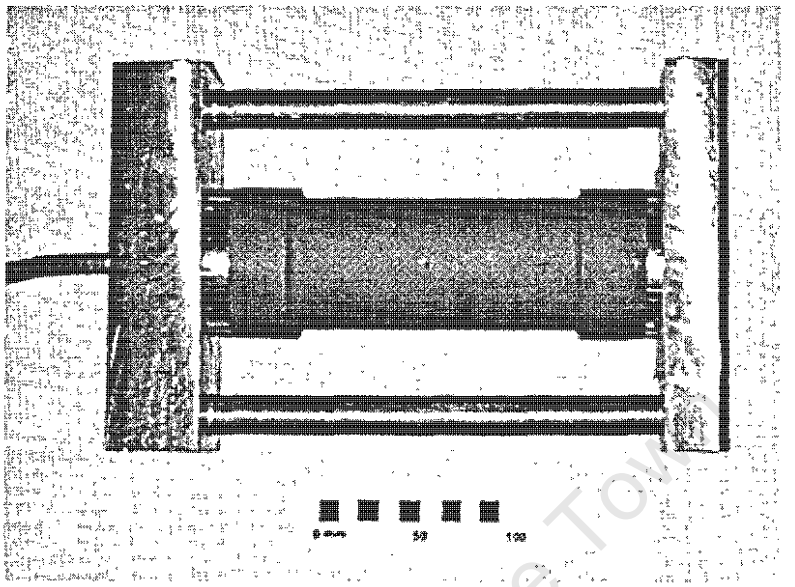

Figure 4-10 Cylinder mounted in the jig

The jig shown in Figure 4-10 was placed on the table and held firmly in place with magnetic clamps, as shown in Figure 4-11.

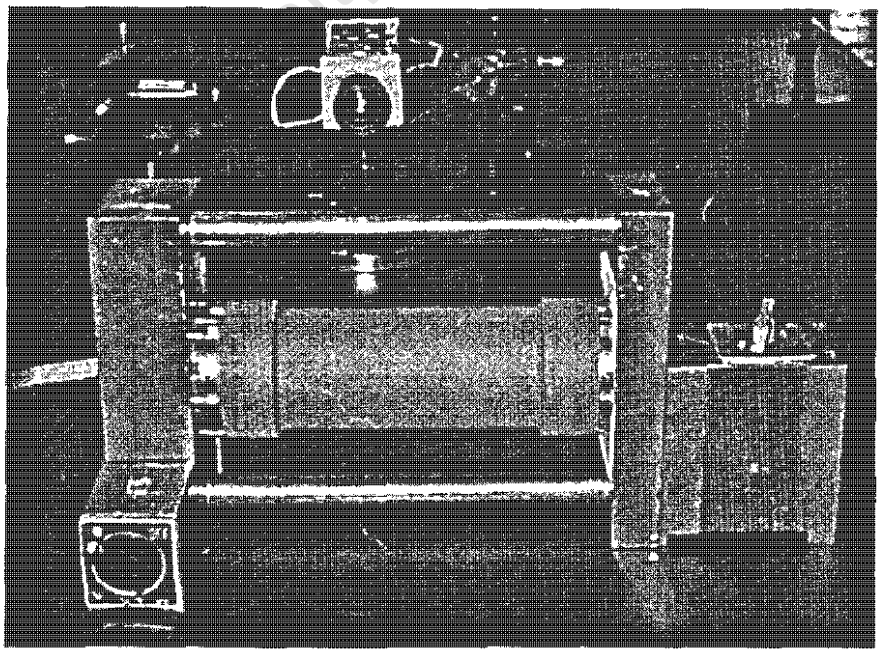

Figure 4-11 Jig and cylinder on the table. The camera is visible in the background.

This arrangement proved very successful. The fringe patterns were symmetrical, easily repeatable and the experiments were carried out using this system of mounting.

4.2.4 Crack Introduction and Location

The cracks which were introduced were all simple thumbnail cracks. It was required that the profile of each crack be accurately known so that it could be modelled accurately in the finite element simulation. The most viable method of introducing these cracks proved to be a 0.2 mm thick, 50 mm diameter slitting saw. This allowed a sufficiently narrow slit to be introduced and allowed the exact depth profile to be calculated for each crack. For all the external cracks the cylinder was clamped on a milling machine's table and moved relative to the rotating slitting saw mounted on the mill head. This arrangement could not be used for the internal crack because the cutter could not be arranged to rotate in the required plane and be manoeuvred inside the cylinder. A dentist drill was employed to make the internal cut. The slitting saw was attached to a custom made arbor for the drill and the drill itself was mounted in a jig. The jig was mounted on the toolpost of a lathe and the cylinder was clamped in the lathe chuck. The dentist drill could then be manoeuvred into the cylinder and the location and depth of the cut could be easily controlled. The arrangement is shown in Figure 4-13.

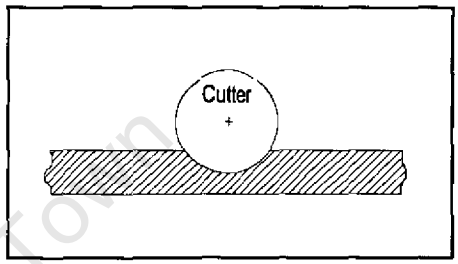

Figure 4-12Method of making cracks in the cylinders

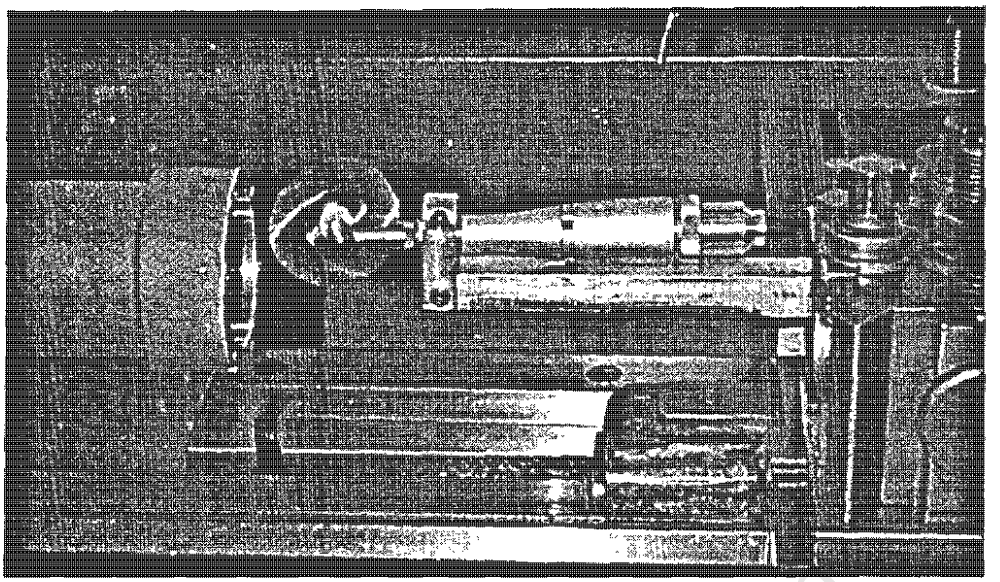

Figure 4-13Dentist drill mounted on the lathe with the cylinder and cutter.

An axial internal crack was introduced rather than the more easily engineered circumferential crack because the displacement profile for an axial internal crack, as predicted by the FE model, was very distinctive, whereas the profile for an internal circumferential crack was predicted to be very similar to the profile for an external circumferential crack. A wide range of displacement profiles would give a more accurate picture of the modelling capabilities of finite elements, so the axial crack was introduced.

Figure 4-12 shows how the cracks were introduced. Figure 4-14 shows the orientation for the single external cracks. An internal axial crack of the same dimensions and in the same location as the external axial crack was introduced into the fourth cylinder. Figure 4-14 also shows the positioning of the second crack in each case to form the crack combinations which were investigated.

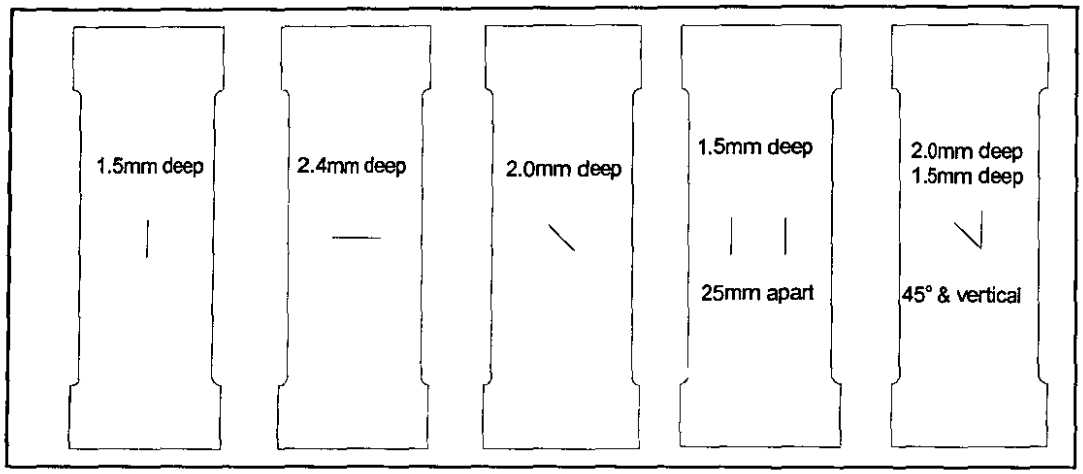

Figure 4-14 Crack locations for single cracks and combinations. All cracks were cut using 50 mm diameter cutter.

The depth profile of the cracks was calculated using a spreadsheet. The maximum depth of the cut was known, along with the diameter of the cylinder and cutter, which provided enough information to calculate the depth at any point along the cut.

4.2.5 ESPI Experimental Set-up

The principals and theory of ESPI have been dealt with in a previous section, so it will not be dealt with here. The actual experimental layout and process will be described in this section.

The actual experimental layout is shown in Figure 4-15. The two mirrors in the object beam are included to allow the object and reference beams to be adjusted independently. The partial mirror is, in practice, a pair of prisms mounted face to face. The prisms are mounted

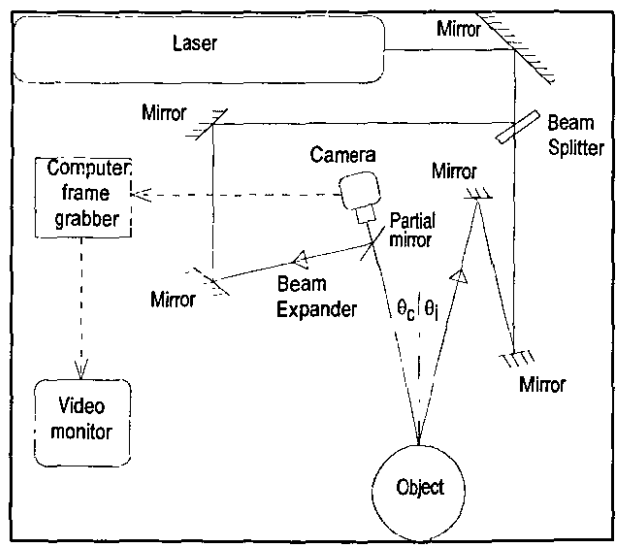

Figure 4-15Experimental layout for ESPI experiments

behind the camera lens and the reference beam is directed onto the prism through a hole in the side of the camera housing. The beam expanders employed were spatial filters, an example is shown in Figure 2 in Appendix A. The spatial filter consists of a microscope objective which is used to focus the laser beam onto a pinhole. This method of beam expansion minimises the diffraction rings which are visible when using a conventional beam expander. The 'cleaner' or spatially filtered expanded beam provides more even illumination for the object and prism. The path lengths of the reference and object beams had to be within about 50 mm of one another for the particular laser used to satisfy the coherence length requirements. A variable beamsplitter, shown in Figure 2 of Appendix A was also included in the reference beam path to allow easy adjustment of the reference beam intensity without refocusing the beam expander.

The components shown in Figure 4-15 were mounted magnetically on a steel vibration isolation table which is shown in Figure 3 of Appendix A. The table surface is a 25 mm steel plate which lies on inflated rubber tubes which rest on a solid base.

The angles θ_1 and θ_2 were kept as small as possible (between 5° and 10°) to minimise the sensitivity to in-plane displacement and maximise the out-of-plane sensitivity. Keeping the angles approximately equal also minimises the in-plane sensitivity, as shown in Section 2.1.5.

The cylinders all had shiny aluminium surfaces so a bright stripe was observed by the camera. This is caused by the curved surface reflecting the incident light in various directions, with only one strip reflecting most of the incident light towards the camera. The brightness of the strip in contrast to the rest of the cylinder prevents fringes being

observed over the whole cylinder surface. The camera aperture can either be adjusted so that fringes can be observed along the strip, in which case the rest of the cylinder is too dimly imaged to form fringes, or the rest of the cylinder is imaged and the strip is too bright. To overcome this problem the cylinder was painted with matt grey primer which lowers the intensity of the bright strip and allows a more even image intensity over the whole cylinder image.

The cylinder was mounted on the table in the jig as shown in Figure 4-11 above. The hydraulic dead weight tester, which provided the pressure load via a flexible pipe is shown in Figure 4 of Appendix A. The tester was located next to the vibration isolation table so that the process of increasing the load, which involved rotating the wheel on the tester, did not cause the table to vibrate so the fringe pattern could be watched as it formed form zero load to the final load. The point of maximum displacement could be determined by observing where the fringes formed and the fringes could be counted as they formed. It was observed that the number of fringes that formed was larger than the number that could be counted on the final interferogram because the fringes 'run together' at the edges of the interferogram and thus cannot be distinguished from one another.

4.2.6 Experimental Program

The experimental program which was followed is described in this section.

4.2.6.1 Cylinders

Four identical cylinders were manufactured from the same solid round bar (6261 T6 Aluminium). Each of these was examined by ESPI to ensure there were no defects. A

photograph of these cylinders is shown in Figure 4-9, the dimensions of these cylinders is shown in Figure 1 of Appendix A.

4.2.6.2 Loading

As discussed above the loading was provided by the dead weight tester. The tester that was used was calibrated in pounds per square inch (psi) (1 psi = 6.89 kPa). The loading range that produced a fringe pattern of satisfactory density across the whole range was determined by rough calculation and checked by experiment. It was found to be between 60 and 120 psi (approx. 414 to 827 kPa).

4.2.6.3 Experimental procedure

Once the cylinders were shown to be free of defects a series of interferograms was captured and stored. Each cylinder was mounted on the table and subjected to a 152 kPa (22 psi) preload to ensure that any friction or other effects in the dead weight tester were overcome. This provided a reliable baseline to which additional load could be applied. The first image was captured with this preload and then, with a higher load applied, the second image was captured to form the interferogram which was stored. The total load was then removed and the preload replaced, the first image captured, the same additional load applied and the second image captured. This process was repeated three times for each load, with each interferogram being stored for later analysis. As discussed in section 4.2.5 the fringes 'run together' at the edges of the cylinder image so it was necessary to apply the load slowly and count the fringes as they formed to ensure that the correct fringe number was used during the analysis of the interferograms. The number of fringes counted was recorded for each interferogram.

The load ranged from 60 psi (414 kPa) to 120 psi (827 kPa) in increments of 10 psi (69 kPa). Thus a total of 21 interferograms (3 interferograms at each of 7 different loads) was stored for each cylinder.

The results from each cylinder were analysed and compared to the finite element predictions for the crack free cylinder in order to both check the finite element model and calibrate the material properties. Malan and Paterson (1987) give 63 to 70 GPa as the accepted range of the modulus of elasticity for Aluminium alloy 6261. The accepted value for Poisson's ratio is 0.3. The calibration showed that 70 GPa provided a good correlation.

Once the calibration was completed a single crack was introduced into each cylinder, each cylinder having a crack of different orientation, and the same experimental procedure as described above was carried out. These results were then analysed and compared to the finite element predictions for each crack orientation.

A second crack was then introduced into two of the cylinders to form a combination of two cracks located near one another. The same experimental and analytical procedure was also carried out for these crack combinations.

4.3 Finite Element Model

With the aims of the investigation in mind, the following criteria were used during the modelling process:

1. The fringes must be simulated as accurately as possible.

2. The crack geometry should be simple to alter.

3. The model should not require excessive computer time to run.

The following sections describe the element choice for the models and the modelling process itself.

4.3.1 Element choice

The requirement of the best possible accuracy suggests the use of a fully three dimensional model, made up of 3D brick elements and a 3D crack model. Such a model would require a complicated mesh, particularly around the crack site, as can be seen in Figure 3-2 above. Implementing changes in crack size and orientation in a 3D model requires extensive remeshing and is therefore time-consuming and complicated, thus point 2 and 3 above were not satisfied.

The cases investigated can be modelled using shell elements with no significant loss of accuracy. The use of shell elements allows line spring elements to be used to model the cracks. The implementation of these elements in ABAQUS allows the depth, length and orientation of the crack, as well as the surface on which the crack occurs to be changed easily with little or no change in the mesh. Previous work in this field and others, as discussed in section 3 has shown that the combination of shell and line spring elements can produce suitably accurate results, particularly when the area of interest is not the region near the crack tip (Kumar et al., 1985). In this investigation the displacement field around the crack site is of interest and not the variables associated with the crack itself, such as stress intensity factors.

The shell-line spring combination has a major advantage over a 3D model in analysis time. Inclusion of even a small section of 3D brick elements into a model of one of the cylinders approximately tripled the analysis time compared to the same model using

only shell elements. The line spring elements do not increase analysis time significantly over the analysis of the crack free geometry.

Another advantage of the line-spring elements in ABAQUS is that they calculate the J-integral and stress intensity factors along the crack front automatically. This may be useful for any future work.

For these reasons the combination of shell and line spring elements was chosen to model the cylinders. The model of the large cylinder required the use of some 3D elements to model the end caps.

The geometry of the crack free cylinders would allow an axisymmetrical analysis of half the cylinder to be performed, but the inclusion of a crack removes the property of axisymmetry. If the axial and circumferential cracks are centred along the length of the cylinder, do not deviate from the axial and circumferential directions respectively, only one quarter of the cylinder needs to be modelled, as shown in Figure 4-16. The cracks will then run along the horizontal and vertical planes of symmetry, but if the cracks are not limited to these positions, as in this case with the angled crack and the crack combinations, the entire cylinder must be modelled because there no longer exist any lines of symmetry. It would be possible to model half the cylinder with the crack or crack combination in the centre of the half cylinder, but the symmetry imposed would mean that a cylinder

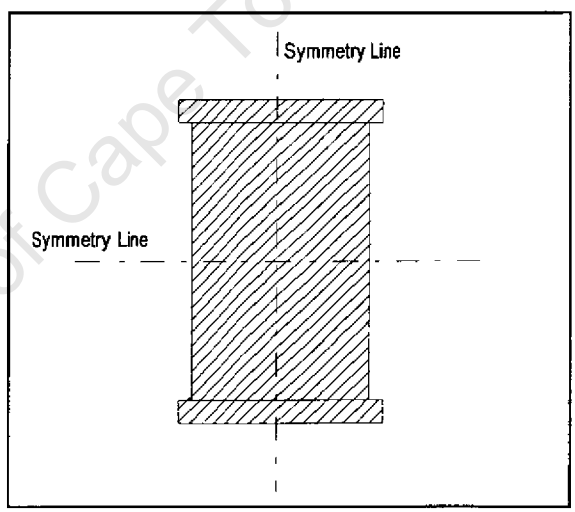

Figure 4-16 Schematic showing symmetry lines for a closed cylinder.

with identical cracks on opposite sides of the centre line was modelled. This investigation was aimed at evaluating the accuracy of the crack models, so it was undesirable to introduce a second crack into the model which was not present in the physical cylinder.

ABAQUS offers two basic groups among its non-axisymmetrical shell elements. The first group are designed for use with thin shells and the second for use in thick shell applications or in cases where the transverse shear flexibility is important in a thin shell. It is suggested that thick elements be used where the thickness of the shell is more than about 1/15 of a characteristic length on the shell surface. In this case the characteristic length is the length of the cylinder because it is along this length that bending occurs, which is the loading type that introduces transverse shear. For the cylinders used in this investigation the ratio was approximately 0.6/15 if the wall thickness was taken as 8 mm along the whole length (i.e. the worst case). Thus the cylinders fall into the thin shell category. However, according to Kumar et al. (1985), the transverse shear deformation is important around the crack site, thus, despite the fact that the cylinders are thin shells, thick shell elements were used.

Thin shell elements were investigated for use in the areas away from the cracks to improve accuracy, but no difference in the results was observed when the elements were changed from thick to thin. The thin shell elements implement the Kirchoff thin shell constraints algebraically, while the shear flexibility implements these constraints approximately when the shells are thin. Therefore the thick shell elements can be used for both thick and thin shell applications (ABAQUS Theory manual, section 4.3.1). These factors led to the use of thick shell elements throughout the cylinder so as to

simplify the model and, more importantly, to allow the crack position to be altered with minimal model changes.

The thick and thin shell element groups can be further subdivided into linear and quadratic elements. The quadratic elements allow the element to follow a curved surface closely, while a curve must be approximated by a series of straight lines when linear elements are used. Either of these groups of elements could be used for the crack free cylinders in this case, but the use of linear elements require a large number of small elements. Far fewer quadratic elements are required for the same level of accuracy, and the reduced number of elements reduces computer time. Quadratic elements are required adjacent to the line spring elements because the line springs available in ABAQUS are 6 noded elements - 3 nodes for each side of the crack. 3 noded line spring elements are also available for use only along symmetry planes. The same basic mesh was to be used for both the cracked and crack free models, so linear elements were not considered for use in the crack free models.

For the abovementioned reasons the 8-noded quadratic shell element S8R, a 6 noded quadratic quadrilateral shell element using reduced integration, was used to model all the shells, and the line spring elements LS6 were used for all the cracks.

4.3.2 Modelling

As discussed in the previous section the whole cylinder was to be modelled using the combination of S8R and LS6 elements. This section describes the model in more detail.

The cylinder was mounted in a very stiff jig, shown in Figure 4-10, so axial expansion under internal pressure could effectively be neglected. It could therefore be modelled

without including the end caps. Constraints were placed on the ends to prevent axial and radial motion. These correspond to the constraint of the jig in the axial direction and the closure of the end cap in the radial direction. The thickness of the cylinder wall will prevent rotation of the mid point of the wall when butted up against the cap, as shown in Figure 4-17. The shell elements are placed at the centre of the wall thickness, so the end nodes were also constrained in rotation.

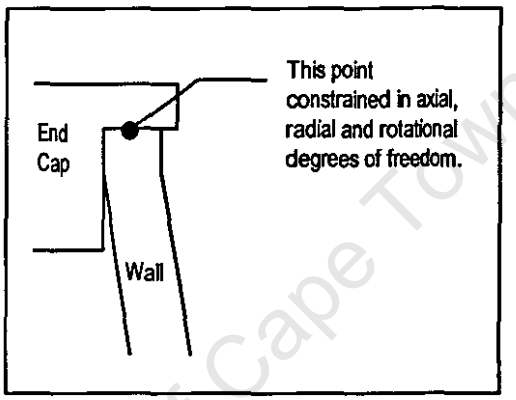

Figure 4-17 Constraints on ends of the cylinders.

The screws holding the end cap penetrate the wall for a short distance. The screw material has a different stiffness to that of the cylinder material and will therefore alter the response of the ends of the cylinder. The end of the cylinder may therefore be held against the end cap for a short distance, or it may be free to move away from the cap right up to the end of the wall. These effects will be very small and, according to St Venant's principle, any effect that it may have will be negligible at a distance from the end. The investigation is focused on the mid line of the cylinder so the uncertainty of the behaviour at the ends should have no effect on the fringe patterns at the centre. This was borne out by experimenting with the boundary conditions at the end of the cylinder.

The variation in wall thickness was modelled by placing shell elements along the centres of the thick and thin sections and then joining these by an angled straight section where the radius occurs on the cylinder, as shown in Figure 4-18. The wall thickness along the angled straight section was varied by interpolating between the wall thicknesses of the thick and thin parts. The mesh was defined specifying that the nodes must lie on a circle with the start and end nodes separate but in the same place. The mesh thus effectively had a split down the length which would open under load. The start and end nodes along this 'split' were thus 'zipped' up using the ABAQUS multi-point constraint 'TIE' to join the start and end nodes.

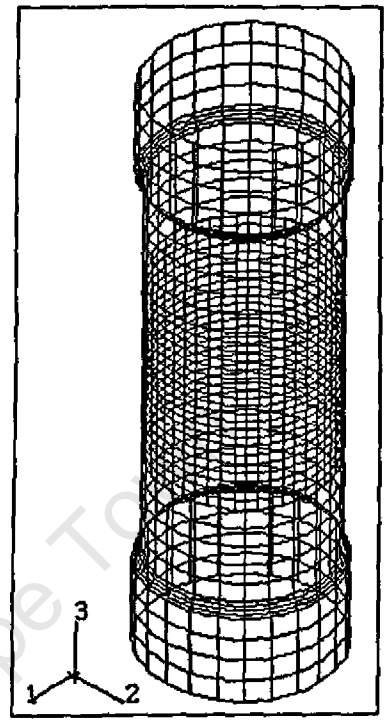

Figure 4-18 Final mesh for the FE model

Line spring elements are implemented by simply defining the nodes making up the element, specifying the depth at each node and defining whether the crack is internal or external. These nodes must be shared by or tied to the edge nodes of the adjacent quadratic shell elements. The thickness of the crack free shell must also be given.

The angled crack could not be implemented in the partially refined mesh shown in Figure 4-18 because the line springs have to

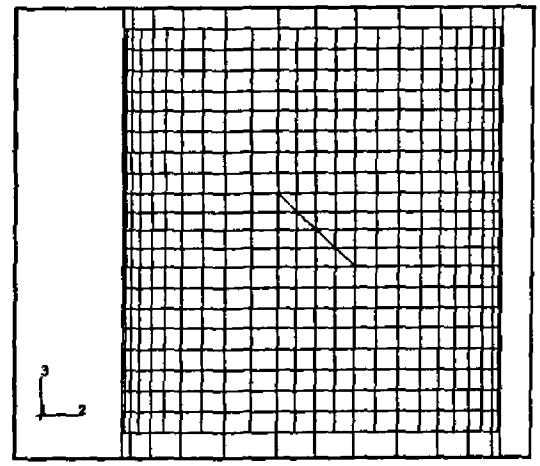

Figure 4-19 Mesh with triangular elements to implement angled crack

run along the edge of elements. The mesh was altered to include a series of triangular quadratic elements (STRI65) in the region where the crack was located as shown in Figure 4-19. STRI65 elements are 6 noded quadratic triangular elements which use reduced integration and five degrees of freedom per node. Although the STRI65 element implements the Kirchoff constraints numerically they may produce inaccurate results in some cases where shear flexibility is important. They are, however, the only 6 noded triangular shell element available in ABAQUS and have been successfully used with line spring elements. The crack free mesh with the triangular elements was compared with the crack free mesh with only rectangular elements to ensure that no numerical errors were introduced by the inclusion of the narrow band of triangles.

To allow the length of the crack to be altered easily without distorting the mesh, the mesh was refined around the crack site. The ABAQUS manual warns against using mesh refinement too close to a discontinuity such as a crack or hole because this can introduce significant errors. The mesh was thus refined over quite a wide area, as shown in Figure 4-18 above. With such a scheme the length of the crack could be compared to the relevant co-ordinate of the element corners. The element corner closest to the crack tip was then defined, as shown in Figure 4-20, so that its co-ordinates coincided with the co-ordinates of the crack tip. The nodes were then generated from the end of the cylinder to the end of the crack, then to the other end of the crack and finally to the other end of the cylinder. This led to the least possible mesh distortion without resorting to extensive re-meshing.

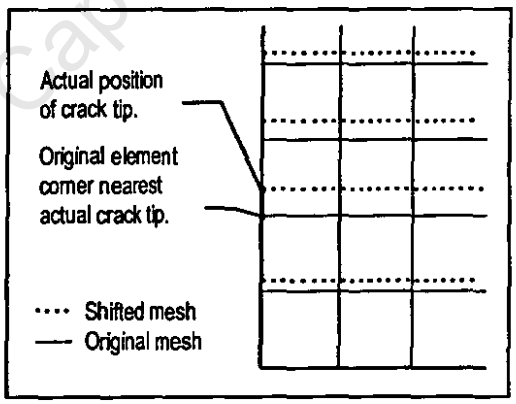

Figure 4-20 Diagram of mesh-shifting technique to locate crack tip.

Once the length of the crack was modelled a 'split' in the mesh had to be created for the line spring crack. This was achieved for the single axial crack by removing the multi-point constraints along the length of the crack, leaving a split. For the other cases the split was achieved by copying the existing nodes along the crack length and placing the copied nodes in the same position as the original nodes. The elements on one side of the crack were then redefined to use the copied nodes instead of sharing the original nodes with the elements on the other side of the crack. A split was thus introduced into the model which was the length of the crack and in the correct position. The line spring element was then defined using the nodes along each side of the split.

ABAQUS imposes a minimum crack depth of 2% of the shell thickness because useful results are not obtained for shallower cracks. If a crack is specified with a depth less than the minimum it is reset to 2% of the depth.

The diameter of the cutter used to introduce the cracks, the depth of the cut, the diameter of the cylinder and the angle of the cut were all known so the depth of the crack could be calculated as a function of position along the crack using a spreadsheet. The depth of the crack could thus be calculated at each node position. The curvature of the cylinder surface affects the depth of the crack for the circumferential and angled cracks. This was taken into account in the depth calculations.

Care was taken to ensure that all elements had an aspect ratio of as close to unity as possible in order to minimise errors due to distorted element shapes. If the surface normals for the elements are not specified in the input deck they are calculated by ABAQUS. The surface normals that ABAQUS calculated for the elements were

checked. They were correct so it proved unnecessary to define the normals explicitly. The ABAQUS input decks are found in Appendix B.

A mesh refinement exercise was performed on the models to determine whether the element size was small enough and to check that no errors were introduced by the mesh refinement around the crack. The partially refined mesh was compared with the fully refined mesh for the crack free cylinder model, the model with a single axial crack and the model containing a single circumferential crack. The element size in the refined areas was half that of the unrefined areas. An example of the comparison is shown in Figure 4-21, which clearly indicates that the partially refined model provides acceptable accuracy. The difference in the results for the two meshes is less than 2% in all cases. The partially refined model provided substantial savings in computer time over the fully refined mesh - of the order of 60% less CPU time was required for the partially refined mesh.

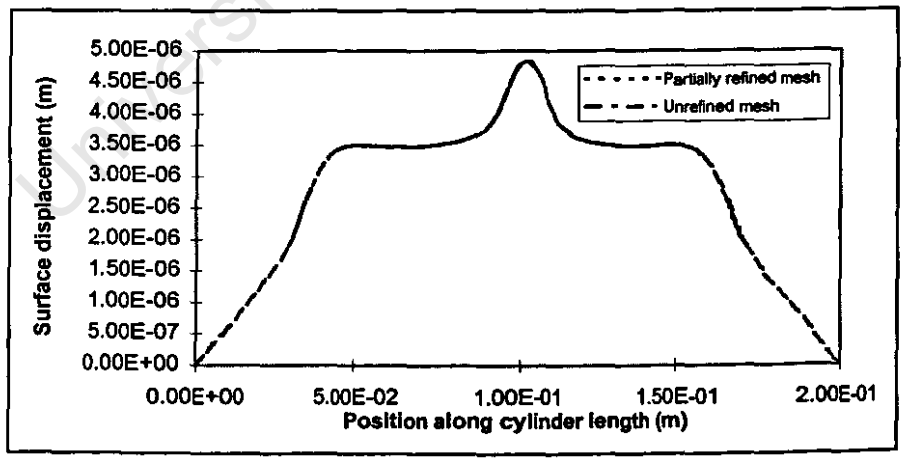

Figure 4-21 Mesh refinement comparison for the Axial crack.

The partially refined model was used for the final comparisons, with alterations to the basic mesh shown in Figure 4-19 being made to include the various crack configurations.

4.4 Analysis and Post Processing

The data provided by the ESPI experiments and that produced by the finite element models requires further processing and analysis before useful comparisons can be made. This section describes the processing of these results to provide the quantitative comparisons.

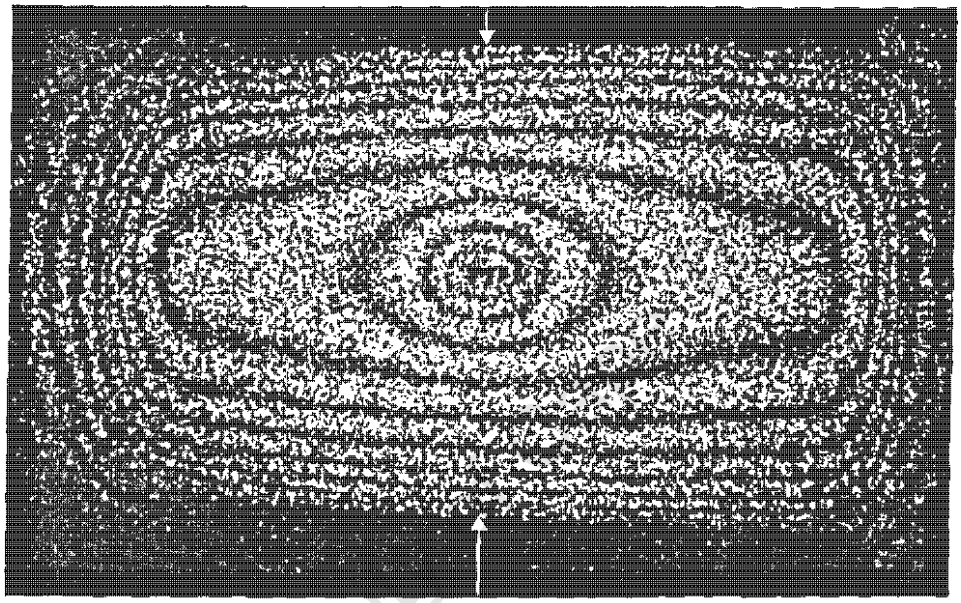

Figure 4-22 Typical interferogram for a cracked cylinder (axial crack at 120psi). The arrows indicate the mid-line.

A typical interferogram for a cylinder with a crack is shown in Figure 4-22. The fringe pattern in such an image can be compared with a similar image produced by FE analysis, but the comparison is limited to a qualitative comparison. The number of fringes can be compared, but the exact position and shape can only really be compared qualitatively. For this investigation it was desirable to have a more reliable comparison. A graph of the out-of-plane displacement profile across the cylinder would provide a good method of comparison of the FE prediction and experimental data. The mid-line of the cylinder (as shown in Figure 4-22) was chosen as the line along which the displacement profile would be plotted. This was the most satisfactory

because the cracks were located across this line, so the profile here would be most affected by the introduction of the crack. The effects of the ends of the cylinder are also at a minimum at the mid-line.

4.4.1 Interferogram Analysis

Once a set of interferograms, consisting of three interferograms for each load for a particular cylinder/crack combination, was complete they were analysed and the data entered on a spreadsheet. The FE data were added to the spreadsheet and the displacement profile plotted. The manual analysis of the interferograms proceeded as follows:

Each interferogram was enhanced using Adobe Photoshop (an image processing package) to enhance the fringe visibility and printed using a laser printer. The diameter of the image on the printed interferogram was then measured. The actual diameter of the cylinder was known, so a scale factor, S, could be calculated where S=(actual diam.)/(image diam.). The position of each fringe could then be measured on the interferogram, and scaled to provide the position on the actual cylinder. The highest fringe number (i.e. the fringe number of the central fringe) was recorded when the interferogram was made, so the fringe number of each visible fringe could be determined. The fringe number was entered in the fringe equation $d = \frac{n \cdot \lambda}{2}$ to give a displacement associated with each fringe position. From these data a plot of displacement vs. fringe position on the cylinder could be plotted.

4.4.2 FE Data Analysis

ABAQUS calculates the displacement and rotations for every node in the model. The post processor can then be used to plot the data or extract the data of interest for any node or group of nodes. The post processor was used to plot contours of the out-of-plane displacement for visual comparison with the ESPI interferograms and to extract the out-of-plane displacement values for the nodes along the mid-line for use in the spreadsheet for comparison with the ESPI data.

4.4.2.1 FE Contour Plots

The ABAQUS post processor is capable of plotting contours of various variables including any component of displacement. The model was arranged so that the x-component of the nodal displacement corresponded to the out-of-plane displacement measured by ESPI, with the crack or crack combination in the centre of the model when viewed along the X axis. The maximum and minimum value for the contour plot can be adjusted along with the number of contours. The maximum out-of-plane displacement was extracted from the FE data. This displacement was substituted into the fringe equation $n = \frac{2 \cdot d}{\lambda}$. The result is the number of fringes that will be visible for the maximum displacement. The number n is truncated because only a whole number of fringes can be seen. This number of fringes is then substituted into the fringe equation $d = \frac{n \cdot \lambda}{2}$ to give the displacement corresponding to the highest fringe number. This result was used as the maximum for the contour plot, the minimum was set to zero and the number of contours to (1+n). ABAQUS provided a contour at zero displacement and counted it as one of the contours, whereas the n obtained is the

number of fringes counted from the first visible fringe, which is at a displacement greater than zero. These calculations were carried out automatically in a MathCad worksheet. Only the maximum displacement needed to be entered and the rest of the calculations were carried out automatically. A spreadsheet could also have been used for this purpose.

The ABAQUS post processor can plot the contour plots either as line plots or as filled colour plots. It was found that filled colour plots were clearer, so these were used for the visual comparisons with the ESPI interferograms. The plots consist of bands of solid colour. The transition between one colour and the next indicates the location of a fringe.

4.4.2.2 Nodal Displacements

A group of nodes was defined which contained all the nodes along the mid-line of the cylinder and which would be visible when observing the cylinder from the front. The post processor was then used to extract the nodal displacements for this group of nodes. The resulting text file was imported into the spreadsheet using a macro. The macro imported the data from the text file, converting it from text to numerical values, stripping the unwanted data and sorting the remaining data so that it could be plotted on the same axes as the ESPI data.

The graphs which were produced in this manner provide a good indication of the accuracy of the finite element model. The results of the investigation are dealt with in the next section.

5. Results and Discussion

The comparisons between the experimental and FE results are briefly presented here. The simulated and actual fringe patterns are shown for each crack configuration at 100 psi (689 kPa). The comparison graphs of out of plane displacement are shown alongside with their corresponding fringe pattern. The complete set of graphs is shown in Appendix C. The results will also be discussed in this section.

Figure 5-1 shows the simulated and actual interferogram for the whole cylinder with a single axial crack at 100 psi (689 kPa). The remaining comparisons show only the centre of the cylinder for greater detail.

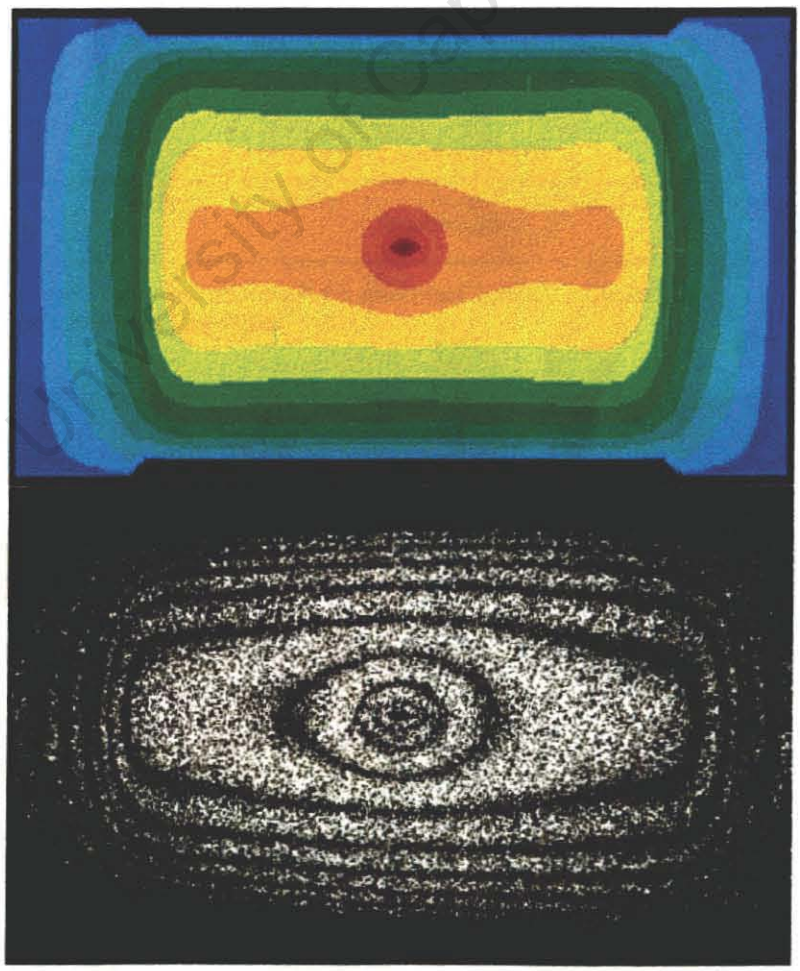

Figure 5-1 Comparison of whole cylinder with axial crack at 100 psi.

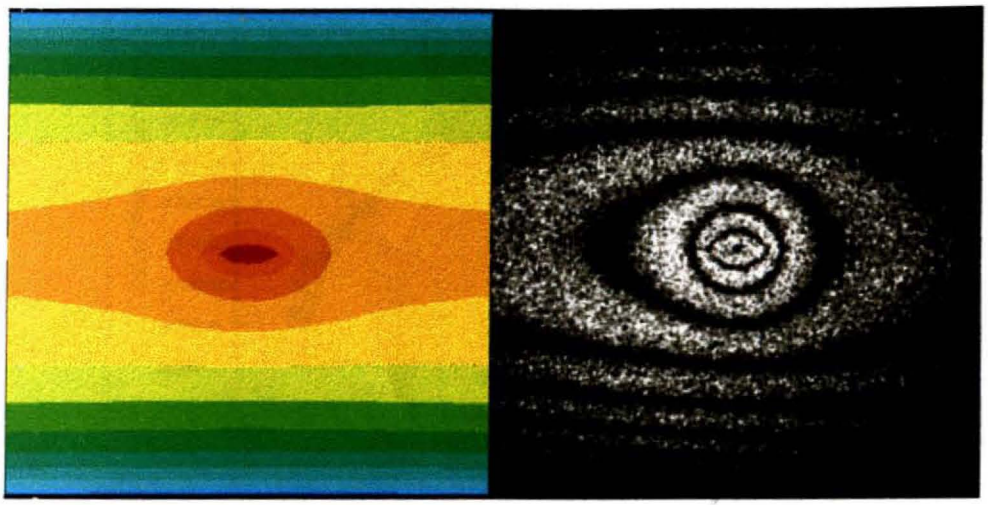

Figure 5-2 Comparison for axial crack at 100 psi

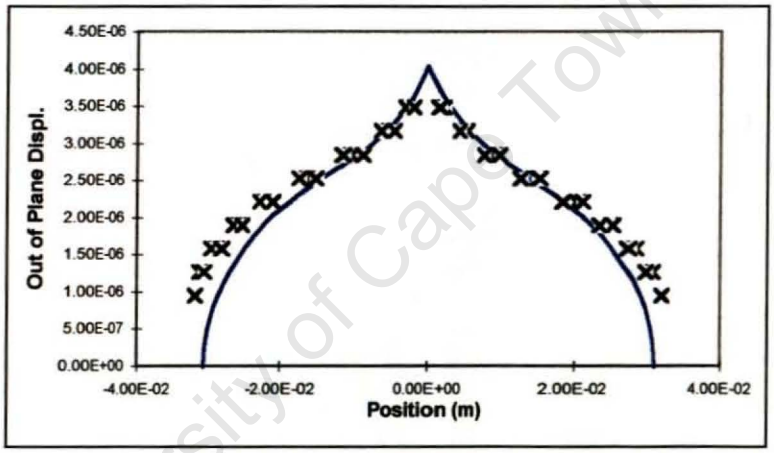

Figure 5-3 Comparison graph for axial crack at 100 psi. The solid line indicates the FE prediction.

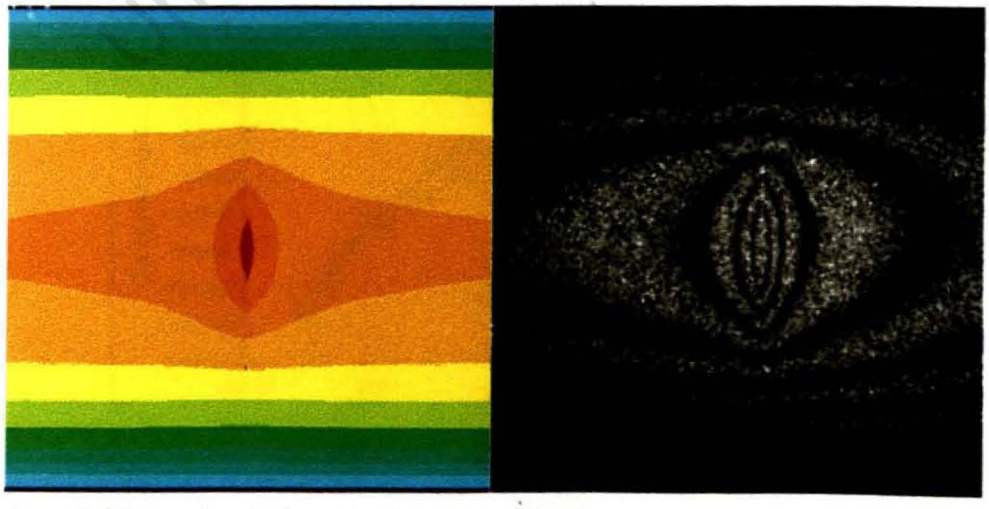

Figure 5-4 Comparison for circumferential crack at 100 psi

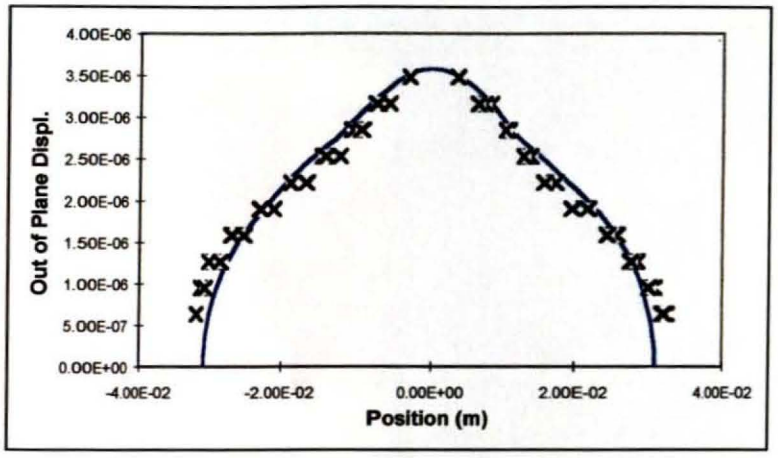

Figure 5-5 Comparison graph for circumferential crack at 100 psi. The solid line indicates the FE prediction.

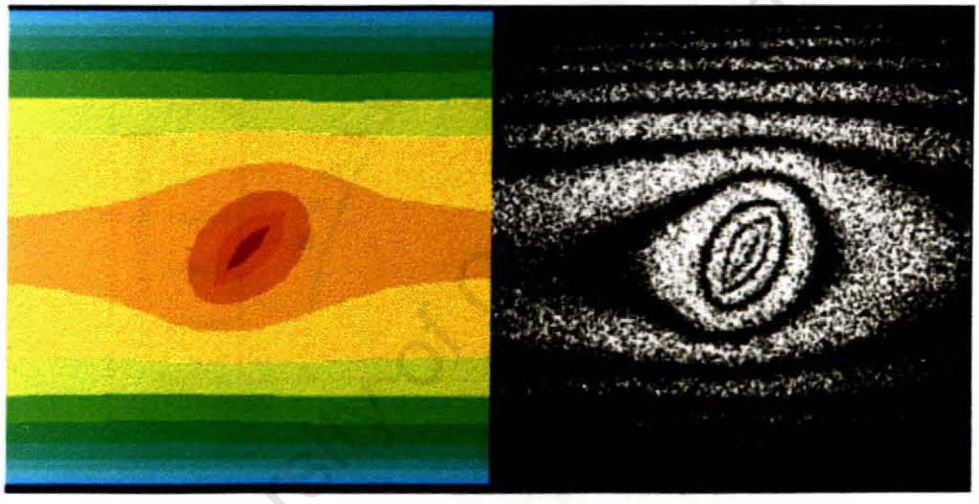

Figure 5-6 Comparison for 45° crack at 100psi

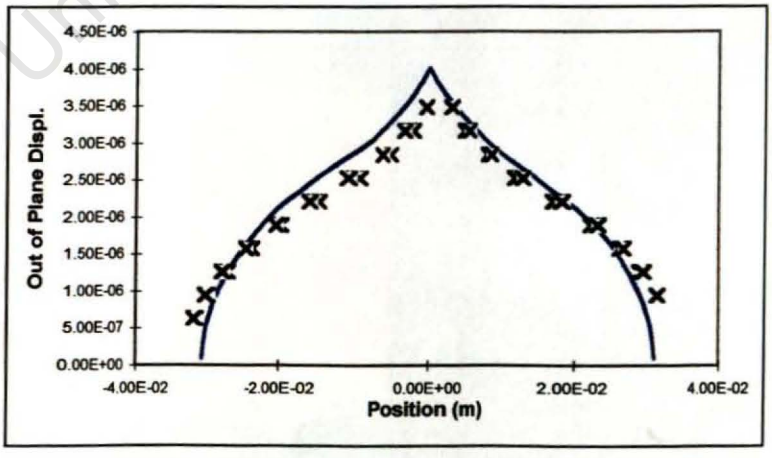

Figure 5-7 Comparison graph for 45° crack at 100 psi. . The solid line indicates the FE prediction.

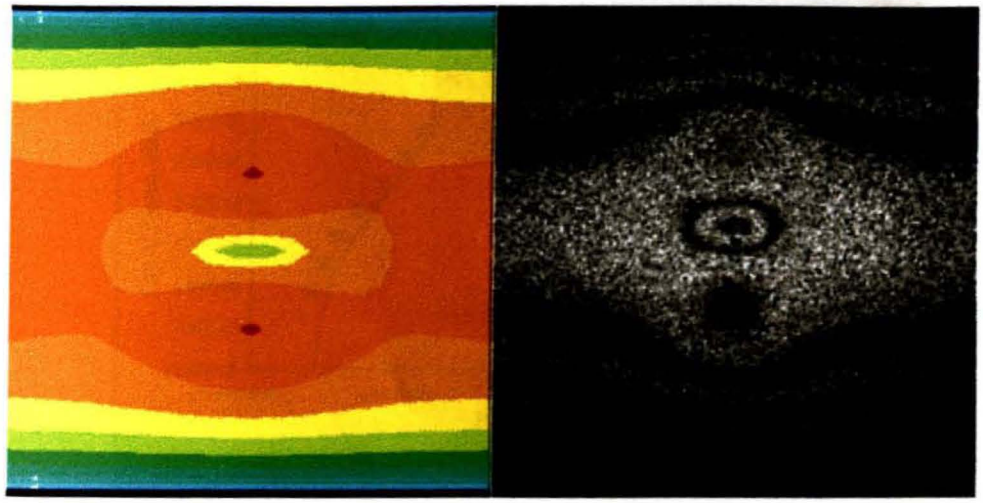

Figure 5-8 Comparison for axial internal crack at 100 psi

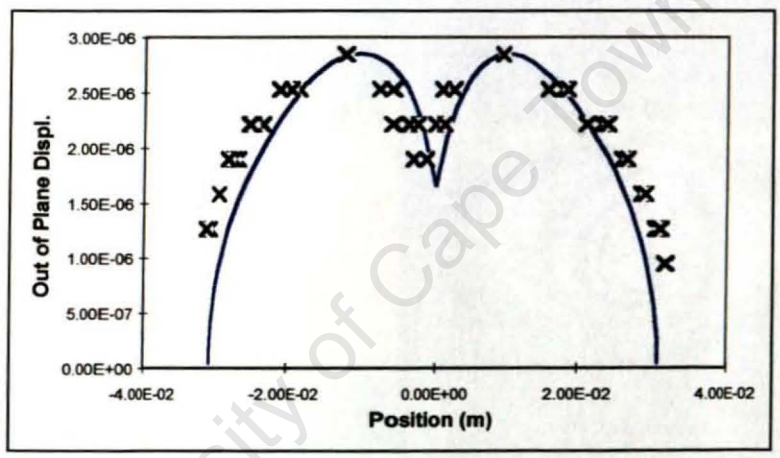

Figure 5-9 Comparison graph for axial internal crack at 100 psi. . The solid line indicates the FE prediction.

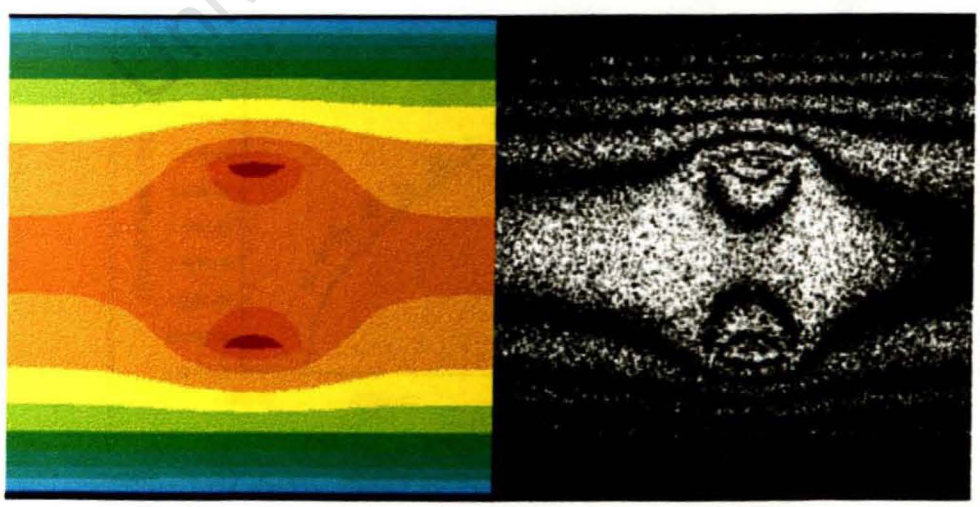

Figure 5-10 Comparison for 2 parallel axial cracks at 100 psi

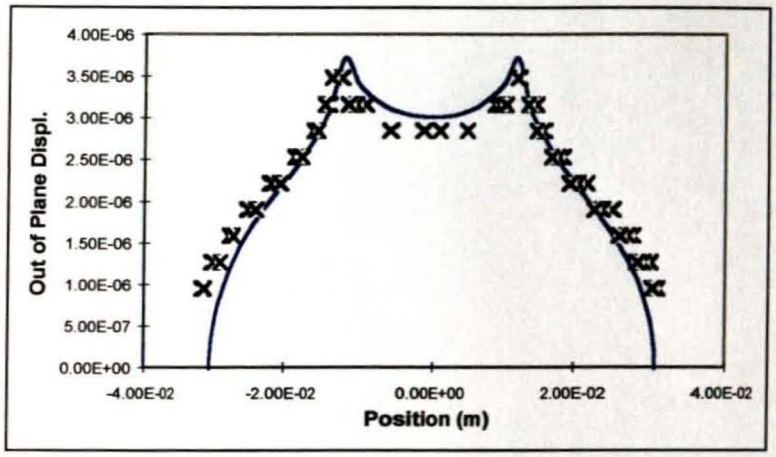

Figure 5-11 Comparison graph for 2 parallel axial cracks at 100 psi. . The solid line indicates the FE prediction.

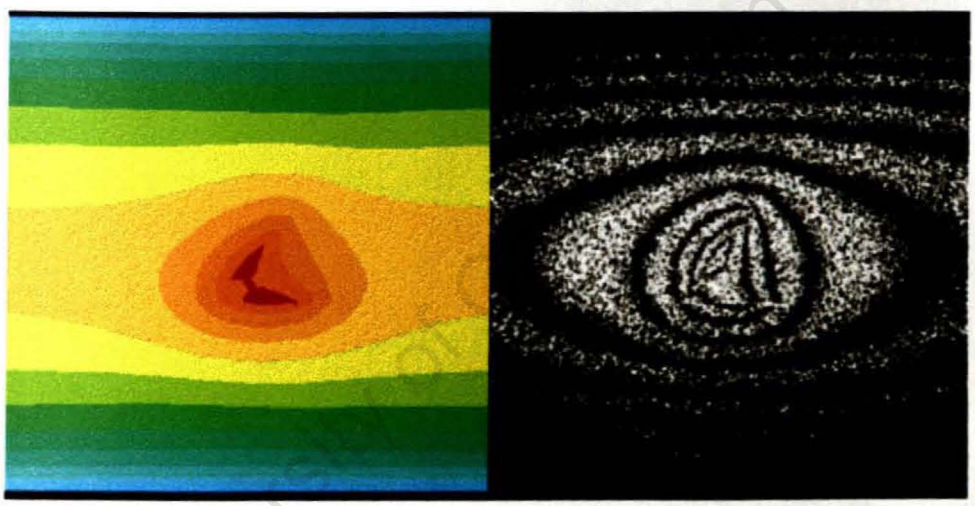

Figure 5-12 Comparison for V-shaped crack at 100 psi

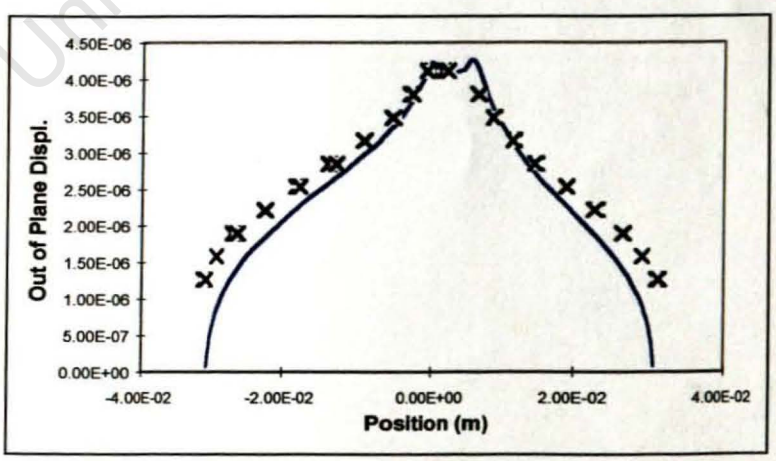

Figure 5-13 Comparison graph for V-shaped crack at 100 psi. . The solid line indicates the FE prediction.

The results show good correlation between the FE and experimental data. The interferograms are matched in general form and fringe number. The number of fringes that formed in the ESPI interferograms was recorded as discussed previously and these were checked against the fringe number predicted by the FE model. The slight difference in shape of the fringes between prediction and experiment can be ascribed to the random effects present in the experimental set-up. The material of the cylinder cannot be expected to be perfectly uniform so the material response will not be perfectly uniform. The jig holding the cylinder during the experiments may also have been subject to very slight movement which would also introduce slight fringe distortion. The end closures with the O-ring and screws along with the pressure inlet and end closure-jig interaction also introduce uncertainties, although small, into the experimental set-up. The scatter of the experimental data obtained from the multiple interferograms, which were used when plotting the graphs, indicates the random nature of these uncertainties. The multiple interferograms give a clearer picture of the 'ideal' system by averaging out the uncertainties.

In every case the experimental data 'flares' slightly outside the FE prediction at the edges of the cylinder regardless of whether the prediction lies above or below the experimental data across the rest of the cylinder. This is accounted for by the nature of the shell finite element model. The shell elements are placed along the centre of the wall thickness when constructing the model, so the displacements predicted by the FE model are the displacements of the centre of the cylinder wall. This does not affect the results where the point of observation is nearly parallel to the cylinder normal, i.e. towards the middle of the cylinder's width, but does introduce a small error at the edges where the viewing angle is almost perpendicular to the tube surface normal. At

the edges of the cylinder the maximum position co-ordinate will thus be larger for the experimental data than for the FE data, introducing this slight 'flare' at the edges. The effect is small and is confined to the edges of the cylinder which are not the areas of primary interest.

To obtain a numerical measure of the accuracy the graphs were analysed to provide an estimate of their accuracy. A best fit line was drawn through the experimental data and the point of worst correlation was chosen for measurement. The difference between the experimentally measured displacement and the FE prediction for that point was measured and converted to a percentage difference from the experimental displacement. This process was followed for each crack configuration and each load. The results are summarised in the following tables. For each crack the pressure value displaying the best correlation and the one displaying the worst correlation are listed along with the mean percentage error and standard deviation for that crack configuration.

Table 5-1 Axial crack results

	Pressure	% error
Best	90 psi	6%
Worst	120 psi	15%
Mean		11.2%
Std. Dev.		3.7%

Table 5-2 Circumferential crack results

	Pressure	% error
Best	90 psi	5.3%
Worst	110 psi	9.3%
Mean		6.6%
Std. Dev.		1.5%

Table 5-3 45° crack results

	Pressure	% error
Best	90 psi	6.6%
Worst	120 psi	14.5%
Mean		10.5%
Std. Dev.		2.9%

Table 5-4 Axial internal crack results

	Pressure	% error
Best	60 psi	8.6%
Worst	110 psi	23.5%
Mean		15.1%
Std. Dev.		6.1%

Table 5-5 Parallel crack results

	Pressure	% error
Best	60 psi	3.4%
Worst	90 psi	7.7%
Mean		6.3%
Std. Dev.		1.5%

Table 5-6 V-shape crack results

	Pressure	% error
Best	70 psi	4.4%
Worst	120 psi	12.5%
Mean		7.7%
Std. Dev.		2.95%

Table 5-7 Overall results summary

	Pressure/ Config	% error
Best	90 psi Parallel	3.4%
Worst	110 psi Internal	23.5%
Mean		9.6%
Std. Dev.		4.5%

The results show a mean error of approximately 10% for the Finite Element predictions of the surface displacement around the crack site. The worst correlation was observed for the internal crack with a maximum error of 23.5%. This large error may have been due to error in applying the load, but the errors for other load values for the internal crack are also quite large, ranging from 10% to 22%. The other crack configurations all show much better correlation. The fact that the poorest correlation is exhibited by the only example of an internal crack that was investigated may indicate a problem with the simulation of internal cracks, but it may also be coincidence. More evidence is required before such a theory can be entertained.

One source of error in this analysis is the use of the simplified fringe equation. The simplified equation assumes that the viewing and illumination points are coincident and normal to a flat object. Neither of these assumptions could be satisfied in practice due to the nature of the object and the experimental equipment. The viewing and illumination angles were minimised to reduce this source of error as far as possible.

There are errors present in the finite element data due to the nature of finite element analysis - it is an approximate technique. The line spring elements, in particular, are approximate. They make use of a linear elastic fracture mechanics equation, which is an approximation, to model the compliance of an edge notched specimen in tension and bending. The element uses the resulting value for the compliance in the shell model of the cracked specimen. The values for the material properties used in the FE model are also a possible cause of error. The literature gives a range of values for any particular alloy which introduces some uncertainty in the appropriate value for the cylinders used in this investigation. This uncertainty was, however, minimised by the calibration procedure that was adopted.

Based on the sample results shown here and those appearing in Appendix C, the assumptions used and the approximations made in the finite element analysis have been proven valid without over-simplifying the physical situation.

6. Conclusions

The results obtained in this investigation show that the shell - line spring model is a satisfactory method of modelling the displacements and fringe patterns of external cracks in pressure vessels.

The simplicity of the model and the ease with which the crack can be moved and altered coupled with the accuracy demonstrated in the investigation make the finite element model a viable tool when investigating the relationship between crack geometry and fringe patterns.

The poor correlation observed for the internal crack may indicate that the line spring model is inaccurate when used for internal cracks. The general fringe pattern and displacement profile were, however, similar to the experimentally observed patterns. The model does show promise for simulating internal cracks, but more data are required to draw useful conclusions.

The problems encountered in ensuring the stability of the cylinders shows that the model may be limited in its applicability to determining crack size from experimental fringe patterns. The difficulties illustrated the uncertainties that can be encountered when securing a vessel for observation. The uncertainty makes it difficult to determine whether a fringe pattern is the result of a flaw or body motion when it is not known what flaws do or do not exist. It may therefore be impossible to match the FE fringe pattern to the experimental because of the uncertainties in the boundary conditions.

The FE model may be useful in predicting the smallest flaw detectable by ESPI at any given load. This could be helpful when testing pressure vessels and attempting to

predict residual life. If the maximum acceptable flaw size is known then the load level for the test can be set so that if no flaws are observed then it is known that any flaws that do exist are below the critical size.

7. Recommendations

The following recommendations are made based on the findings and conclusions of the investigation:

1. The line spring model should be evaluated further for internal cracks and crack combinations to determine if it is a sufficiently accurate method of simulating internal cracks.

2. A reliable system of securing pressure vessels and other objects for observation by ESPI should be investigated and developed. Such a system could be developed either for use on the optical table or off the table.

3. Actual cracks should be 'grown' in a controlled specimen using fracture mechanics methods to allow the model to be tested with a very 'sharp' crack. There would be some uncertainty in the crack profile for these experiments, but if they are carefully controlled the investigation should provide useful information on the potential of the FE model.

8. References

ASM Handbook (1989) (various authors) — *ASM Handbook vol. 17: Non-destructive Evaluation and Quality Control*, American Society for Metals, 1989

Cordes, J, Yazici, R & Seo, M (1993) — 'Mixed-mode Fracture in Plastically Deforming Materials' , *Journal of Pressure Vessel Technology*, Trans. ASME, v115 p348-52, November 1993

Deng, X, Rosakis, AJ — 'Dynamic crack propagation in elastic perfectly plastic solids under plane stress conditions', *J. Mech. Phys. Solids*, v39 p683-722, 1991

Ewalds, HL & Wanhill, RJH (1989) — *Fracture Mechanics*, Edward Arnold (Hodder and Stoughton), London, 1989

Gensheimer, VM & Packman, PF (1988) — 'Variation in Stress-Intensity Factor and Back-Surface Displacement for Surface Cracks' , *Experimental Mechanics*, v28 p182-7, June 1988

Hearn, EJ (1985) — *Mechanics of Materials, Vol. 1*, Pergamon Press, Oxford, 1985

Hibbitt, Karlsson & Sorenson — *ABAQUS ver. 5.3 Manuals*, Providence,

Rhode Island, USA.

Hulett, C & Penny, RK (1992) 'Interferometric patterns at discontinuities in pressurised cylindrical shells' , *Proc. 11th Symposium on Finite Element Methods in South Africa (FEMSA '92),* Cape Town, January 1992

Jones, R & Wykes, C (1983) *Holographic and Speckle Interferometry,* Cambridge University Press, Cambridge, 1983

Kaufmann, GH, Lopergolo, AM & Idelsohn, SR (1987) 'Evaluation of finite-element calculations in a part-circular crack by coherent optical techniques' , *Experimental Mechanics*, v27 p154-7, June 1987

Kumar, V, German, MD, Schumacher, BI (1985) 'Analysis of Elastic Surface Cracks Using the Line Spring Model and Shell Finite Element Method' , *Journal of Pressure Vessel Technology*, Trans. ASME, v107 p403-11, November 1985

Kwon, YW 'Analysis of Composite Plates containing Cracks', *Journal of Pressure Vessel Technology,* v114 p358-363, August 1992

Maji, AK & Shah, SP (1990) 'Measurement of Mixed-mode Crack Profiles by Holographic Interferometry' , *Experimental Mechanics*, v30 p201-7, June 1990

Malan, SF and Paterson, AE (1987) *Introduction to Aluminium*, Aluminium Federation of South Africa, 1987

Miller, RA, Shah, SP, Bjelkhagen, HI 'Crack Profiles in Mortar Measured by Holographic Interferometry' , *Experimental Mechanics*, v28 p388-394, December 1988

Miyoshi, T, Shiratori, & Yoshida, Y (1986) 'Analysis of J-integral and Crack Growth for Surface Cracks by Line Spring Method' , *Journal of Pressure Vessel Technology*, Trans. ASME, v108 p305-11 August 1986

Parks, DM & White, CS (1982) 'Elastic-Plastic Line-Spring Finite Elements for Surface-Cracked Plates and Shells' , *Journal of Pressure Vessel Technology*, Trans. ASME, v104 p287-92, November 1982

Penny, RK & Gryzagoridis, J. (1994) 'Holographic NDE in pressure vessels and piping' , *International Journal of*

Pressure Vessels and Piping, v58 (1994) p223-30

Raju, IS & Newman, JC (1982) 'Stress Intensity Factors for Internal and External Cracks in Cylindrical Vessels' , *Journal of Pressure Vessel Technology*, Trans. ASME, 104, p293-8 (1982)

Ratnam, MM & Evans, WT (1993) 'Comparison of Measurement of Piston Deformation Using Holographic Interferometry and Finite Elements' , *Experimental Mechanics*, v33 p336-42, December 1993.

Rice, JR & Levy, N (1972) 'The Part-through Surface Crack in an Elastic Plate' , *Journal of Applied Mechanics*, Trans. ASME, p185-94, March 1972

9. Bibliography

Caulfield, JH (1984) 'The wonder of Holography' , *National Geographic*, v165 no.3 p 364-77, March 1984

Garza, R & Sharp, B (1987) 'Holographic Interferometry: A Primer' , *Automotive Engineering*, p69-72, August 1987

Hemmick, TK, Huang, JW, Song, YD 'Holographic detection of defects under the surface of solid objects', *American Journal of Physics*, v51 p984-987, November 1983

Klisinski, M, Runesson, K, Sture, S (1991) 'Finite Element with Inner Softening Band' , *Journal of Engineering Mechanics*, v117 no 3 p575-87, March 1991

Li, QB & Chiang, FP (1988) 'Studies of Holospeckle Interferometry', *Optical Engineering*, v27 no. 3 p200-6, March 1988

Miller, RA, Castro-Montero, A, Shah, SP 'Use of Laser Holographic Interferometry and Image Analysis for the study of Fracture Specimens', *Experimental Techniques*, v15 p14-18, May/June 1991

Rubayi, NA, Liew, SH — 'Vacuum Stressing Techniques for Composite Laminates Inspection by Optical Methods', *Experimental Techniques,* v13 p17-20, March 1989

Sih, GC — *Mechanics of Fracture 3: Plates and shells with cracks*, Noordhof International Publishing, Leyden, 1977

Simonen, FA — 'The impact of NDE Unreliability on Pressure Vessel Fracture Predictions' , *Journal of Pressure Vessel Technology,* Trans. ASME, v108 p18-24, February 1985

Stetson, KA — 'The origins of Hologram Interferometry', *Experimental Techniques*, v15 p15-18, March/April 1991

Tada, H — *The Stress Analysis of Cracks Handbook*, Del Research Company, Hellertown, Pa, 1973

Timoshenko and Woinowsky-Krieger — *Theory of Plates and Shells*, Mcgraw Hill, New York, 1959

Timoshenko, S — *Strength of Materials part II*, van

Nostrand, New York, 1941

Wang, YY, Chen, DJ, Chiang, FP — 'Material testing by Computer Aided Speckle Interferometry', *Experimental Techniques*, v17 p30-32, September/October 1993

Zienkiewicz & Taylor — *The Finite Element Method*, vol.2, McGraw Hill, 1991

Appendix A - Supplementary Pictures and Diagrams

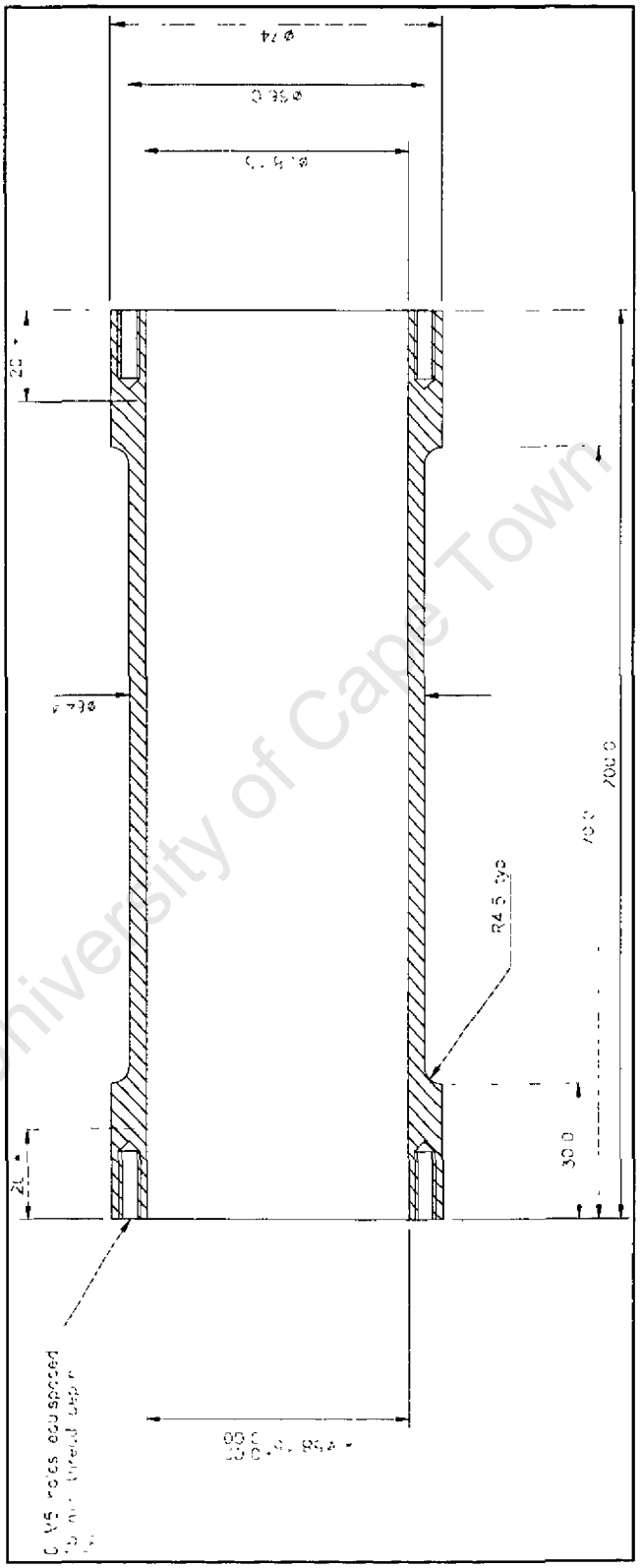

Figure 1 Diagram of cylinder design

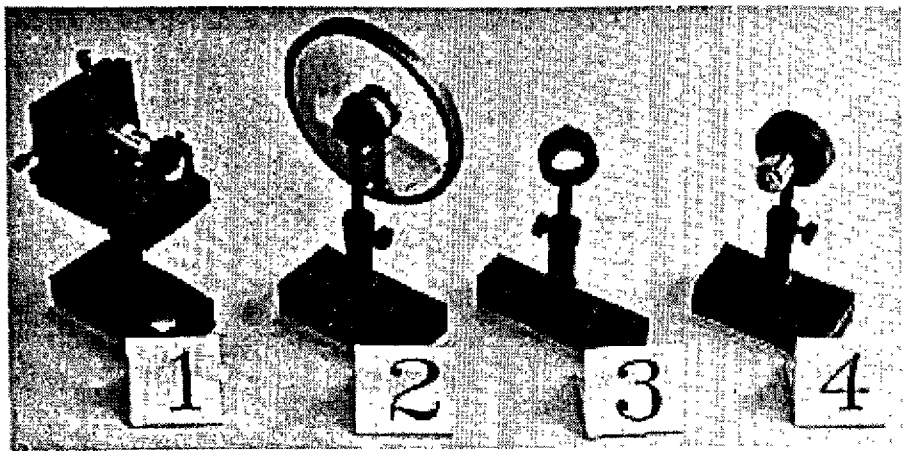

Figure 2 Optical components. 1. Spatial Filter 2. Variable beam splitter 3. Beam splitter 4. Conventional beam splitter

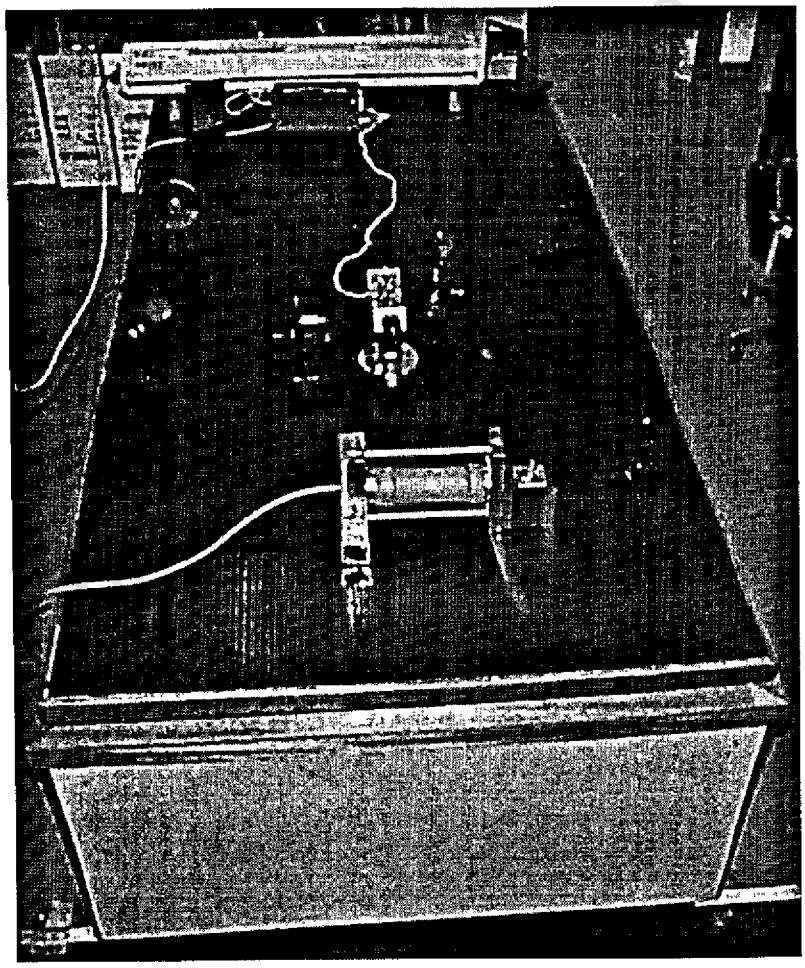

Figure 3 Vibration isolation table used for experiments

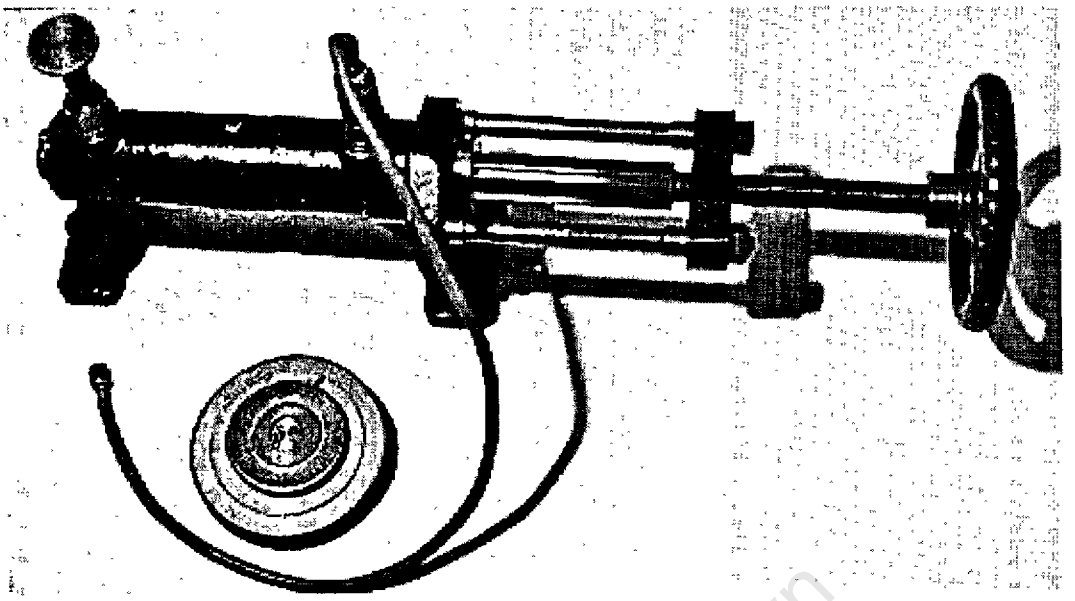

Figure 4 Dead weight tester

Appendix B - ABAQUS Input Decks

Axial Crack

```
*HEADING
LARGE CYLINDER, MACHINED FROM SOLID, partially refined
74 mm max OD, modelling whole cylinder
SINGLE AXIAL CRACK, 1.5mm DEEP
**
**
**-------------------------------------------------------------
**                  Define corner nodes of SHELL
**
*NODE
10,  0.033, 0., 0.
202,  0.033, 0., 0.
394, 0.033, 0., 0.
**
6410,  0.033, 0., 0.030
6602,  0.033, 0., 0.030
6794, 0.033, 0., 0.030
**
12810, 0.0305, 0., 0.0345
13002, 0.0305, 0., 0.0345
13194, 0.0305, 0., 0.0345
**
44810,  0.0305, 0., 0.1655
45002,  0.0305, 0., 0.1655
45194, 0.0305, 0., 0.1655
**
51210,  0.033, 0., 0.170
51402,  0.033, 0., 0.170
51594, 0.033, 0., 0.170
**
57610,  0.033, 0., 0.200
57802,  0.033, 0., 0.200
57994, 0.033, 0., 0.200
**
**
**---------CRACK DATA-------
26410,  0.0305, 0., 0.0914706
26794,  0.0305, 0., 0.0914706
**
31210,  0.0305, 0., 0.1085294
31594,  0.0305, 0., 0.1085294
**
*NGEN, LINE=C, NSET=BOTCRK
26410, 26794, 4, , 0., 0., 0.0914706, 0., 0., 1.
*NGEN, LINE=C, NSET=TOPCRK
31210, 31594, 4, , 0., 0., 0.1085294, 0., 0., 1.
**---------END CRACK--------
**
**
**-------------------------------------------------------------
**
**   Generate the shell nodes using node sets and node filling
```

```
**
*NGEN, LINE=C, NSET=BOTT
10, 394, 4, , 0., 0., 0., 0., 0., 1.
*NGEN, LINE=C, NSET=ENDTHCK
6410, 6794, 4, , 0., 0., 0.030, 0., 0., 1.
*NGEN, LINE=C, NSET=STRTTHN
12810, 13194, 4, , 0., 0., 0.0345, 0., 0., 1.
*NGEN, LINE=C, NSET=B_RAD
44810, 45194, 4, , 0., 0., 0.1655, 0., 0., 1.
*NGEN, LINE=C, NSET=TOP_RAD
51210, 51594, 4, , 0., 0., 0.170, 0., 0., 1.
*NGEN, LINE=C, NSET=TOP
57610, 57994, 4, , 0., 0., 0.200, 0., 0., 1.
**
**          Generate shell wall for thick bottom end
**
*NFILL, NSET=THICK1
BOTT, ENDTHCK, 16, 400
**
**          Generate shell wall for first radius
**
*NFILL, NSET=RAD1
ENDTHCK, STRTTHN, 16, 400
**
**          Generate shell wall for main body
**
**--------CRACK DATA--------
*NFILL, NSET=WALL
STRTTHN, BOTCRK, 34, 400
BOTCRK, TOPCRK, 12, 400
TOPCRK, B_RAD, 34, 400
**--------END CRACK---------
**
**           Generate shell wall for second radius
**
*NFILL, NSET=RAD2
B_RAD, TOP_RAD, 16, 400
**
**          Generate shell wall for thickened top end
**
*NFILL, NSET=THICK2
TOP_RAD, TOP, 16, 400
**
**
**------------------------------------------------------------
**                Define master element for SHELL
**
*ELEMENT, TYPE=S8R
1,  10, 26, 1626, 1610, 18, 826, 1618, 810
400, 6410, 6426, 8026, 8010, 6418, 7226, 8018, 7210
800, 12810, 12826, 14426, 14410, 12818, 13626, 14418, 13610
1280, 20810, 20818, 21618, 21610, 20814, 21218, 21614, 21210
2240, 36810, 36826, 38426, 38410, 36818, 37626, 38418, 37610
3000, 44810, 44826, 46426, 46410, 44818, 45626, 46418, 45610
3400, 51210, 51226, 52826, 52810, 51218, 52026, 52818, 52010
**
**------------------------------------------------------------
**
```

```
**    Generate the other elements using the master elements
**
*ELGEN, ELSET=THICK1
1, 24, 16, 1,  4, 1600, 24
**
*ELGEN, ELSET=RAD1_1
400, 24, 16, 1
*ELCOPY,ELEMENTSHIFT=24,OLDSET=RAD1_1,SHIFTNODES=1600,NEWSET=RAD1_2
*ELCOPY,ELEMENTSHIFT=24,OLDSET=RAD1_2,SHIFTNODES=1600,NEWSET=RAD1_3
*ELCOPY,ELEMENTSHIFT=24,OLDSET=RAD1_3,SHIFTNODES=1600,NEWSET=RAD1_4
**
*ELGEN, ELSET=THIN
800,  24, 16, 1, 5, 1600, 24
1280,  48, 8, 1,  20, 800, 48
2240, 24, 16, 1, 5, 1600, 24
**
*ELGEN, ELSET=RAD2_1
3000, 24, 16, 1
*ELCOPY,ELEMENTSHIFT=24,OLDSET=RAD2_1,SHIFTNODES=1600,NEWSET=RAD2_2
*ELCOPY,ELEMENTSHIFT=24,OLDSET=RAD2_2,SHIFTNODES=1600,NEWSET=RAD2_3
*ELCOPY,ELEMENTSHIFT=24,OLDSET=RAD2_3,SHIFTNODES=1600,NEWSET=RAD2_4
**
*ELGEN, ELSET=THICK2
3400, 24, 16, 1,  4, 1600, 24
**
**
*ELSET, ELSET=CYLIN
THICK1, RAD1_1, RAD1_2, RAD1_3, RAD1_4
THIN, RAD2_1, RAD2_2, RAD2_3, RAD2_4, THICK2
**
**------------------------------------------------------------
**
**          Define the boundary conditions and MPC's
**
**
**
**     Define node sets for zipping up mesh
**
*NSET, NSET=JOIN1, GENERATE
10, 20810, 800
20810, 26010, 400
31610, 36810, 400
36810, 57610, 800
*NSET, NSET=JOIN2, GENERATE
394, 21194, 800
21194, 26394, 400
31994, 37194, 400
37194, 57994, 800
**
**
**     Define node sets for tying refined mesh
**
*NSET, NSET=PB1, GENERATE
20814, 21182, 16
*NSET, NSET=AB, GENERATE
20810, 21178, 16
*NSET, NSET=BB, GENERATE
20818, 21186, 16
```

```
*NSET, NSET=CB, GENERATE
20826, 21194, 16
*NSET, NSET=PB2, GENERATE
20822, 21190, 16
**
*NSET, NSET=PT1, GENERATE
36814, 37182, 16
*NSET, NSET=AT, GENERATE
36810, 37178, 16
*NSET, NSET=BT, GENERATE
36818, 37186, 16
*NSET, NSET=CT, GENERATE
36826, 37194, 16
*NSET, NSET=PT2, GENERATE
36822, 37190, 16
**
*MPC
QUADRATIC, PB1, AB, BB, CB
QUADRATIC, PB2, AB, BB, CB
QUADRATIC, PT1, AT, BT, CT
QUADRATIC, PT2, AT, BT, CT
TIE, JOIN1, JOIN2
**
*NSET, NSET=BTML1, GENERATE
10, 394, 8
*NSET, NSET=BTML2, GENERATE
810, 1194, 16
*NSET, NSET=BTML3, GENERATE
1610, 1994, 8
*NSET, NSET=BTML4, GENERATE
2410, 2794, 16
*NSET, NSET=BTML5, GENERATE
3210, 3594, 8
**
*NSET, NSET=BTM
BTML1, BTML2, BTML3, BTML4, BTML5
**
*NSET, NSET=TPL1, GENERATE
57610, 57994, 8
*NSET, NSET=TPL2, GENERATE
56810, 57194, 16
*NSET, NSET=TPL3, GENERATE
56010, 56394, 8
*NSET, NSET=TPL4, GENERATE
55210, 55594, 16
*NSET, NSET=TPL5, GENERATE
54410, 54794, 8
**
*NSET, NSET=TP
TPL1, TPL2, TPL3, TPL4, TPL5
**
*BOUNDARY
BTML1, 1
BTML1, 2
BTML1, 3
BTML1, 4
BTML1, 5
BTML1, 6
```

```
TPL1, 1
TPL1, 2
TPL1, 3
TPL1, 4
TPL1, 5
TPL1, 6
**
*NSET, NSET=PLOT, GENERATE
10, 20810, 800
20810, 36810, 400
36810, 57610, 800
*NSET, NSET=MIDSEC, GENERATE
28810, 29194, 4
*NSET, NSET=PLOT2, GENERATE
28810, 28906, 4
29098, 29194, 4
**
**------------------------------------------------------------
**
**------------------------------------------------------------
**
**         Define the material properties
**
*SHELL SECTION, ELSET=THIN, MATERIAL=ALUM
0.003
*SHELL SECTION, ELSET=RAD2_1, MATERIAL=ALUM
0.004
*SHELL SECTION, ELSET=RAD1_4, MATERIAL=ALUM
0.004
*SHELL SECTION, ELSET=RAD2_2, MATERIAL=ALUM
0.005
*SHELL SECTION, ELSET=RAD1_3, MATERIAL=ALUM
0.005
*SHELL SECTION, ELSET=RAD2_3, MATERIAL=ALUM
0.006
*SHELL SECTION, ELSET=RAD1_2, MATERIAL=ALUM
0.006
*SHELL SECTION, ELSET=RAD2_4, MATERIAL=ALUM
0.007
*SHELL SECTION, ELSET=RAD1_1, MATERIAL=ALUM
0.007
*SHELL SECTION, ELSET=THICK1, MATERIAL=ALUM
0.008
*SHELL SECTION, ELSET=THICK2, MATERIAL=ALUM
0.008
**
*MATERIAL, NAME=ALUM
*ELASTIC
70.E9,  0.3
**
**------------------------------------------------------------
**
**
**                      CRACK DATA
**     NB: change JOIN nset if crack length changes
**
*ELEMENT, TYPE=LS6, ELSET=ACRACK
10000, 31594, 31194, 30794, 31210, 30810, 30410
```

```
10001, 30794, 30394, 29994, 30410, 30010, 29610
10002, 29994, 29594, 29194, 29610, 29210, 28810
10003, 29194, 28794, 28394, 28810, 28410, 28010
10004, 28394, 27994, 27594, 28010, 27610, 27210
10005, 27594, 27194, 26794, 27210, 26810, 26410
**
*SURFACE FLAW, SIDE=POSITIVE
31594, 0.0
31194, 0.467643E-3
30794, 0.843868E-3
30394, 1.134374E-3
29994, 1.338164E-3
29594, 1.459639E-3
29194, 1.5E-3
28794, 1.459639E-3
28394, 1.338164E-3
27994, 1.134374E-3
27594, 0.843868E-3
27194, 0.467643E-3
26794, 0.0
**
*SHELL SECTION, ELSET=ACRACK, MATERIAL=ALUM
0.003
**
************************************************************
**              Define analysis type and loading
************************************************************
**
*STEP
*STATIC
**
**------------------------------------------------------------
**
**     Define the distributed load, NB load per unit area
**
*DLOAD
CYLIN, P, 689475.73
**------------------------------------------------------------
**
*NODE PRINT, NSET=PLOT
U1
*RESTART, WRITE
**
*END STEP
**
**
**                   End of Analysis
```

Circumferential Crack

```
*HEADING
LARGE CYLINDER, MACHINED FROM SOLID, partially refined
74 mm max OD, modelling whole cylinder
CIRCUMFERENTIAL CRACK
**
**
**------------------------------------------------------------
```

```
**                Define corner nodes of SHELL
**
*NODE
10,  0.033, 0., 0.
202,  0.033, 0., 0.
394, 0.033, 0., 0.
**
6410,  0.033, 0., 0.030
6602,  0.033, 0., 0.030
6794, 0.033, 0., 0.030
**
12810, 0.0305, 0., 0.0345
13002, 0.0305, 0., 0.0345
13194, 0.0305, 0., 0.0345
**
44810,  0.0305, 0., 0.1655
45002,  0.0305, 0., 0.1655
45194, 0.0305, 0., 0.1655
**
51210,  0.033, 0., 0.170
51402,  0.033, 0., 0.170
51594, 0.033, 0., 0.170
**
57610,  0.033, 0., 0.200
57802,  0.033, 0., 0.200
57994, 0.033, 0., 0.200
**
**-------------------------------------------------------------
**
**   Generate the shell nodes using node sets and node filling
**
*NGEN, LINE=C, NSET=BOTT
10, 394, 4, , 0., 0., 0., 0., 0., 1.
*NGEN, LINE=C, NSET=ENDTHCK
6410, 6794, 4, , 0., 0., 0.030, 0., 0., 1.
*NGEN, LINE=C, NSET=STRTTHN
12810, 13194, 4, , 0., 0., 0.0345, 0., 0., 1.
*NGEN, LINE=C, NSET=B_RAD
44810, 45194, 4, , 0., 0., 0.1655, 0., 0., 1.
*NGEN, LINE=C, NSET=TOP_RAD
51210, 51594, 4, , 0., 0., 0.170, 0., 0., 1.
*NGEN, LINE=C, NSET=TOP
57610, 57994, 4, , 0., 0., 0.200, 0., 0., 1.
**
**----------CRACK DATA------
*NODE
34, 0.030268552491, 0.0131459016393, 0.
370, 0.030268552491, -0.0131459016393, 0.
**
6434, 0.030268552491, 0.0131459016393, 0.030
6770, 0.030268552491, -0.0131459016393, 0.030
**
12834, 0.0279754803355, 0.01215, 0.0345
13170, 0.0279754803355, -0.01215, 0.0345
**
44834, 0.0279754803355, 0.01215, 0.1655
45170, 0.0279754803355, -0.01215, 0.1655
**
```

```
51234, 0.030268552491, 0.0131459016393, 0.170
51570, 0.030268552491, -0.0131459016393, 0.170
**
57634, 0.030268552491, 0.0131459016393, 0.200
57970, 0.030268552491, -0.0131459016393, 0.200
**
**----------END CRACK---------
**
**          Generate shell wall for thick bottom end
**
*NFILL, NSET=THICK1
BOTT, ENDTHCK, 16, 400
**
**          Generate shell wall for first radius
**
*NFILL, NSET=RAD1
ENDTHCK, STRTTHN, 16, 400
**
**          Generate shell wall for main body
**
*NFILL, NSET=WALL
STRTTHN, B_RAD, 80, 400
**
**           Generate shell wall for second radius
**
*NFILL, NSET=RAD2
B_RAD, TOP_RAD, 16, 400
**
**          Generate shell wall for thickened top end
**
*NFILL, NSET=THICK2
TOP_RAD, TOP, 16, 400
**
**
**-------------------------------------------------------------
**              Define master element for SHELL
**
*ELEMENT, TYPE=S8R
1,  10, 26, 1626, 1610, 18, 826, 1618, 810
400, 6410, 6426, 8026, 8010, 6418, 7226, 8018, 7210
800, 12810, 12826, 14426, 14410, 12818, 13626, 14418, 13610
1280, 20810, 20818, 21618, 21610, 20814, 21218, 21614, 21210
2240, 36810, 36826, 38426, 38410, 36818, 37626, 38418, 37610
3000, 44810, 44826, 46426, 46410, 44818, 45626, 46418, 45610
3400, 51210, 51226, 52826, 52810, 51218, 52026, 52818, 52010
**
**-------------------------------------------------------------
**
**    Generate the other elements using the master elements
**
*ELGEN, ELSET=THICK1
1, 24, 16, 1,  4, 1600, 24
**
*ELGEN, ELSET=RAD1_1
400, 24, 16, 1
*ELCOPY,ELEMENTSHIFT=24,OLDSET=RAD1_1,SHIFTNODES=1600,NEWSET=RAD1_2
*ELCOPY,ELEMENTSHIFT=24,OLDSET=RAD1_2,SHIFTNODES=1600,NEWSET=RAD1_3
*ELCOPY,ELEMENTSHIFT=24,OLDSET=RAD1_3,SHIFTNODES=1600,NEWSET=RAD1_4
```

```
**
*ELGEN, ELSET=THIN
800,  24, 16, 1, 5, 1600, 24
1280,  48, 8, 1,  20, 800, 48
2240, 24, 16, 1, 5, 1600, 24
**
*ELGEN, ELSET=RAD2_1
3000, 24, 16, 1
*ELCOPY,ELEMENTSHIFT=24,OLDSET=RAD2_1,SHIFTNODES=1600,NEWSET=RAD2_2
*ELCOPY,ELEMENTSHIFT=24,OLDSET=RAD2_2,SHIFTNODES=1600,NEWSET=RAD2_3
*ELCOPY,ELEMENTSHIFT=24,OLDSET=RAD2_3,SHIFTNODES=1600,NEWSET=RAD2_4
**
*ELGEN, ELSET=THICK2
3400, 24, 16, 1,  4, 1600, 24
**
**
*ELSET, ELSET=CYLIN
THICK1, RAD1_1, RAD1_2, RAD1_3, RAD1_4
THIN, RAD2_1, RAD2_2, RAD2_3, RAD2_4, THICK2
**
**-------------------------------------------------------------
**
**          Define the boundary conditions and MPC's
**
**
**
**     Define node sets for zipping up mesh
**
*NSET, NSET=JOIN1, GENERATE
10, 20810, 800
20810, 36810, 400
36810, 57610, 800
*NSET, NSET=JOIN2, GENERATE
394, 21194, 800
21194, 37194, 400
37194, 57994, 800
**
**
**     Define node sets for tieing refined mesh
**
*NSET, NSET=PB1, GENERATE
20814, 21182, 16
*NSET, NSET=AB, GENERATE
20810, 21178, 16
*NSET, NSET=BB, GENERATE
20818, 21186, 16
*NSET, NSET=CB, GENERATE
20826, 21194, 16
*NSET, NSET=PB2, GENERATE
20822, 21190, 16
**
*NSET, NSET=PT1, GENERATE
36814, 37182, 16
*NSET, NSET=AT, GENERATE
36810, 37178, 16
*NSET, NSET=BT, GENERATE
36818, 37186, 16
*NSET, NSET=CT, GENERATE
```

```
36826, 37194, 16
*NSET, NSET=PT2, GENERATE
36822, 37190, 16
**
*MPC
QUADRATIC, PB1, AB, BB, CB
QUADRATIC, PB2, AB, BB, CB
QUADRATIC, PT1, AT, BT, CT
QUADRATIC, PT2, AT, BT, CT
TIE, JOIN1, JOIN2
**
*NSET, NSET=BTML1, GENERATE
10, 394, 8
*NSET, NSET=BTML2, GENERATE
810, 1194, 16
*NSET, NSET=BTML3, GENERATE
1610, 1994, 8
*NSET, NSET=BTML4, GENERATE
2410, 2794, 16
*NSET, NSET=BTML5, GENERATE
3210, 3594, 8
**
*NSET, NSET=BTM
BTML1, BTML2, BTML3, BTML4, BTML5
**
*NSET, NSET=TPL1, GENERATE
57610, 57994, 8
*NSET, NSET=TPL2, GENERATE
56810, 57194, 16
*NSET, NSET=TPL3, GENERATE
56010, 56394, 8
*NSET, NSET=TPL4, GENERATE
55210, 55594, 16
*NSET, NSET=TPL5, GENERATE
54410, 54794, 8
**
*NSET, NSET=TP
TPL1, TPL2, TPL3, TPL4, TPL5
**
*BOUNDARY
BTML1, 1
BTML1, 2
BTML1, 3
BTML1, 4
BTML1, 5
BTML1, 6
TPL1, 1
TPL1, 2
TPL1, 3
TPL1, 4
TPL1, 5
TPL1, 6
**
*NSET, NSET=PLOT, GENERATE
10, 20810, 800
20810, 36810, 400
36810, 57610, 800
*NSET, NSET=MIDSEC, GENERATE
```

```
28810, 29194, 4
*NSET, NSET=PLOT2, GENERATE
28810, 28906, 4
29098, 29194, 4
**
**-------------------------------------------------------------
**
**-------------------------------------------------------------
**
**         Define the material properties
**
*SHELL SECTION, ELSET=THIN, MATERIAL=ALUM
0.003
*SHELL SECTION, ELSET=RAD2_1, MATERIAL=ALUM
0.004
*SHELL SECTION, ELSET=RAD1_4, MATERIAL=ALUM
0.004
*SHELL SECTION, ELSET=RAD2_2, MATERIAL=ALUM
0.005
*SHELL SECTION, ELSET=RAD1_3, MATERIAL=ALUM
0.005
*SHELL SECTION, ELSET=RAD2_3, MATERIAL=ALUM
0.006
*SHELL SECTION, ELSET=RAD1_2, MATERIAL=ALUM
0.006
*SHELL SECTION, ELSET=RAD2_4, MATERIAL=ALUM
0.007
*SHELL SECTION, ELSET=RAD1_1, MATERIAL=ALUM
0.007
*SHELL SECTION, ELSET=THICK1, MATERIAL=ALUM
0.008
*SHELL SECTION, ELSET=THICK2, MATERIAL=ALUM
0.008
**
*MATERIAL, NAME=ALUM
*ELASTIC
70.E9,  0.3
**
**-------------------------------------------------------------
**
**
**                      CRACK DATA
**
**
*NSET, NSET=CRKCOPY, GENERATE
29170, 29194, 4
28810, 28834, 4
**
*NCOPY, CHANGENUMBER=100000, OLDSET=CRKCOPY, SHIFT
0., 0., 0.
0., 0., 0., 0., 0., 1., 0.
**
*ELEMENT, TYPE=S8R, ELSET=TPCRK
1804, 29162, 129170, 29970, 29962, 29166, 29570, 29966, 29562
1805, 129170, 129178, 29978, 29970, 129174, 29578, 29974, 29570
1806, 129178, 129186, 29986, 29978, 129182, 29586, 29982, 29578
1807, 129186, 129194, 29994, 29986, 129190, 29594, 29990, 29586
1760, 128810, 128818, 29618, 29610, 128814, 29218, 29614, 29210
```

```
1761, 128818, 128826, 29626, 29618, 128822, 29226, 29622, 29218
1762, 128826, 128834, 29634, 29626, 128830, 29234, 29630, 29226
1763, 128834, 28842, 29642, 29634, 28838, 29242, 29638, 29234
**
*MPC
TIE, 129194, 128810
**
**
*ELEMENT, TYPE=LS6, ELSET=CCRACK
10000, 129178, 129174, 129170, 29178, 29174, 29170
10001, 129186, 129182, 129178, 29186, 29182, 29178
10002, 129194, 129190, 129186, 29194, 29190, 29186
10003, 128818, 128814, 128810, 28818, 28814, 28810
10004, 128826, 128822, 128818, 28826, 28822, 28818
10005, 128834, 128830, 128826, 28834, 28830, 28826
**
*SURFACE FLAW, SIDE=POSITIVE
29170, 0.
29174, 0.850865E-3
29178, 1.397152E-3
29182, 1.825328E-3
29186, 2.132897E-3
29190, 2.318139E-3
29194, 2.38E-3
28834, 0.
28830, 0.850865E-3
28826, 1.397152E-3
28822, 1.825328E-3
28818, 2.132897E-3
28814, 2.318139E-3
28810, 2.38E-3
**
*SHELL SECTION, ELSET=CCRACK, MATERIAL=ALUM
0.003
**
*ELSET, ELSET=CYLIN2
CYLIN, CCRACK
**
**
**************************************************************
**              Define analysis type and loading
**************************************************************
**
*STEP
*STATIC
**
**-------------------------------------------------------------
**
**      Define the distributed load, NB load per unit area
**
*DLOAD
CYLIN, P, 689475.73
**-------------------------------------------------------------
**
*NODE PRINT, NSET=PLOT
U1
*RESTART, WRITE
**
```

```
*END STEP
**
**
**                    End of Analysis
```

45° Crack

```
*HEADING
LARGE CYLINDER, MACHINED FROM SOLID, partially refined
74 mm max OD, modelling whole cylinder
45 DEGREE CRACK WITH TRIANGULAR ELEMENTS
**
**
**-------------------------------------------------------------
**                  Define corner nodes of SHELL
**
*NODE
10,   0.033, 0., 0.
26,   0.032360566, 0.006464808, 0.
378,  0.032360566, -0.006464808, 0.
394,  0.033, 0., 0.
**
6410,   0.033, 0., 0.030
6426,  0.032360566, 0.006464808, 0.030
6778,  0.032360566, -0.006464808, 0.030
6794,  0.033, 0., 0.030
**
12810,  0.0305, 0., 0.0345
12826,  0.029909008, 0.00597505, 0.0345
13178,  0.029909008, -0.00597505, 0.0345
13194,  0.0305, 0., 0.0345
**
44810,   0.0305, 0., 0.1655
44826,  0.029909008, 0.00597505, 0.1655
45178,  0.029909008, -0.00597505, 0.1655
45194,  0.0305, 0., 0.1655
**
51210,   0.033, 0., 0.170
51226,  0.032360566, 0.006464808, 0.170
51578,  0.032360566, -0.006464808, 0.170
51594,  0.033, 0., 0.170
**
57610,   0.033, 0., 0.200
57626,  0.032360566, 0.006464808, 0.200
57978,  0.032360566, -0.006464808, 0.200
57994,  0.033, 0., 0.200
**
**--------CRACK DATA--------
*NODE
27210,  0.0305, 0., 0.09402495
27226,  0.029909008, 0.00597505, 0.09402495
27578,  0.029909008, -0.00597505, 0.09402495
27594,  0.0305, 0., 0.09402495
**
30410,  0.0305, 0., 0.10597505
30426,  0.029909008, 0.00597505, 0.10597505
30778,  0.029909008, -0.00597505, 0.10597505
```

```
30794, 0.0305, 0., 0.10597505
**
**---------END CRACK---------
**
**-------------------------------------------------------------
**
**    Generate the shell nodes using node sets and node filling
**
*NGEN, LINE=C, NSET=BOTT
10, 26, 4, , 0., 0., 0., 0., 0., 1.
26, 378, 4, , 0., 0., 0., 0., 0., 1.
378, 394, 4, , 0., 0., 0., 0., 0., 1.
*NGEN, LINE=C, NSET=ENDTHCK
6410, 6426, 4, , 0., 0., 0.030, 0., 0., 1.
6426, 6778, 4, , 0., 0., 0.030, 0., 0., 1.
6778, 6794, 4, , 0., 0., 0.030, 0., 0., 1.
*NGEN, LINE=C, NSET=STRTTHN
12810, 12826, 4, , 0., 0., 0.0345, 0., 0., 1.
12826, 13178, 4, , 0., 0., 0.0345, 0., 0., 1.
13178, 13194, 4, , 0., 0., 0.0345, 0., 0., 1.
*NGEN, LINE=C, NSET=B_RAD
44810, 44826, 4, , 0., 0., 0.1655, 0., 0., 1.
44826, 45178, 4, , 0., 0., 0.1655, 0., 0., 1.
45178, 45194, 4, , 0., 0., 0.1655, 0., 0., 1.
*NGEN, LINE=C, NSET=TOP_RAD
51210, 51226, 4, , 0., 0., 0.170, 0., 0., 1.
51226, 51578, 4, , 0., 0., 0.170, 0., 0., 1.
51578, 51594, 4, , 0., 0., 0.170, 0., 0., 1.
*NGEN, LINE=C, NSET=TOP
57610, 57626, 4, , 0., 0., 0.200, 0., 0., 1.
57626, 57978, 4, , 0., 0., 0.200, 0., 0., 1.
57978, 57994, 4, , 0., 0., 0.200, 0., 0., 1.
**
**---------CRACK DATA-------
**
*NGEN, LINE=C, NSET=BCRK
27210, 27226, 4, , 0., 0., 0.09402495, 0., 0., 1.
27226, 27578, 4, , 0., 0., 0.09402495, 0., 0., 1.
27578, 27594, 4, , 0., 0., 0.09402495, 0., 0., 1.
**
*NGEN, LINE=C, NSET=TCRK
30410, 30426, 4, , 0., 0., 0.10597505, 0., 0., 1.
30426, 30778, 4, , 0., 0., 0.10597505, 0., 0., 1.
30778, 30794, 4, , 0., 0., 0.10597505, 0., 0., 1.
**
**---------END CRACK---------
**
**          Generate shell wall for thick bottom end
**
*NFILL, NSET=THICK1
BOTT, ENDTHCK, 16, 400
**
**          Generate shell wall for first radius
**
*NFILL, NSET=RAD1
ENDTHCK, STRTTHN, 16, 400
**
**          Generate shell wall for main body
```

```
**
**------CRACK DATA--------
**
*NFILL, NSET=WALL
STRTTHN, BCRK, 36, 400
BCRK, TCRK, 8, 400
TCRK, B_RAD, 36, 400
**
**-----END CRACK----------
**
**            Generate shell wall for second radius
**
*NFILL, NSET=RAD2
B_RAD, TOP_RAD, 16, 400
**
**          Generate shell wall for thickened top end
**
*NFILL, NSET=THICK2
TOP_RAD, TOP, 16, 400
**
**
**-------------------------------------------------------------
**                Define master element for SHELL
**
*ELEMENT, TYPE=S8R
1,  10, 26, 1626, 1610, 18, 826, 1618, 810
400, 6410, 6426, 8026, 8010, 6418, 7226, 8018, 7210
800, 12810, 12826, 14426, 14410, 12818, 13626, 14418, 13610
1280, 20810, 20818, 21618, 21610, 20814, 21218, 21614, 21210
2240, 36810, 36826, 38426, 38410, 36818, 37626, 38418, 37610
3000, 44810, 44826, 46426, 46410, 44818, 45626, 46418, 45610
3400, 51210, 51226, 52826, 52810, 51218, 52026, 52818, 52010
**
**-------------------------------------------------------------
**
**    Generate the other elements using the master elements
**
*ELGEN, ELSET=THICK1
1, 24, 16, 1,  4, 1600, 24
**
*ELGEN, ELSET=RAD1_1
400, 24, 16, 1
*ELCOPY,ELEMENTSHIFT=24,OLDSET=RAD1_1,SHIFTNODES=1600,NEWSET=RAD1_2
*ELCOPY,ELEMENTSHIFT=24,OLDSET=RAD1_2,SHIFTNODES=1600,NEWSET=RAD1_3
*ELCOPY,ELEMENTSHIFT=24,OLDSET=RAD1_3,SHIFTNODES=1600,NEWSET=RAD1_4
**
*ELGEN, ELSET=THIN
800,  24, 16, 1, 5, 1600, 24
1280,  48, 8, 1,  20, 800, 48
2240, 24, 16, 1, 5, 1600, 24
**
*ELGEN, ELSET=RAD2_1
3000, 24, 16, 1
*ELCOPY,ELEMENTSHIFT=24,OLDSET=RAD2_1,SHIFTNODES=1600,NEWSET=RAD2_2
*ELCOPY,ELEMENTSHIFT=24,OLDSET=RAD2_2,SHIFTNODES=1600,NEWSET=RAD2_3
*ELCOPY,ELEMENTSHIFT=24,OLDSET=RAD2_3,SHIFTNODES=1600,NEWSET=RAD2_4
**
*ELGEN, ELSET=THICK2
```

```
3400, 24, 16, 1,  4, 1600, 24
**
**
*ELSET, ELSET=CYLIN
THICK1, RAD1_1, RAD1_2, RAD1_3, RAD1_4
THIN, RAD2_1, RAD2_2, RAD2_3, RAD2_4, THICK2
**
**------------------------------------------------------------
**
**           Define the boundary conditions and MPC's
**
**
**
**      Define node sets for zipping up mesh
**
*NSET, NSET=JOIN1, GENERATE
10, 20810, 800
20810, 36810, 400
36810, 57610, 800
*NSET, NSET=JOIN2, GENERATE
394, 21194, 800
21194, 37194, 400
37194, 57994, 800
**
**
**      Define node sets for tieing refined mesh
**
*NSET, NSET=PB1, GENERATE
20814, 21182, 16
*NSET, NSET=AB, GENERATE
20810, 21178, 16
*NSET, NSET=BB, GENERATE
20818, 21186, 16
*NSET, NSET=CB, GENERATE
20826, 21194, 16
*NSET, NSET=PB2, GENERATE
20822, 21190, 16
**
*NSET, NSET=PT1, GENERATE
36814, 37182, 16
*NSET, NSET=AT, GENERATE
36810, 37178, 16
*NSET, NSET=BT, GENERATE
36818, 37186, 16
*NSET, NSET=CT, GENERATE
36826, 37194, 16
*NSET, NSET=PT2, GENERATE
36822, 37190, 16
**
*MPC
QUADRATIC, PB1, AB, BB, CB
QUADRATIC, PB2, AB, BB, CB
QUADRATIC, PT1, AT, BT, CT
QUADRATIC, PT2, AT, BT, CT
TIE, JOIN1, JOIN2
**
*NSET, NSET=BTML1, GENERATE
10, 394, 8
```

```
*NSET, NSET=BTML2, GENERATE
810, 1194, 16
*NSET, NSET=BTML3, GENERATE
1610, 1994, 8
*NSET, NSET=BTML4, GENERATE
2410, 2794, 16
*NSET, NSET=BTML5, GENERATE
3210, 3594, 8
**
*NSET, NSET=BTM
BTML1, BTML2, BTML3, BTML4, BTML5
**
*NSET, NSET=TPL1, GENERATE
57610, 57994, 8
*NSET, NSET=TPL2, GENERATE
56810, 57194, 16
*NSET, NSET=TPL3, GENERATE
56010, 56394, 8
*NSET, NSET=TPL4, GENERATE
55210, 55594, 16
*NSET, NSET=TPL5, GENERATE
54410, 54794, 8
**
*NSET, NSET=TP
TPL1, TPL2, TPL3, TPL4, TPL5
**
*BOUNDARY
BTML1, 1
BTML1, 2
BTML1, 3
BTML1, 4
BTML1, 5
BTML1, 6
TPL1, 1
TPL1, 2
TPL1, 3
TPL1, 4
TPL1, 5
TPL1, 6
**
*NSET, NSET=PLOT, GENERATE
10, 20810, 800
20810, 36810, 400
36810, 57610, 800
*NSET, NSET=MIDSEC, GENERATE
28810, 29194, 4
*NSET, NSET=PLOT2, GENERATE
28810, 28906, 4
29098, 29194, 4
**
**-----------------------------------------------------------------
**
**-----------------------------------------------------------------
**
**          Define the material properties
**
*SHELL SECTION, ELSET=THIN, MATERIAL=ALUM
0.003
```

```
*SHELL SECTION, ELSET=RAD2_1, MATERIAL=ALUM
0.004
*SHELL SECTION, ELSET=RAD1_4, MATERIAL=ALUM
0.004
*SHELL SECTION, ELSET=RAD2_2, MATERIAL=ALUM
0.005
*SHELL SECTION, ELSET=RAD1_3, MATERIAL=ALUM
0.005
*SHELL SECTION, ELSET=RAD2_3, MATERIAL=ALUM
0.006
*SHELL SECTION, ELSET=RAD1_2, MATERIAL=ALUM
0.006
*SHELL SECTION, ELSET=RAD2_4, MATERIAL=ALUM
0.007
*SHELL SECTION, ELSET=RAD1_1, MATERIAL=ALUM
0.007
*SHELL SECTION, ELSET=THICK1, MATERIAL=ALUM
0.008
*SHELL SECTION, ELSET=THICK2, MATERIAL=ALUM
0.008
**
*MATERIAL, NAME=ALUM
*ELASTIC
70.E9,  0.3
**
**------------------------------------------------------------
**
**
**                        CRACK DATA
**
**
*NSET, NSET=CRKCOPY
30778, 30382, 29986, 29590, 29194, 28414, 28018, 27622, 27226
**
*NCOPY, CHANGENUMBER=100000, OLDSET=CRKCOPY, SHIFT
0., 0., 0.
0., 0., 0., 0., 0., 1., 0.
**
*ELEMENT, TYPE=STRI65, ELSET=TRIANG
1807, 29186, 29194, 29986, 29190, 29590, 29586
11807, 129194, 29994, 129986, 29594, 29990, 129590
1854, 29978, 29986, 30778, 29982, 30382, 30378
11854, 129986, 30786, 130778, 30386, 30782, 130382
1712, 28010, 28018, 29194, 28014, 28414, 28410
11712, 128018, 28818, 129194, 28418, 28814, 128414
1665, 27218, 27226, 28018, 27222, 27622, 27618
11665, 127226, 28026, 128018, 27626, 28022, 127622
**
*ELEMENT, TYPE=S8R, ELSET=THIN
1855, 129986, 29994, 30794, 30786, 29990, 30394, 30790, 30386
1760, 129194, 28818, 29618, 29610, 28814, 29218, 29614, 29210
1713, 128018, 28026, 28826, 28818, 28022, 28426, 28822, 28418
1666, 127226, 27234, 28034, 28026, 27230, 27634, 28030, 27626
**
**
*ELEMENT, TYPE=LS6, ELSET=ANGCRK
10000, 129986, 130382, 130778, 29986, 30382, 30778
10001, 129194, 129590, 129986, 29194, 29590, 29986
```

```
10002, 128018, 128414, 129194, 28018, 28414, 29194
10003, 127226, 127622, 128018, 27226, 27622, 28018
**
*MPC
TIE, 30778, 130778
TIE, 27226, 127226
**
*SURFACE FLAW, SIDE=POSITIVE
30778, 0.0
30382, 0.893522E-3
29986, 1.526606E-3
29590, 1.904396E-3
29194, 2.03E-3
28414, 1.904396E-3
28018, 1.526606E-3
27622, 0.893522E-3
27226, 0.0
**
*SHELL SECTION, ELSET=ANGCRK, MATERIAL=ALUM
0.003
**
*SHELL SECTION, ELSET=TRIANG, MATERIAL=ALUM
0.003
**
*ELSET, ELSET=CYLIN2
CYLIN, TRIANG
**
**
**************************************************************
**              Define analysis type and loading
**************************************************************
**
*STEP
*STATIC
**
**-------------------------------------------------------------
**
**      Define the distributed load, NB load per unit area
**
*DLOAD
CYLIN2, P, 689475.73
**-------------------------------------------------------------
**
*NODE PRINT, NSET=PLOT
U1
*RESTART, WRITE
**
*END STEP
**
**
**                  End of Analysis
```

Internal Crack

```
*HEADING
LARGE CYLINDER, MACHINED FROM SOLID, partially refined
74 mm max OD, modelling whole cylinder
```

```
1.5mm DEEP INTERNAL AXIAL CRACK
**
**
**------------------------------------------------------------
**                  Define corner nodes of SHELL
**
*NODE
10,   0.033, 0., 0.
202,   0.033, 0., 0.
394, 0.033, 0., 0.
**
6410,   0.033, 0., 0.030
6602,   0.033, 0., 0.030
6794, 0.033, 0., 0.030
**
12810, 0.0305, 0., 0.0345
13002, 0.0305, 0., 0.0345
13194, 0.0305, 0., 0.0345
**
44810,   0.0305, 0., 0.1655
45002,   0.0305, 0., 0.1655
45194, 0.0305, 0., 0.1655
**
51210,   0.033, 0., 0.170
51402,   0.033, 0., 0.170
51594, 0.033, 0., 0.170
**
57610,   0.033, 0., 0.200
57802,   0.033, 0., 0.200
57994, 0.033, 0., 0.200
**
**
**----------CRACK DATA-------
26410,   0.0305, 0., 0.09065
26794,   0.0305, 0., 0.09065
**
31210,   0.0305, 0., 0.10935
31594,   0.0305, 0., 0.10935
**
*NGEN, LINE=C, NSET=BOTCRK
26410, 26794, 4, , 0., 0., 0.09065, 0., 0., 1.
*NGEN, LINE=C, NSET=TOPCRK
31210, 31594, 4, , 0., 0., 0.10935, 0., 0., 1.
**---------END CRACK--------
**
**
**------------------------------------------------------------
**
**   Generate the shell nodes using node sets and node filling
**
*NGEN, LINE=C, NSET=BOTT
10, 394, 4, , 0., 0., 0., 0., 0., 1.
*NGEN, LINE=C, NSET=ENDTHCK
6410, 6794, 4, , 0., 0., 0.030, 0., 0., 1.
*NGEN, LINE=C, NSET=STRTTHN
12810, 13194, 4, , 0., 0., 0.0345, 0., 0., 1.
*NGEN, LINE=C, NSET=B_RAD
44810, 45194, 4, , 0., 0., 0.1655, 0., 0., 1.
```

```
*NGEN, LINE=C, NSET=TOP_RAD
51210, 51594, 4, , 0., 0., 0.170, 0., 0., 1.
*NGEN, LINE=C, NSET=TOP
57610, 57994, 4, , 0., 0., 0.200, 0., 0., 1.
**
**          Generate shell wall for thick bottom end
**
*NFILL, NSET=THICK1
BOTT, ENDTHCK, 16, 400
**
**          Generate shell wall for first radius
**
*NFILL, NSET=RAD1
ENDTHCK, STRTTHN, 16, 400
**
**          Generate shell wall for main body
**
**--------CRACK DATA--------
*NFILL, NSET=WALL
STRTTHN, BOTCRK, 34, 400
BOTCRK, TOPCRK, 12, 400
TOPCRK, B_RAD, 34, 400
**---------END CRACK---------
**
**           Generate shell wall for second radius
**
*NFILL, NSET=RAD2
B_RAD, TOP_RAD, 16, 400
**
**          Generate shell wall for thickened top end
**
*NFILL, NSET=THICK2
TOP_RAD, TOP, 16, 400
**
**
**-------------------------------------------------------------
**                Define master element for SHELL
**
*ELEMENT, TYPE=S8R
1,  10, 26, 1626, 1610, 18, 826, 1618, 810
400, 6410, 6426, 8026, 8010, 6418, 7226, 8018, 7210
800, 12810, 12826, 14426, 14410, 12818, 13626, 14418, 13610
1280, 20810, 20818, 21618, 21610, 20814, 21218, 21614, 21210
2240, 36810, 36826, 38426, 38410, 36818, 37626, 38418, 37610
3000, 44810, 44826, 46426, 46410, 44818, 45626, 46418, 45610
3400, 51210, 51226, 52826, 52810, 51218, 52026, 52818, 52010
**
**-------------------------------------------------------------
**
**    Generate the other elements using the master elements
**
*ELGEN, ELSET=THICK1
1, 24, 16, 1,  4, 1600, 24
**
*ELGEN, ELSET=RAD1_1
400, 24, 16, 1
*ELCOPY,ELEMENTSHIFT=24,OLDSET=RAD1_1,SHIFTNODES=1600,NEWSET=RAD1_2
*ELCOPY,ELEMENTSHIFT=24,OLDSET=RAD1_2,SHIFTNODES=1600,NEWSET=RAD1_3
```

```
*NSET, NSET=BT, GENERATE
36818, 37186, 16
*NSET, NSET=CT, GENERATE
36826, 37194, 16
*NSET, NSET=PT2, GENERATE
36822, 37190, 16
**
*MPC
QUADRATIC, PB1, AB, BB, CB
QUADRATIC, PB2, AB, BB, CB
QUADRATIC, PT1, AT, BT, CT
QUADRATIC, PT2, AT, BT, CT
TIE, JOIN1, JOIN2
**
*NSET, NSET=BTML1, GENERATE
10, 394, 8
*NSET, NSET=BTML2, GENERATE
810, 1194, 16
*NSET, NSET=BTML3, GENERATE
1610, 1994, 8
*NSET, NSET=BTML4, GENERATE
2410, 2794, 16
*NSET, NSET=BTML5, GENERATE
3210, 3594, 8
**
*NSET, NSET=BTM
BTML1, BTML2, BTML3, BTML4, BTML5
**
*NSET, NSET=TPL1, GENERATE
57610, 57994, 8
*NSET, NSET=TPL2, GENERATE
56810, 57194, 16
*NSET, NSET=TPL3, GENERATE
56010, 56394, 8
*NSET, NSET=TPL4, GENERATE
55210, 55594, 16
*NSET, NSET=TPL5, GENERATE
54410, 54794, 8
**
*NSET, NSET=TP
TPL1, TPL2, TPL3, TPL4, TPL5
**
*BOUNDARY
BTML1, 1
BTML1, 2
BTML1, 3
BTML1, 4
BTML1, 5
BTML1, 6
TPL1, 1
TPL1, 2
TPL1, 3
TPL1, 4
TPL1, 5
TPL1, 6
**
*NSET, NSET=PLOT, GENERATE
10, 20810, 800
```

```
20810, 36810, 400
36810, 57610, 800
*NSET, NSET=MIDSEC, GENERATE
28810, 29194, 4
*NSET, NSET=PLOT2, GENERATE
28810, 28906, 4
29098, 29194, 4
**
**------------------------------------------------------------
**
**------------------------------------------------------------
**
**         Define the material properties
**
*SHELL SECTION, ELSET=THIN, MATERIAL=ALUM
0.003
*SHELL SECTION, ELSET=RAD2_1, MATERIAL=ALUM
0.004
*SHELL SECTION, ELSET=RAD1_4, MATERIAL=ALUM
0.004
*SHELL SECTION, ELSET=RAD2_2, MATERIAL=ALUM
0.005
*SHELL SECTION, ELSET=RAD1_3, MATERIAL=ALUM
0.005
*SHELL SECTION, ELSET=RAD2_3, MATERIAL=ALUM
0.006
*SHELL SECTION, ELSET=RAD1_2, MATERIAL=ALUM
0.006
*SHELL SECTION, ELSET=RAD2_4, MATERIAL=ALUM
0.007
*SHELL SECTION, ELSET=RAD1_1, MATERIAL=ALUM
0.007
*SHELL SECTION, ELSET=THICK1, MATERIAL=ALUM
0.008
*SHELL SECTION, ELSET=THICK2, MATERIAL=ALUM
0.008
**
*MATERIAL, NAME=ALUM
*ELASTIC
70.E9,  0.3
**
**------------------------------------------------------------
**
**
**                    CRACK DATA
**     NB: change JOIN nset if crack length changes
**
*ELEMENT, TYPE=LS6, ELSET=ACRACK
10000, 31594, 31194, 30794, 31210, 30810, 30410
10001, 30794, 30394, 29994, 30410, 30010, 29610
10002, 29994, 29594, 29194, 29610, 29210, 28810
10003, 29194, 28794, 28394, 28810, 28410, 28010
10004, 28394, 27994, 27594, 28010, 27610, 27210
10005, 27594, 27194, 26794, 27210, 26810, 26410
**
*SURFACE FLAW, SIDE=NEGATIVE
31594, 0.0
31194, 0.569E-3
```

```
30794, 1.025E-3
30394, 1.373E-3
29994, 1.619E-3
29594, 1.765E-3
29194, 1.814E-3
28794, 1.765E-3
28394, 1.619E-3
27994, 1.373E-3
27594, 1.025E-3
27194, 0.569E-3
26794, 0.0
**
*SHELL SECTION, ELSET=ACRACK, MATERIAL=ALUM
0.003
**
**************************************************************
**              Define analysis type and loading
**************************************************************
**
*STEP
*STATIC
**
**-------------------------------------------------------------
**
**      Define the distributed load, NB load per unit area
**
*DLOAD
CYLIN, P, 689475.729
ACRACK, P, 689475.729
**-------------------------------------------------------------
**
*NODE PRINT, NSET=PLOT
U1
*RESTART, WRITE
**
*END STEP
**
**
**                End of Analysis
```

Parallel Cracks

```
*HEADING
LARGE CYLINDER, MACHINED FROM SOLID, partially refined
74 mm max OD, modelling whole cylinder
2 PARALLEL CRACKS 1.5mm deep
**
**
**-------------------------------------------------------------
**                Define corner nodes of SHELL
**
*NODE
10,  0.033, 0., 0.
394, 0.033, 0., 0.
**
6410,  0.033, 0., 0.030
6794, 0.033,  0., 0.030
```

```
**
12810, 0.0305, 0., 0.0345
13194, 0.0305, 0., 0.0345
**
44810,  0.0305, 0., 0.1655
45194, 0.0305, 0., 0.1655
**
51210,  0.033, 0., 0.170
51594, 0.033, 0., 0.170
**
57610,  0.033, 0., 0.200
57994, 0.033, 0., 0.200
**
**
**---------CRACK DATA-------
26410,  0.0305, 0., 0.0914706
26794,  0.0305, 0., 0.0914706
**
31210,  0.0305, 0., 0.1085294
31594,  0.0305, 0., 0.1085294
**
*NGEN, LINE=C, NSET=BOTCRK
26410, 26794, 4, , 0., 0., 0.0914706, 0., 0., 1.
*NGEN, LINE=C, NSET=TOPCRK
31210, 31594, 4, , 0., 0., 0.1085294, 0., 0., 1.
**----------END CRACK--------
**
**
**-----------------------------------------------------------
**
**   Generate the shell nodes using node sets and node filling
**
*NGEN, LINE=C, NSET=BOTT
10, 394, 4, , 0., 0., 0., 0., 0., 1.
*NGEN, LINE=C, NSET=ENDTHCK
6410, 6794, 4, , 0., 0., 0.030, 0., 0., 1.
*NGEN, LINE=C, NSET=STRTTHN
12810, 13194, 4, , 0., 0., 0.0345, 0., 0., 1.
*NGEN, LINE=C, NSET=B_RAD
44810, 45194, 4, , 0., 0., 0.1655, 0., 0., 1.
*NGEN, LINE=C, NSET=TOP_RAD
51210, 51594, 4, , 0., 0., 0.170, 0., 0., 1.
*NGEN, LINE=C, NSET=TOP
57610, 57994, 4, , 0., 0., 0.200, 0., 0., 1.
**
**          Generate shell wall for thick bottom end
**
*NFILL, NSET=THICK1
BOTT, ENDTHCK, 16, 400
**
**          Generate shell wall for first radius
**
*NFILL, NSET=RAD1
ENDTHCK, STRTTHN, 16, 400
**
**          Generate shell wall for main body
**
**---------CRACK DATA-------
```

```
*NFILL, NSET=WALL
STRTTHN, BOTCRK, 34, 400
BOTCRK, TOPCRK, 12, 400
TOPCRK, B_RAD, 34, 400
**---------END CRACK---------
**
**            Generate shell wall for second radius
**
*NFILL, NSET=RAD2
B_RAD, TOP_RAD, 16, 400
**
**          Generate shell wall for thickened top end
**
*NFILL, NSET=THICK2
TOP_RAD, TOP, 16, 400
**
**
**-------------------------------------------------------------
**                Define master element for SHELL
**
*ELEMENT, TYPE=S8R
1,  10, 26, 1626, 1610, 18, 826, 1618, 810
400, 6410, 6426, 8026, 8010, 6418, 7226, 8018, 7210
800, 12810, 12826, 14426, 14410, 12818, 13626, 14418, 13610
1280, 20810, 20818, 21618, 21610, 20814, 21218, 21614, 21210
2240, 36810, 36826, 38426, 38410, 36818, 37626, 38418, 37610
3000, 44810, 44826, 46426, 46410, 44818, 45626, 46418, 45610
3400, 51210, 51226, 52826, 52810, 51218, 52026, 52818, 52010
**
**-------------------------------------------------------------
**
**    Generate the other elements using the master elements
**
*ELGEN, ELSET=THICK1
1, 24, 16, 1,  4, 1600, 24
**
*ELGEN, ELSET=RAD1_1
400, 24, 16, 1
*ELCOPY,ELEMENTSHIFT=24,OLDSET=RAD1_1,SHIFTNODES=1600,NEWSET=RAD1_2
*ELCOPY,ELEMENTSHIFT=24,OLDSET=RAD1_2,SHIFTNODES=1600,NEWSET=RAD1_3
*ELCOPY,ELEMENTSHIFT=24,OLDSET=RAD1_3,SHIFTNODES=1600,NEWSET=RAD1_4
**
*ELGEN, ELSET=THIN
800,  24, 16, 1, 5, 1600, 24
1280,  48, 8, 1,  20, 800, 48
2240, 24, 16, 1, 5, 1600, 24
**
*ELGEN, ELSET=RAD2_1
3000, 24, 16, 1
*ELCOPY,ELEMENTSHIFT=24,OLDSET=RAD2_1,SHIFTNODES=1600,NEWSET=RAD2_2
*ELCOPY,ELEMENTSHIFT=24,OLDSET=RAD2_2,SHIFTNODES=1600,NEWSET=RAD2_3
*ELCOPY,ELEMENTSHIFT=24,OLDSET=RAD2_3,SHIFTNODES=1600,NEWSET=RAD2_4
**
*ELGEN, ELSET=THICK2
3400, 24, 16, 1,  4, 1600, 24
**
**
**
```

```
**-------------------------------------------------------------
**
**          Define the boundary conditions and MPC's
**
**
**
**      Define node sets for zipping up mesh
**
*NSET, NSET=JOIN1, GENERATE
10, 20810, 800
20810, 36810, 400
36810, 57610, 800
*NSET, NSET=JOIN2, GENERATE
394, 21194, 800
21194, 37194, 400
37194, 57994, 800
**
**
**      Define node sets for tieing refined mesh
**
*NSET, NSET=PB1, GENERATE
20814, 21182, 16
*NSET, NSET=AB, GENERATE
20810, 21178, 16
*NSET, NSET=BB, GENERATE
20818, 21186, 16
*NSET, NSET=CB, GENERATE
20826, 21194, 16
*NSET, NSET=PB2, GENERATE
20822, 21190, 16
**
*NSET, NSET=PT1, GENERATE
36814, 37182, 16
*NSET, NSET=AT, GENERATE
36810, 37178, 16
*NSET, NSET=BT, GENERATE
36818, 37186, 16
*NSET, NSET=CT, GENERATE
36826, 37194, 16
*NSET, NSET=PT2, GENERATE
36822, 37190, 16
**
*MPC
QUADRATIC, PB1, AB, BB, CB
QUADRATIC, PB2, AB, BB, CB
QUADRATIC, PT1, AT, BT, CT
QUADRATIC, PT2, AT, BT, CT
TIE, JOIN1, JOIN2
**
*NSET, NSET=BTML1, GENERATE
10, 394, 8
*NSET, NSET=BTML2, GENERATE
810, 1194, 16
*NSET, NSET=BTML3, GENERATE
1610, 1994, 8
*NSET, NSET=BTML4, GENERATE
2410, 2794, 16
*NSET, NSET=BTML5, GENERATE
```

```
3210, 3594, 8
**
*NSET, NSET=BTM
BTML1, BTML2, BTML3, BTML4, BTML5
**
*NSET, NSET=TPL1, GENERATE
57610, 57994, 8
*NSET, NSET=TPL2, GENERATE
56810, 57194, 16
*NSET, NSET=TPL3, GENERATE
56010, 56394, 8
*NSET, NSET=TPL4, GENERATE
55210, 55594, 16
*NSET, NSET=TPL5, GENERATE
54410, 54794, 8
**
*NSET, NSET=TP
TPL1, TPL2, TPL3, TPL4, TPL5
**
*BOUNDARY
BTML1, 1
BTML1, 2
BTML1, 3
BTML1, 4
BTML1, 5
BTML1, 6
TPL1, 1
TPL1, 2
TPL1, 3
TPL1, 4
TPL1, 5
TPL1, 6
**
*NSET, NSET=PLOT, GENERATE
10, 20810, 800
20810, 36810, 400
36810, 57610, 800
*NSET, NSET=MIDSEC, GENERATE
28810, 29194, 4
*NSET, NSET=PL2, GENERATE
28810, 28906, 4
29098, 29194, 4
*NSET, NSET=PLOT2
PL2, 129170, 128834
**
**-----------------------------------------------------------------
**
**-----------------------------------------------------------------
**
**         Define the material properties
**
*SHELL SECTION, ELSET=THIN, MATERIAL=ALUM
0.003
*SHELL SECTION, ELSET=RAD2_1, MATERIAL=ALUM
0.004
*SHELL SECTION, ELSET=RAD1_4, MATERIAL=ALUM
0.004
*SHELL SECTION, ELSET=RAD2_2, MATERIAL=ALUM
```

```
0.005
*SHELL SECTION, ELSET=RAD1_3, MATERIAL=ALUM
0.005
*SHELL SECTION, ELSET=RAD2_3, MATERIAL=ALUM
0.006
*SHELL SECTION, ELSET=RAD1_2, MATERIAL=ALUM
0.006
*SHELL SECTION, ELSET=RAD2_4, MATERIAL=ALUM
0.007
*SHELL SECTION, ELSET=RAD1_1, MATERIAL=ALUM
0.007
*SHELL SECTION, ELSET=THICK1, MATERIAL=ALUM
0.008
*SHELL SECTION, ELSET=THICK2, MATERIAL=ALUM
0.008
**
*MATERIAL, NAME=ALUM
*ELASTIC
70.E9,  0.3
**
**------------------------------------------------------------
**
**
**                        CRACK DATA
**
**
*NSET, NSET=CRKCOPY, GENERATE
26434, 31234, 400
26770, 31570, 400
**
*NCOPY, CHANGENUMBER=100000, OLDSET=CRKCOPY, SHIFT
0., 0., 0.
0., 0., 0., 0., 0., 1., 0.
**
**
*ELEMENT, TYPE=S8R, ELSET=LRCRK
1571, 25634, 25642, 26442, 126434, 25638, 26042, 26438, 26034
1619, 126434, 26442, 27242, 127234, 26438, 26842, 27238, 126834
1907, 131234, 31242, 32042, 32034, 31238, 31642, 32038, 31634
**
*ELGEN, ELSET=RRCRK
1619, 6, 800, 48, 1
**
*ELEMENT, TYPE=S8R, ELSET=RLCRK
1612, 25962, 25970, 126770, 26762, 25966, 26370, 26766, 26362
1660, 26762, 126770, 127570, 27562, 26766, 127170, 27566, 27162
1948, 31562, 131570, 32370, 32362, 31566, 31970, 32366, 31962
**
*ELGEN, ELSET=RLCRK
1660, 6, 800, 48, 1
**
*ELSET, ELSET=THIN
RLCRK, RRCRK
**
*ELSET, ELSET=CYLIN
THICK1, RAD1_1, RAD1_2, RAD1_3, RAD1_4
THIN, RAD2_1, RAD2_2, RAD2_3, RAD2_4, THICK2
**
```

```
*ELEMENT, TYPE=LS6, ELSET=LCRK
10000, 131570, 131170, 130770, 31570, 31170, 30770
10001, 130770, 130370, 129970, 30770, 30370, 29970
10002, 129970, 129570, 129170, 29970, 29570, 29170
10003, 129170, 128770, 128370, 29170, 28770, 28370
10004, 128370, 127970, 127570, 28370, 27970, 27570
10005, 127570, 127170, 126770, 27570, 27170, 26770
**
*ELEMENT, TYPE=LS6, ELSET=RCRK
10006, 31234, 30834, 30434, 131234, 130834, 130434
10007, 30434, 30034, 29634, 130434, 130034, 129634
10008, 29634, 29234, 28834, 129634, 129234, 128834
10009, 28834, 28434, 28034, 128834, 128434, 128034
10010, 28034, 27634, 27234, 128034, 127634, 127234
10011, 27234, 26834, 26434, 127234, 126834, 126434
**
*SURFACE FLAW, SIDE=POSITIVE
31234, 0.0
30834, 0.467643E-3
30434, 0.843868E-3
30034, 1.134374E-3
29634, 1.338164E-3
29234, 1.459639E-3
28834, 1.5E-3
28434, 1.459639E-3
28034, 1.338164E-3
27634, 1.134374E-3
27234, 0.843868E-3
26834, 0.467643E-3
26434, 0.0
**
31570, 0.0
31170, 0.467643E-3
30770, 0.843868E-3
30370, 1.134374E-3
29970, 1.338164E-3
29570, 1.459639E-3
29170, 1.5E-3
28770, 1.459639E-3
28370, 1.338164E-3
27970, 1.134374E-3
27570, 0.843868E-3
27170, 0.467643E-3
26770, 0.0
**
*SHELL SECTION, ELSET=LCRK, MATERIAL=ALUM
0.003
**
*SHELL SECTION, ELSET=RCRK, MATERIAL=ALUM
0.003
**
************************************************************
**              Define analysis type and loading
************************************************************
**
*STEP
*STATIC
**
```

```
**-------------------------------------------------------------
**
**      Define the distributed load, NB load per unit area
**
*DLOAD
CYLIN, P, 689475.729
**-------------------------------------------------------------
**
*NODE PRINT, NSET=PLOT
U1
*RESTART, WRITE
**
*END STEP
**
**
**                    End of Analysis
```

V-shaped Crack

```
*HEADING
LARGE CYLINDER, MACHINED FROM SOLID, partially refined
74 mm max OD, modelling whole cylinder
V-SHAPED CRACK
**
**
**-------------------------------------------------------------
**                 Define corner nodes of SHELL
**
*NODE
10,   0.033, 0., 0.
26,   0.032360566, 0.006464808, 0.
378, 0.032360566, -0.006464808, 0.
394, 0.033, 0., 0.
**
6410,   0.033, 0., 0.030
6426, 0.032360566, 0.006464808, 0.030
6778, 0.032360566, -0.006464808, 0.030
6794, 0.033, 0., 0.030
**
12810, 0.0305, 0., 0.0345
12826, 0.029909008, 0.00597505, 0.0345
13178, 0.029909008, -0.00597505, 0.0345
13194, 0.0305, 0., 0.0345
**
44810,   0.0305, 0., 0.1655
44826, 0.029909008, 0.00597505, 0.1655
45178, 0.029909008, -0.00597505, 0.1655
45194, 0.0305, 0., 0.1655
**
51210,   0.033, 0., 0.170
51226, 0.032360566, 0.006464808, 0.170
51578, 0.032360566, -0.006464808, 0.170
51594, 0.033, 0., 0.170
**
57610,   0.033, 0., 0.200
57626, 0.032360566, 0.006464808, 0.200
57978, 0.032360566, -0.006464808, 0.200
```

```
57994, 0.033, 0., 0.200
**
**--------CRACK DATA--------
*NODE
27210, 0.0305, 0., 0.09402495
27226, 0.029909008, 0.00597505, .0.09402495
27578, 0.029909008, -0.00597505, 0.09402495
27594, 0.0305, 0., 0.09402495
**
30410, 0.0305, 0., 0.10597505
30426, 0.029909008, 0.00597505, 0.10597505
30778, 0.029909008, -0.00597505, 0.10597505
30794, 0.0305, 0., 0.10597505
**
32010, 0.0305, 0., 0.111425
32026, 0.029909008, 0.00597505, 0.111425
32378, 0.029909008, -0.00597505, 0.111425
32394, 0.0305, 0., 0.111425
**--------END CRACK---------
**
**-------------------------------------------------------------
**
**   Generate the shell nodes using node sets and node filling
**
*NGEN, LINE=C, NSET=BOTT
10, 26, 4, , 0., 0., 0., 0., 0., 1.
26, 378, 4, , 0., 0., 0., 0., 0., 1.
378, 394, 4, , 0., 0., 0., 0., 0., 1.
*NGEN, LINE=C, NSET=ENDTHCK
6410, 6426, 4, , 0., 0., 0.030, 0., 0., 1.
6426, 6778, 4, , 0., 0., 0.030, 0., 0., 1.
6778, 6794, 4, , 0., 0., 0.030, 0., 0., 1.
*NGEN, LINE=C, NSET=STRTTHN
12810, 12826, 4, , 0., 0., 0.0345, 0., 0., 1.
12826, 13178, 4, , 0., 0., 0.0345, 0., 0., 1.
13178, 13194, 4, , 0., 0., 0.0345, 0., 0., 1.
*NGEN, LINE=C, NSET=B_RAD
44810, 44826, 4, , 0., 0., 0.1655, 0., 0., 1.
44826, 45178, 4, , 0., 0., 0.1655, 0., 0., 1.
45178, 45194, 4, , 0., 0., 0.1655, 0., 0., 1.
*NGEN, LINE=C, NSET=TOP_RAD
51210, 51226, 4, , 0., 0., 0.170, 0., 0., 1.
51226, 51578, 4, , 0., 0., 0.170, 0., 0., 1.
51578, 51594, 4, , 0., 0., 0.170, 0., 0., 1.
*NGEN, LINE=C, NSET=TOP
57610, 57626, 4, , 0., 0., 0.200, 0., 0., 1.
57626, 57978, 4, , 0., 0., 0.200, 0., 0., 1.
57978, 57994, 4, , 0., 0., 0.200, 0., 0., 1.
**
**---------CRACK DATA-------
**
*NGEN, LINE=C, NSET=BCRK
27210, 27226, 4, , 0., 0., 0.09402495, 0., 0., 1.
27226, 27578, 4, , 0., 0., 0.09402495, 0., 0., 1.
27578, 27594, 4, , 0., 0., 0.09402495, 0., 0., 1.
**
*NGEN, LINE=C, NSET=TVCRK
30410, 30426, 4, , 0., 0., 0.10597505, 0., 0., 1.
```

```
30426, 30778, 4, , 0., 0., 0.10597505, 0., 0., 1.
30778, 30794, 4, , 0., 0., 0.10597505, 0., 0., 1.
**
*NGEN, LINE=C, NSET=TSCRK
32010, 32026, 4, , 0., 0., 0.111425, 0., 0., 1.
32026, 32378, 4, , 0., 0., 0.111425, 0., 0., 1.
32378, 32394, 4, , 0., 0., 0.111425, 0., 0., 1.
**
**--------END CRACK---------
**
**          Generate shell wall for thick bottom end
**
*NFILL, NSET=THICK1
BOTT, ENDTHCK, 16, 400
**
**          Generate shell wall for first radius
**
*NFILL, NSET=RAD1
ENDTHCK, STRTTHN, 16, 400
**
**          Generate shell wall for main body
**
**------CRACK DATA--------
**
*NFILL, NSET=WALL
STRTTHN, BCRK, 36, 400
BCRK, TVCRK, 8, 400
TVCRK, TSCRK, 4, 400
TSCRK, B_RAD, 32, 400
**
**-----END CRACK----------
**
**           Generate shell wall for second radius
**
*NFILL, NSET=RAD2
B_RAD, TOP_RAD, 16, 400
**
**          Generate shell wall for thickened top end
**
*NFILL, NSET=THICK2
TOP_RAD, TOP, 16, 400
**
**
**-------------------------------------------------------------
**                Define master element for SHELL
**
*ELEMENT, TYPE=S8R
1,  10, 26, 1626, 1610, 18, 826, 1618, 810
400, 6410, 6426, 8026, 8010, 6418, 7226, 8018, 7210
800, 12810, 12826, 14426, 14410, 12818, 13626, 14418, 13610
1280, 20810, 20818, 21618, 21610, 20814, 21218, 21614, 21210
2240, 36810, 36826, 38426, 38410, 36818, 37626, 38418, 37610
3000, 44810, 44826, 46426, 46410, 44818, 45626, 46418, 45610
3400, 51210, 51226, 52826, 52810, 51218, 52026, 52818, 52010
**
**-------------------------------------------------------------
**
**    Generate the other elements using the master elements
```

```
**
*ELGEN, ELSET=THICK1
1, 24, 16, 1,  4, 1600, 24
**
*ELGEN, ELSET=RAD1_1
400, 24, 16, 1
*ELCOPY,ELEMENTSHIFT=24,OLDSET=RAD1_1,SHIFTNODES=1600,NEWSET=RAD1_2
*ELCOPY,ELEMENTSHIFT=24,OLDSET=RAD1_2,SHIFTNODES=1600,NEWSET=RAD1_3
*ELCOPY,ELEMENTSHIFT=24,OLDSET=RAD1_3,SHIFTNODES=1600,NEWSET=RAD1_4
**
*ELGEN, ELSET=THIN
800,  24, 16, 1, 5, 1600, 24
1280,  48, 8, 1,  20, 800, 48
2240, 24, 16, 1, 5, 1600, 24
**
*ELGEN, ELSET=RAD2_1
3000, 24, 16, 1
*ELCOPY,ELEMENTSHIFT=24,OLDSET=RAD2_1,SHIFTNODES=1600,NEWSET=RAD2_2
*ELCOPY,ELEMENTSHIFT=24,OLDSET=RAD2_2,SHIFTNODES=1600,NEWSET=RAD2_3
*ELCOPY,ELEMENTSHIFT=24,OLDSET=RAD2_3,SHIFTNODES=1600,NEWSET=RAD2_4
**
*ELGEN, ELSET=THICK2
3400, 24, 16, 1,  4, 1600, 24
**
**
*ELSET, ELSET=CYLIN
THICK1, RAD1_1, RAD1_2, RAD1_3, RAD1_4
THIN, RAD2_1, RAD2_2, RAD2_3, RAD2_4, THICK2
**
**--------------------------------------------------------------
**
**          Define the boundary conditions and MPC's
**
**
**
**     Define node sets for zipping up mesh
**
*NSET, NSET=JOIN1, GENERATE
10, 20810, 800
20810, 36810, 400
36810, 57610, 800
*NSET, NSET=JOIN2, GENERATE
394, 21194, 800
21194, 37194, 400
37194, 57994, 800
**
**
**     Define node sets for tieing refined mesh
**
*NSET, NSET=PB1, GENERATE
20814, 21182, 16
*NSET, NSET=AB, GENERATE
20810, 21178, 16
*NSET, NSET=BB, GENERATE
20818, 21186, 16
*NSET, NSET=CB, GENERATE
20826, 21194, 16
*NSET, NSET=PB2, GENERATE
```

```
20822, 21190, 16
**
*NSET, NSET=PT1, GENERATE
36814, 37182, 16
*NSET, NSET=AT, GENERATE
36810, 37178, 16
*NSET, NSET=BT, GENERATE
36818, 37186, 16
*NSET, NSET=CT, GENERATE
36826, 37194, 16
*NSET, NSET=PT2, GENERATE
36822, 37190, 16
**
*MPC
QUADRATIC, PB1, AB, BB, CB
QUADRATIC, PB2, AB, BB, CB
QUADRATIC, PT1, AT, BT, CT
QUADRATIC, PT2, AT, BT, CT
TIE, JOIN1, JOIN2
**
*NSET, NSET=BTML1, GENERATE
10, 394, 8
*NSET, NSET=BTML2, GENERATE
810, 1194, 16
*NSET, NSET=BTML3, GENERATE
1610, 1994, 8
*NSET, NSET=BTML4, GENERATE
2410, 2794, 16
*NSET, NSET=BTML5, GENERATE
3210, 3594, 8
**
*NSET, NSET=BTM
BTML1, BTML2, BTML3, BTML4, BTML5
**
*NSET, NSET=TPL1, GENERATE
57610, 57994, 8
*NSET, NSET=TPL2, GENERATE
56810, 57194, 16
*NSET, NSET=TPL3, GENERATE
56010, 56394, 8
*NSET, NSET=TPL4, GENERATE
55210, 55594, 16
*NSET, NSET=TPL5, GENERATE
54410, 54794, 8
**
*NSET, NSET=TP
TPL1, TPL2, TPL3, TPL4, TPL5
**
*BOUNDARY
BTML1, 1
BTML1, 2
BTML1, 3
BTML1, 4
BTML1, 5
BTML1, 6
TPL1, 1
TPL1, 2
TPL1, 3
```

```
TPL1, 4
TPL1, 5
TPL1, 6
**
*NSET, NSET=PLOT, GENERATE
10, 20810, 800
20810, 36810, 400
36810, 57610, 800
*NSET, NSET=MIDSEC, GENERATE
28810, 29194, 4
*NSET, NSET=PLOT3, GENERATE
28810, 28906, 4
29098, 29194, 4
*NSET, NSET=PLOT2
PLOT3, 129194, 128826
**
**-------------------------------------------------------------
**
**-------------------------------------------------------------
**
**          Define the material properties
**
*SHELL SECTION, ELSET=THIN, MATERIAL=ALUM
0.003
*SHELL SECTION, ELSET=RAD2_1, MATERIAL=ALUM
0.004
*SHELL SECTION, ELSET=RAD1_4, MATERIAL=ALUM
0.004
*SHELL SECTION, ELSET=RAD2_2, MATERIAL=ALUM
0.005
*SHELL SECTION, ELSET=RAD1_3, MATERIAL=ALUM
0.005
*SHELL SECTION, ELSET=RAD2_3, MATERIAL=ALUM
0.006
*SHELL SECTION, ELSET=RAD1_2, MATERIAL=ALUM
0.006
*SHELL SECTION, ELSET=RAD2_4, MATERIAL=ALUM
0.007
*SHELL SECTION, ELSET=RAD1_1, MATERIAL=ALUM
0.007
*SHELL SECTION, ELSET=THICK1, MATERIAL=ALUM
0.008
*SHELL SECTION, ELSET=THICK2, MATERIAL=ALUM
0.008
**
*MATERIAL, NAME=ALUM
*ELASTIC
70.E9,  0.3
**
**-------------------------------------------------------------
**
**
**                      CRACK DATA
**
**
*NSET, NSET=CRKCPY1
30778, 30382, 29986, 29590, 29194, 28414, 28018, 27622, 27226
**
```

```
*NCOPY, CHANGENUMBER=100000, OLDSET=CRKCPY1, SHIFT, NEWSET=CP1B
0., 0., 0.
0., 0., 0., 0., 0., 1., 0.
**
*NSET, NSET=CRKCPY2, GENERATE
27626, 32026, 400
*NSET, NSET=CRKCPY3
CRKCPY2, 127226
**
*NCOPY, CHANGENUMBER=100000, OLDSET=CRKCPY3, SHIFT, NEWSET=CP2B
0., 0., 0.
0., 0., 0., 0., 0., 1., 0.
**
*NSET, NSET=CRKCOPY
CRKCPY1, CRKCPY3
**
*ELEMENT, TYPE=STRI65, ELSET=TRIANG
1807, 29186, 29194, 29986, 29190, 29590, 29586
11807, 129194, 29994, 129986, 29594, 29990, 129590
1854, 29978, 29986, 30778, 29982, 30382, 30378
11854, 129986, 30786, 130778, 30386, 30782, 130382
1712, 28010, 28018, 29194, 28014, 28414, 28410
11712, 128018, 28818, 129194, 28418, 28814, 128414
1665, 27218, 27226, 28018, 27222, 27622, 27618
11665, 127226, 28026, 128018, 27626, 28022, 127622
**
*ELEMENT, TYPE=S8R, ELSET=THIN
1855, 129986, 29994, 30794, 30786, 29990, 30394, 30790, 30386
1760, 129194, 28818, 29618, 29610, 28814, 29218, 29614, 29210
1713, 128018, 28026, 28826, 28818, 28022, 28426, 28822, 28418
1666, 227226, 27234, 28034, 128026, 27230, 27634, 28030, 127626
1714, 128026, 28034, 28834, 128826, 28030, 28434, 28830, 128426
1762, 128826, 28834, 29634, 129626, 28830, 29234, 29630, 129226
1810, 129626, 29634, 30434, 130426, 29630, 30034, 30430, 130026
1858, 130426, 30434, 31234, 131226, 30430, 30834, 31230, 130826
1906, 131226, 31234, 32034, 132026, 31230, 31634, 32030, 131626
1954, 132026, 32034, 32834, 32826, 32030, 32434, 32830, 32426
**
**
*ELEMENT, TYPE=LS6, ELSET=ANGCRK
10000, 129986, 130382, 130778, 29986, 30382, 30778
10001, 129194, 129590, 129986, 29194, 29590, 29986
10002, 128018, 128414, 129194, 28018, 28414, 29194
10003, 127226, 127622, 128018, 27226, 27622, 28018
**
*ELEMENT, TYPE=LS6, ELSET=STRCRK
10004, 32026, 31626, 31226, 132026, 131626, 131226
10005, 31226, 30826, 30426, 131226, 130826, 130426
10006, 30426, 30026, 29626, 130426, 130026, 129626
10007, 29626, 29226, 28826, 129626, 129226, 128826
10008, 28826, 28426, 28026, 128826, 128426, 128026
10009, 28026, 27626, 127226, 128026, 127626, 227226
**
*MPC
TIE, 30778, 130778
TIE, 27226, 127226
**
*SURFACE FLAW, SIDE=POSITIVE
```

```
30778, 0.0
30382, 0.893522E-3
29986, 1.526606E-3
29590, 1.904396E-3
29194, 2.03E-3
28414, 1.904396E-3
28018, 1.526606E-3
27622, 0.893522E-3
27226, 0.0
**
32026, 0.0
31626, 0.529E-3
31226, 0.901E-3
30826, 1.187E-3
30426, 1.380E-3
30026, 1.516E-3
29626, 1.5617E-3
29226, 1.517E-3
28826, 1.3822E-3
28426, 1.157E-3
28026, 0.836E-3
27626, 0.4196E-3
127226, 0.0
**
*SHELL SECTION, ELSET=ANGCRK, MATERIAL=ALUM
0.003
**
*SHELL SECTION, ELSET=TRIANG, MATERIAL=ALUM
0.003
**
*SHELL SECTION, ELSET=STRCRK, MATERIAL=ALUM
0.003
**
*ELSET, ELSET=CYLIN2
CYLIN, TRIANG
**
*NSET, NSET=WALL2
WALL, CP1B, CP2B
**
**************************************************************
**              Define analysis type and loading
**************************************************************
**
*STEP
*STATIC
**
**-------------------------------------------------------------
**
**     Define the distributed load, NB load per unit area
**
*DLOAD
CYLIN2, P, 689475.729
**-------------------------------------------------------------
**
*NODE PRINT, NSET=WALL2
U1
*RESTART, WRITE
**
```

```
*END STEP
**
**
**                    End of Analysis
```

Appendix C - Complete Set of Comparison Graphs

Axial Crack

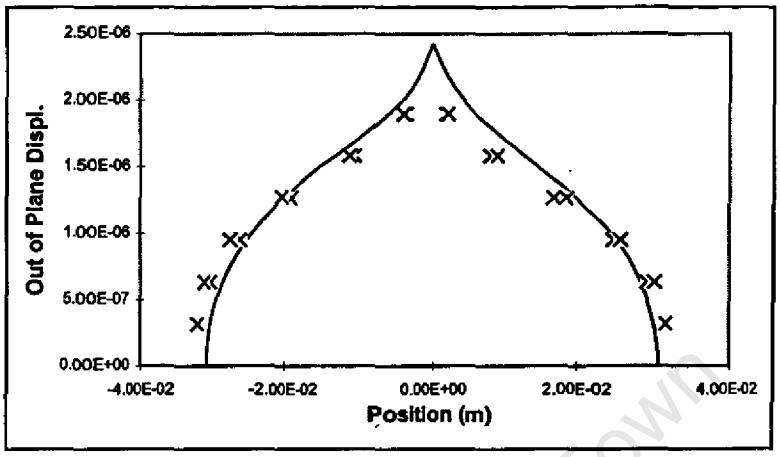

Figure 1 Axial crack at 60 psi

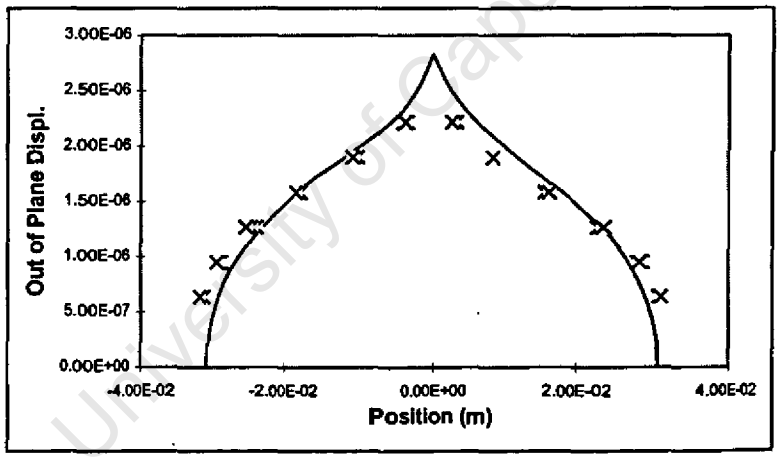

Figure 2 Axial crack at 70 psi

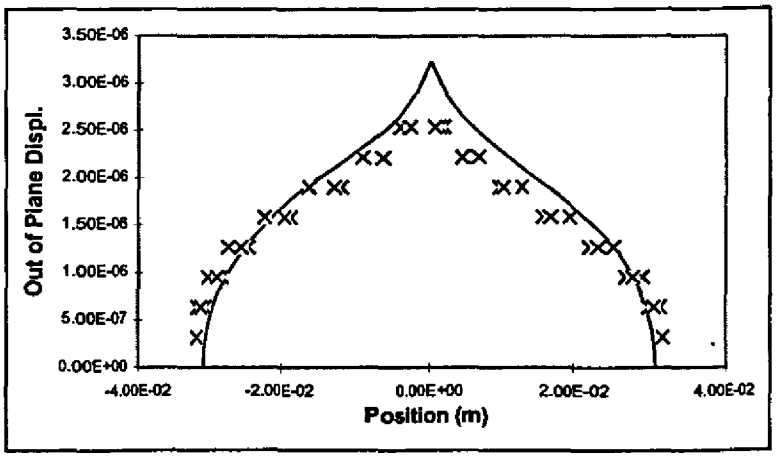

Figure 3 Axial crack at 80 psi

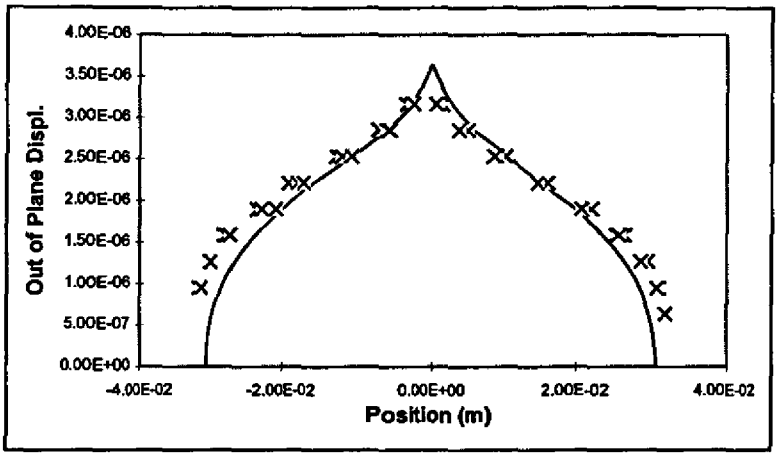

Figure 4 Axial crack at 90 psi

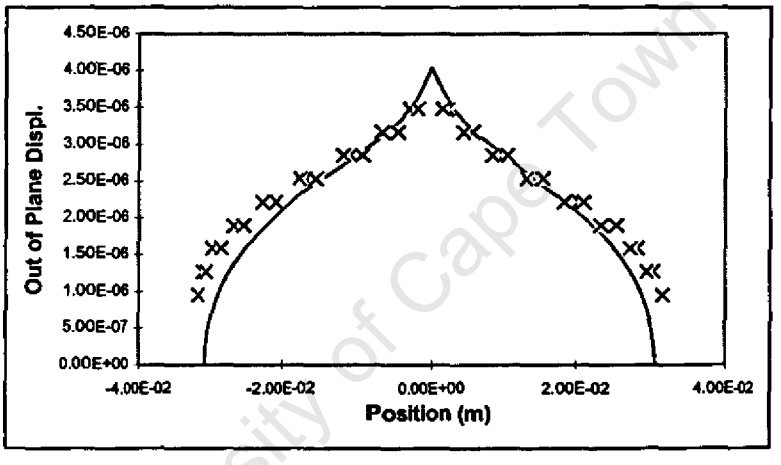

Figure 5 Axial crack at 100 psi

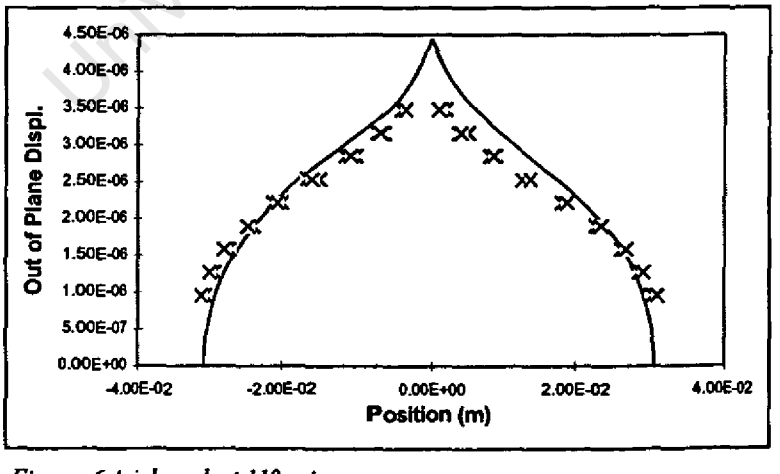

Figure 6 Axial crack at 110 psi

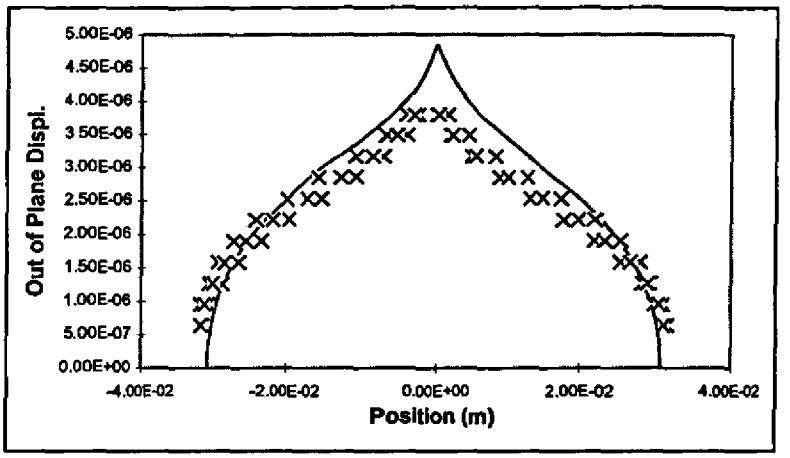

Figure 7 Axial crack at 120 psi

Circumferential Crack

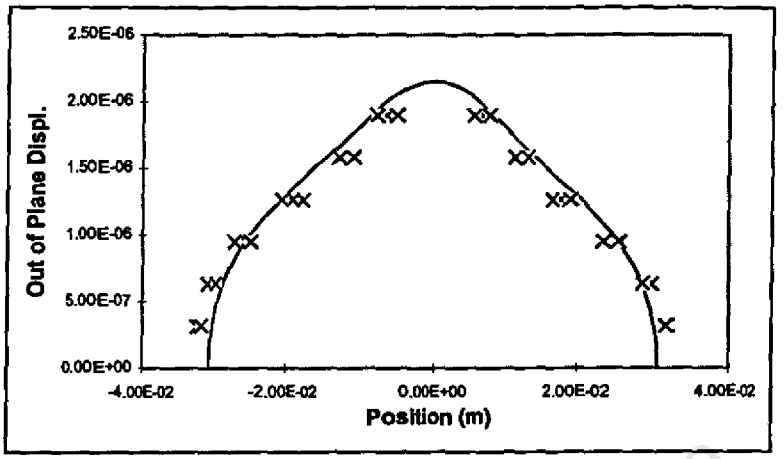

Figure 8 Circumferential crack at 60 psi

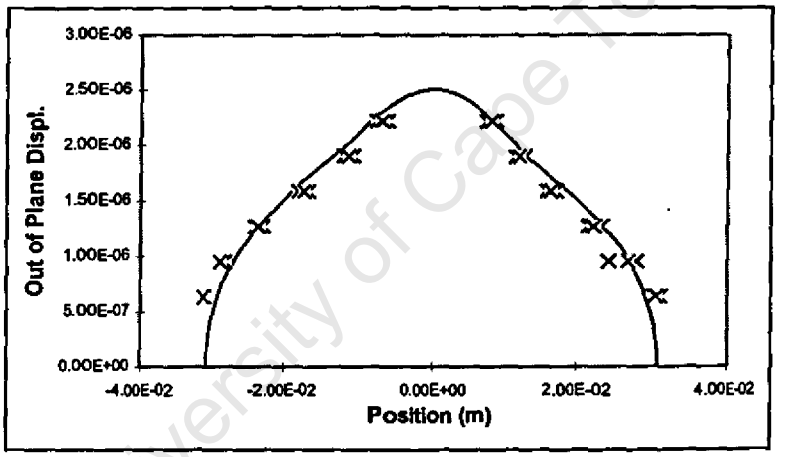

Figure 9 Circumferential crack at 70 psi

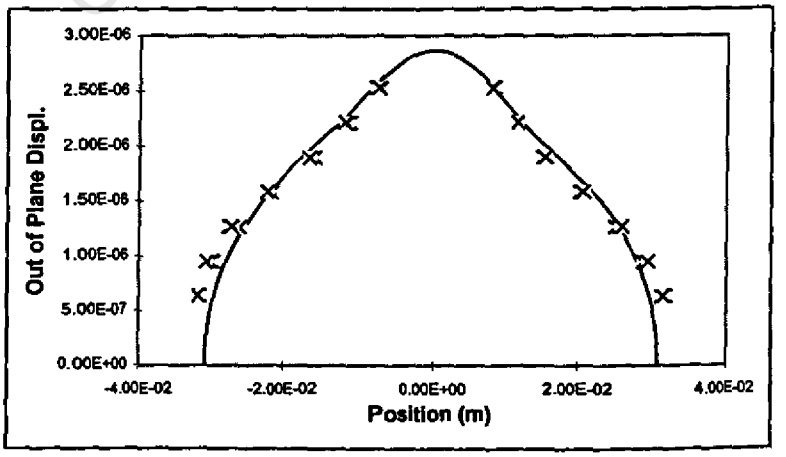

Figure 10 Circumferential crack at 80 psi

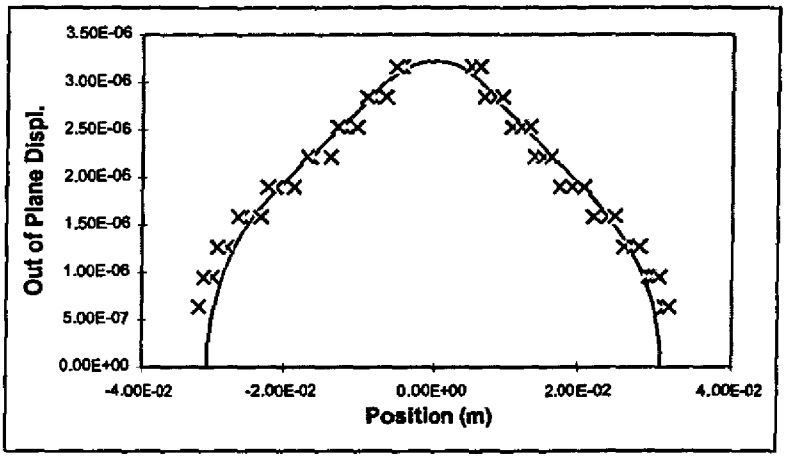

Figure 11 Circumferential crack at 90 psi

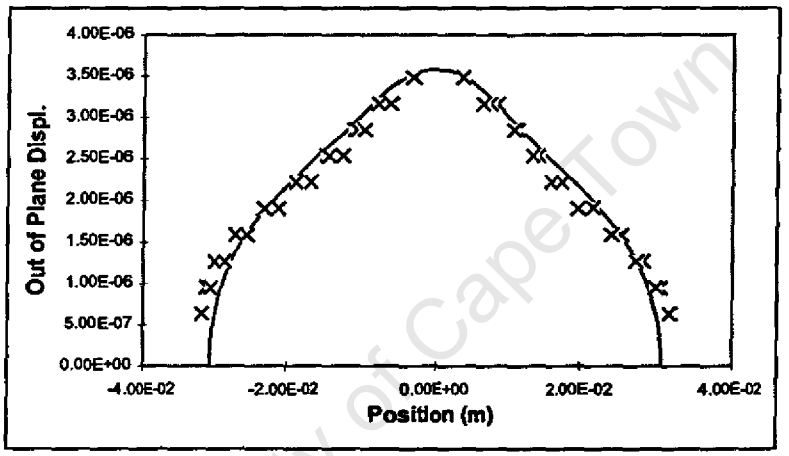

Figure 12 Circumferential crack at 100 psi

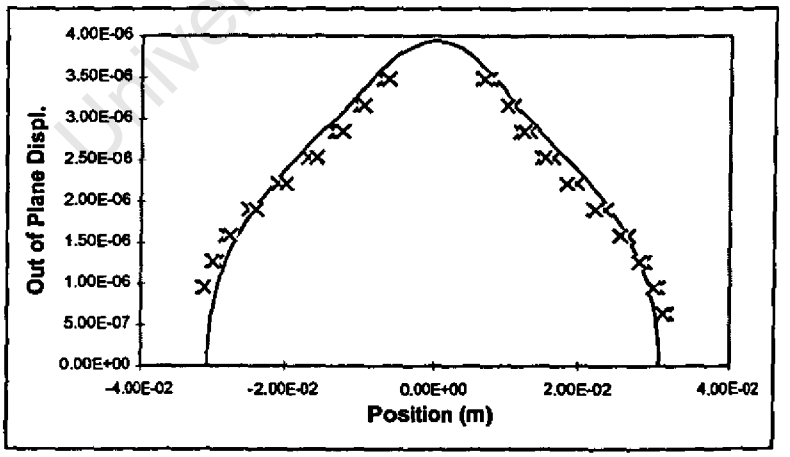

Figure 13 Circumferential crack at 110 psi

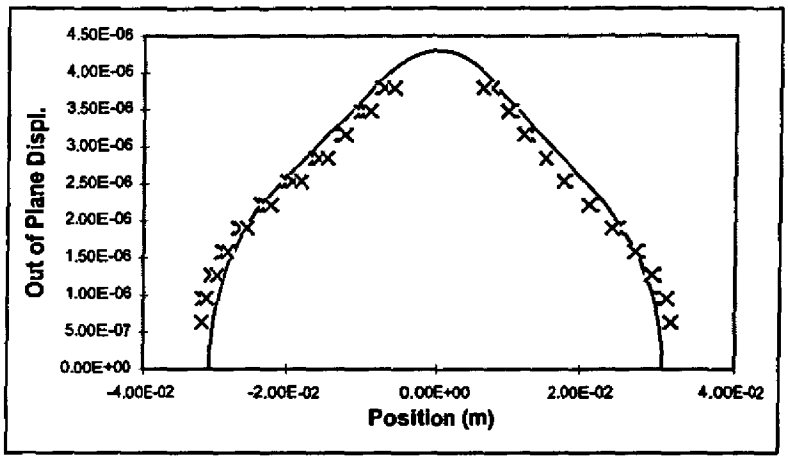

Figure 14 Circumferential crack at 120 psi

45° Crack

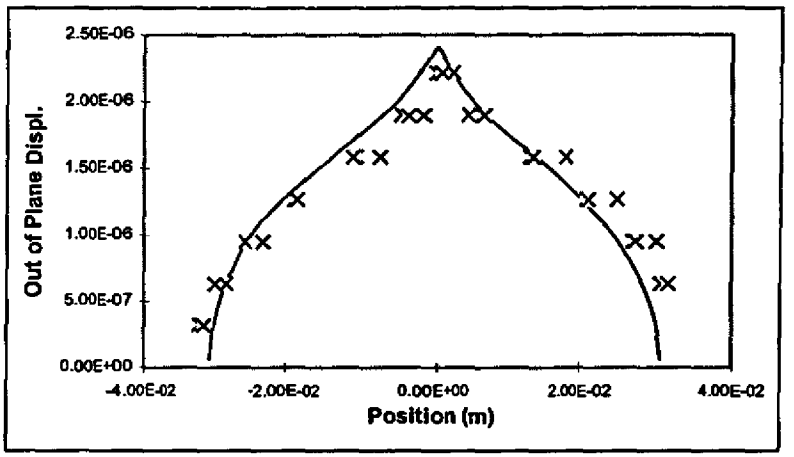

Figure 15 Angled crack at 60 psi

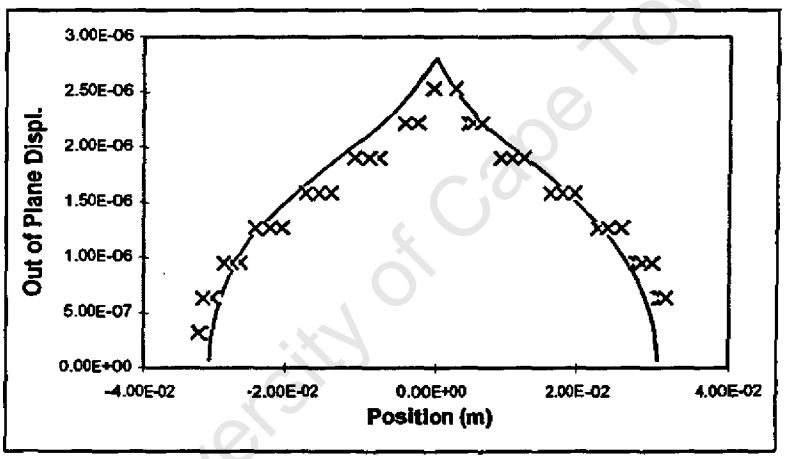

Figure 16 Angled crack at 70 psi

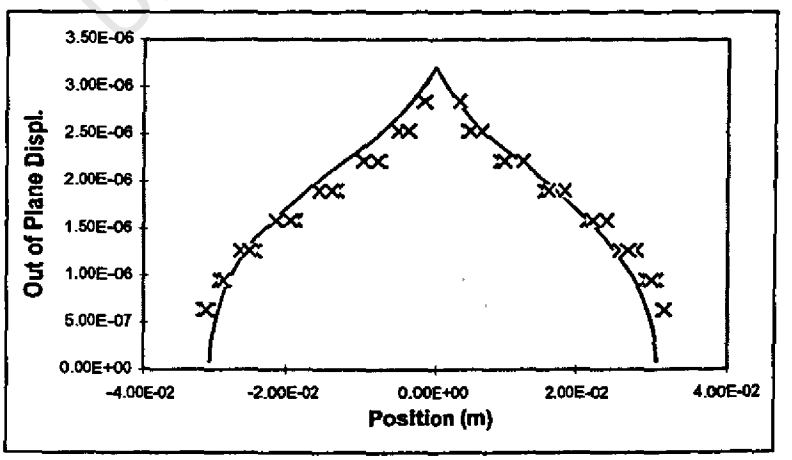

Figure 17 Angled crack at 80 psi

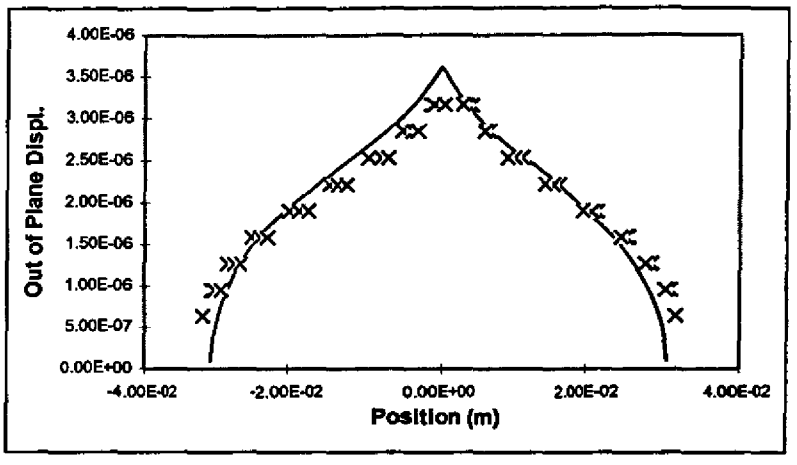

Figure 18 Angled crack at 90 psi

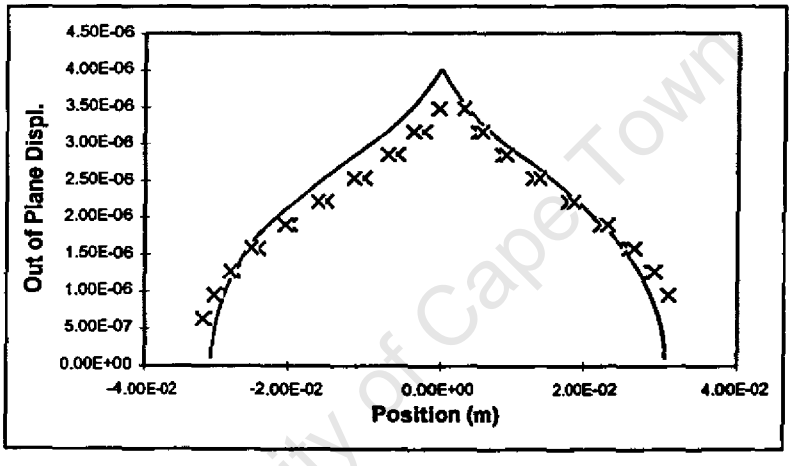

Figure 19 Angled crack at 100 psi

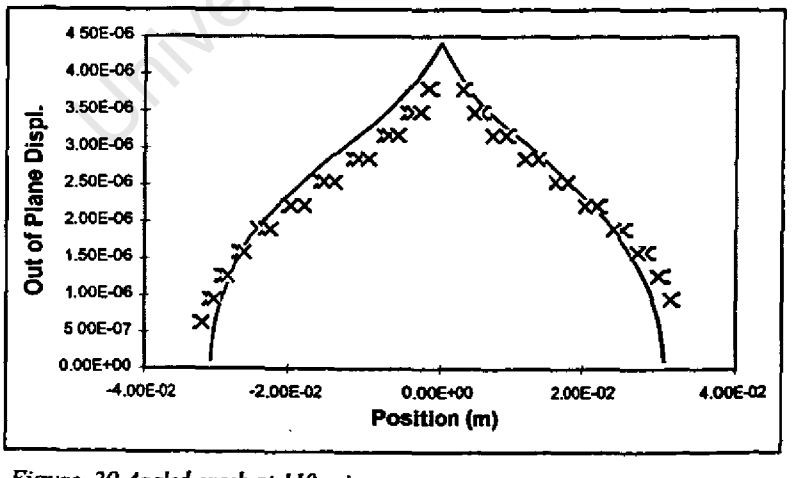

Figure 20 Angled crack at 110 psi

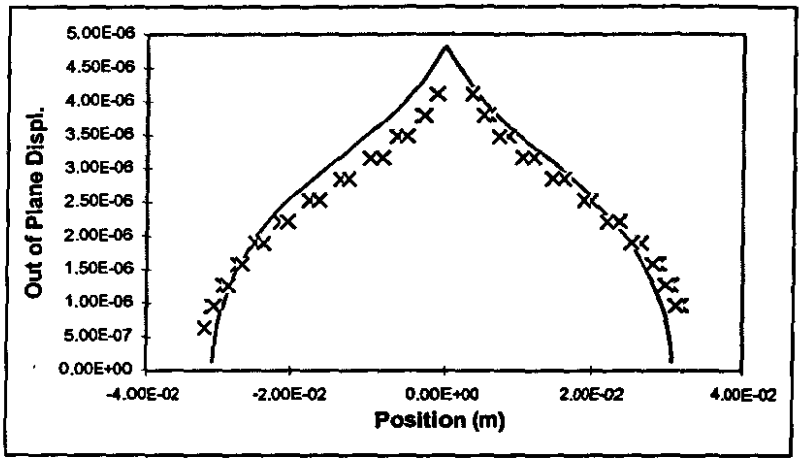

Figure 21 Angled crack at 120 psi

Internal Crack

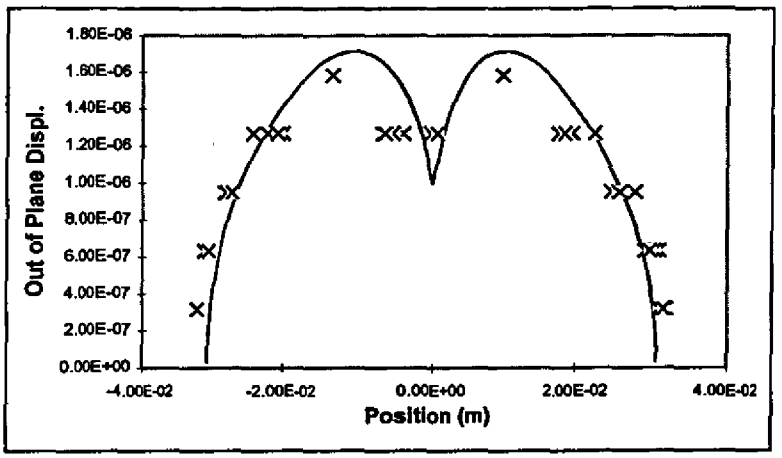

Figure 22 Internal crack at 60 psi

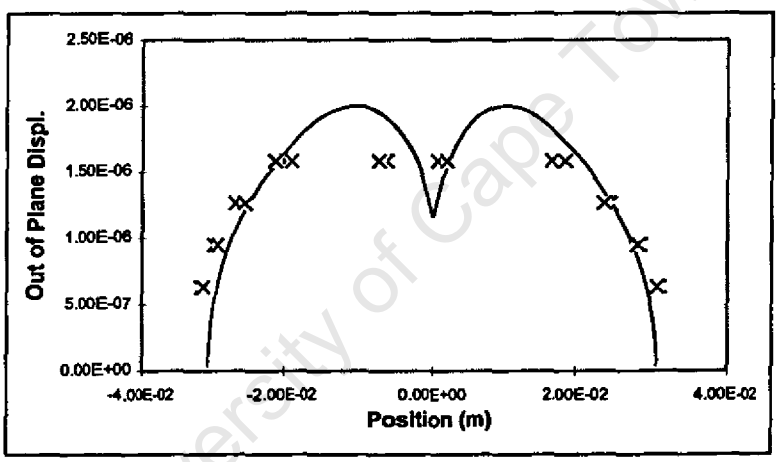

Figure 23 Internal crack at 70 psi

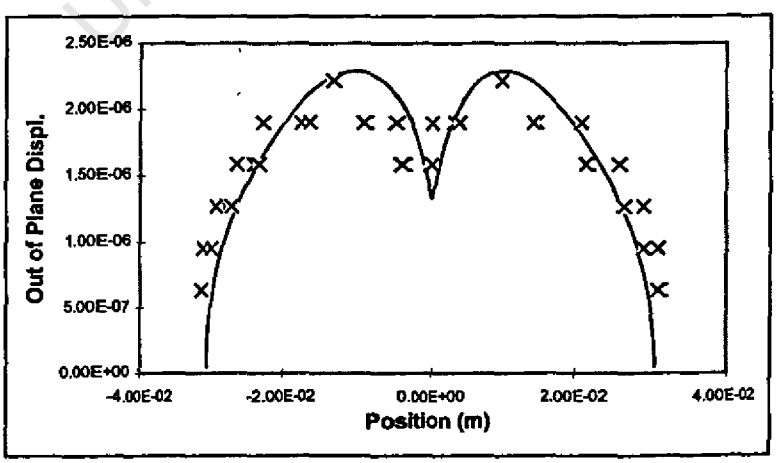

Figure 24 Internal crack at 80 psi

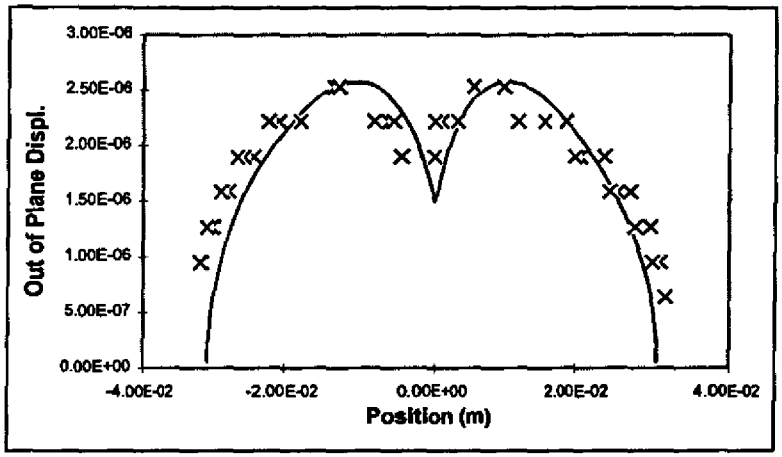

Figure 25 Internal crack at 90 psi

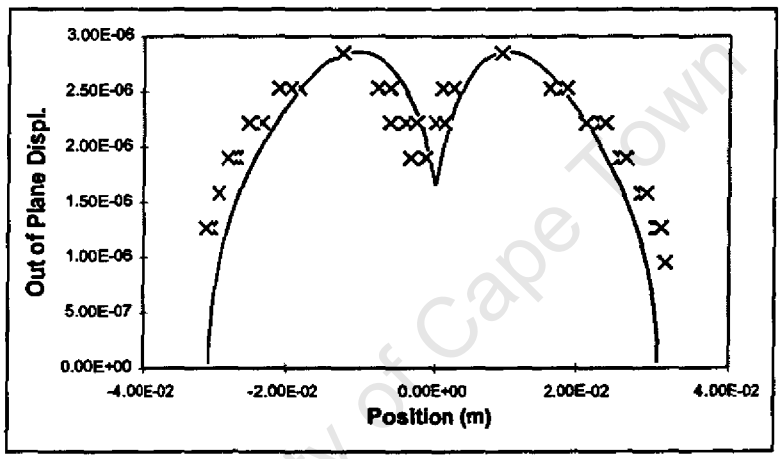

Figure 26 Internal crack at 100 psi

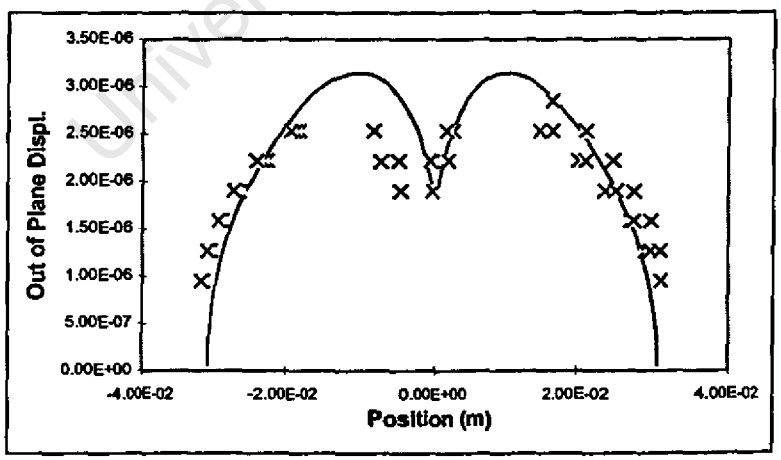

Figure 27 Internal crack at 110 psi

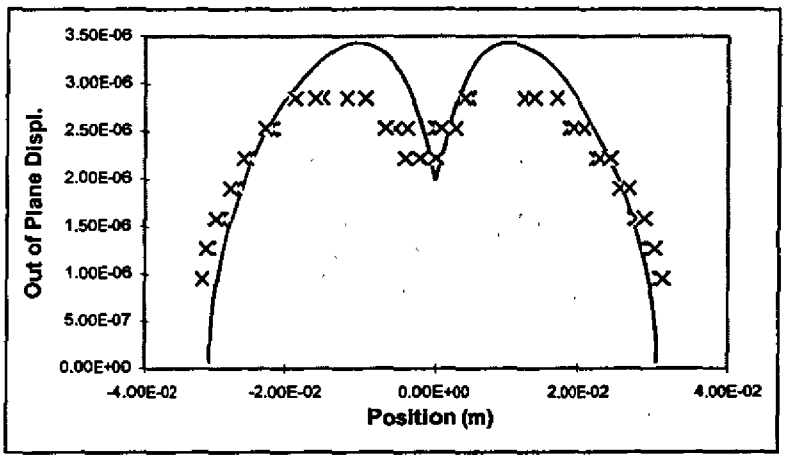

Figure 28 Internal crack at 120 psi

Parallel Cracks

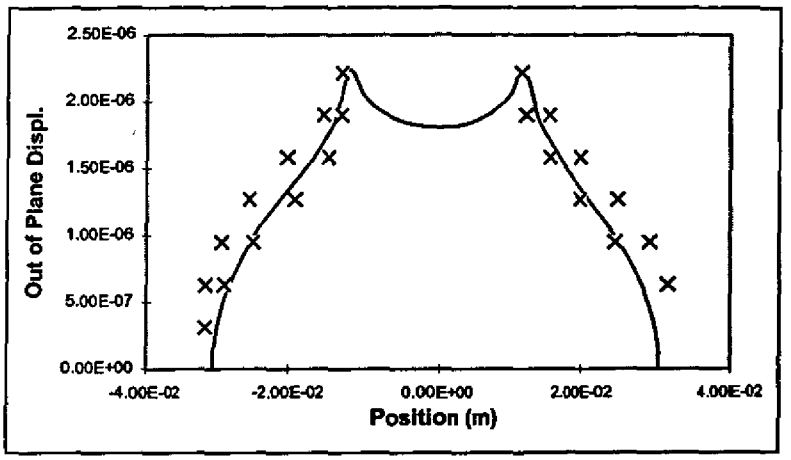

Figure 29 Parallel cracks at 60 psi

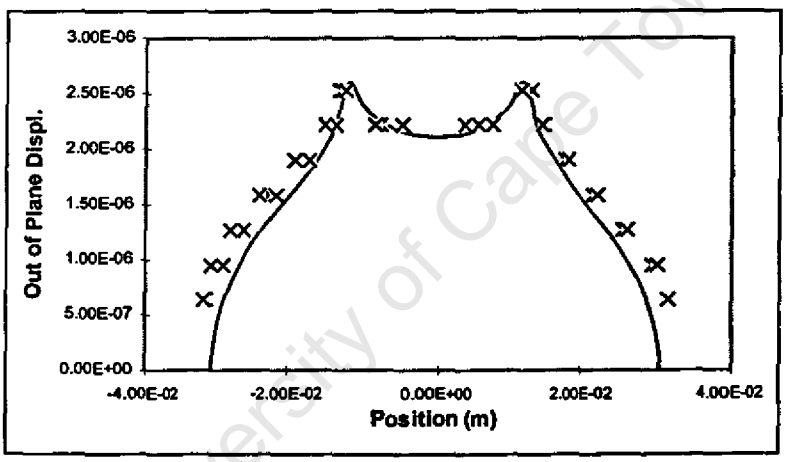

Figure 30 Parallel cracks at 70 psi

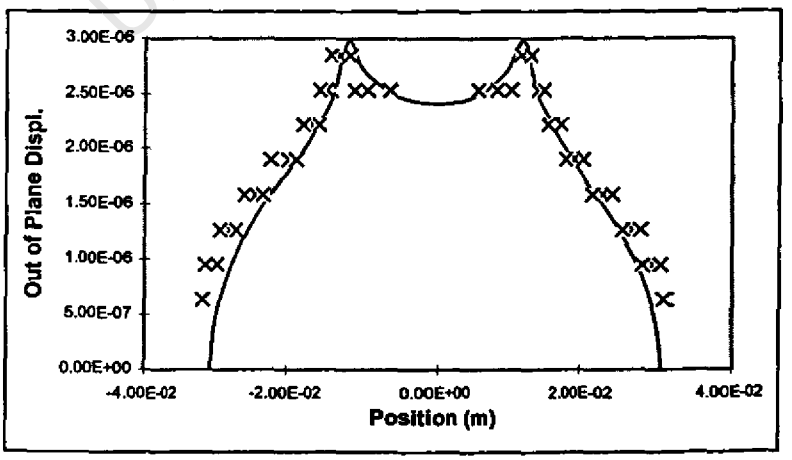

Figure 31 Parallel cracks at 80 psi

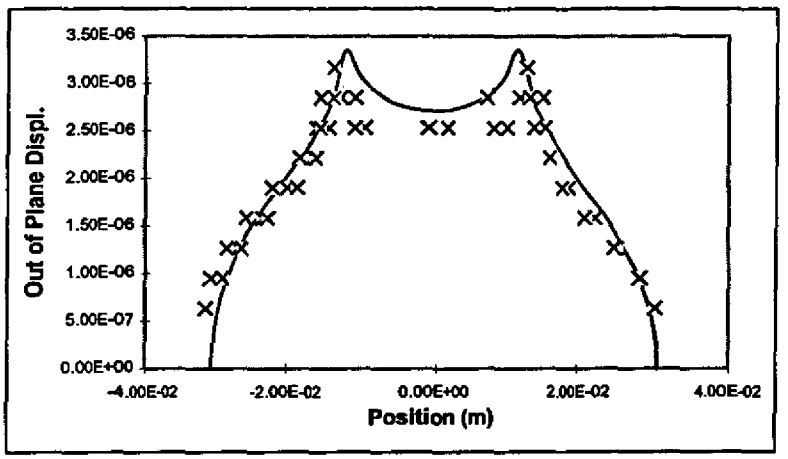

Figure 32 Parallel cracks at 90 psi

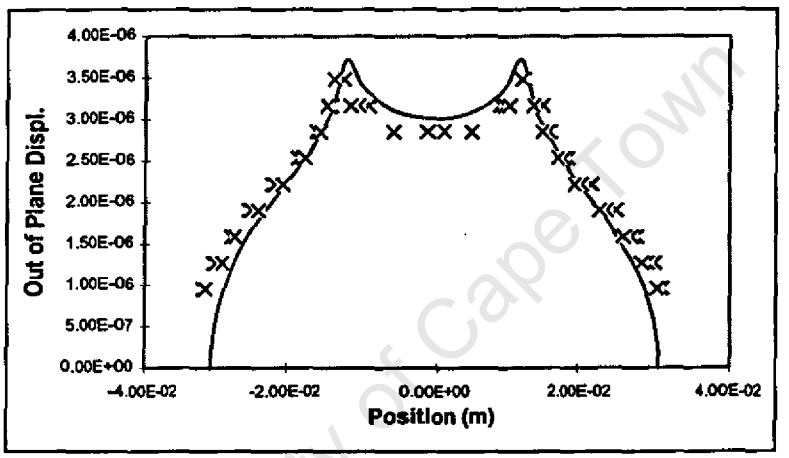

Figure 33 Parallel cracks at 100 psi

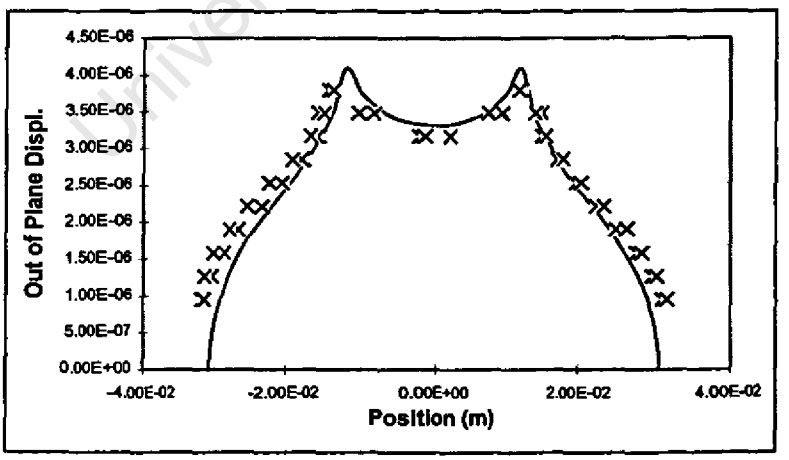

Figure 34 Parallel cracks at 110 psi

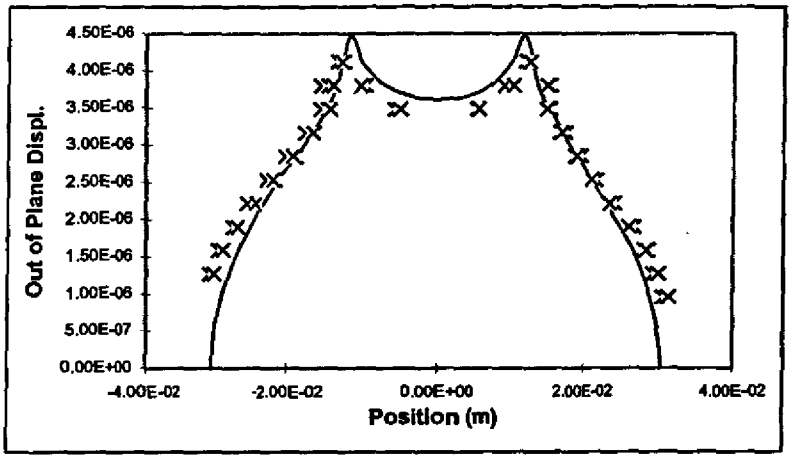

Figure 35 Parallel cracks at 120 psi

V-shaped Crack

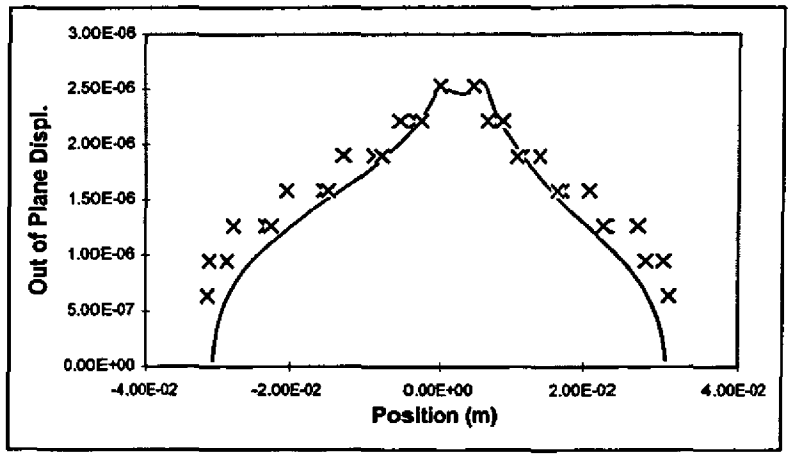

Figure 36 V-shaped crack at 60 psi

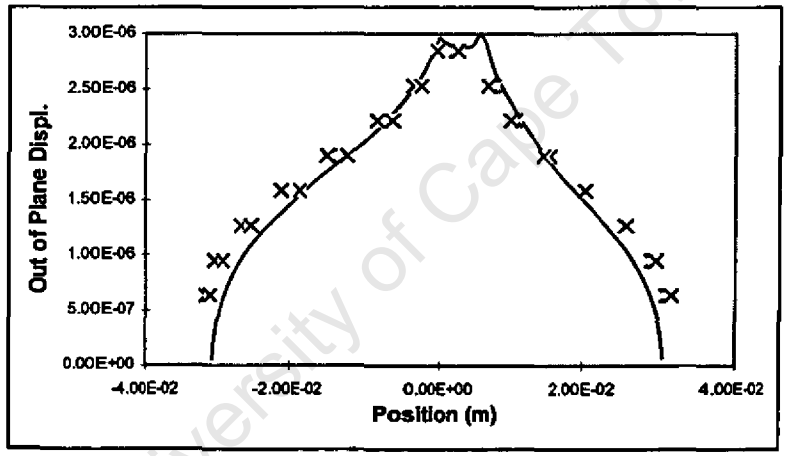

Figure 37 V-shaped crack at 70 psi

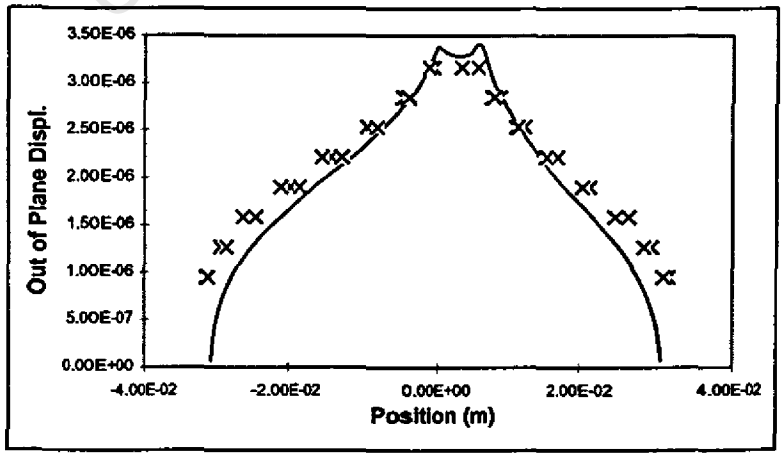

Figure 38 V-shpaed crack at 80 psi

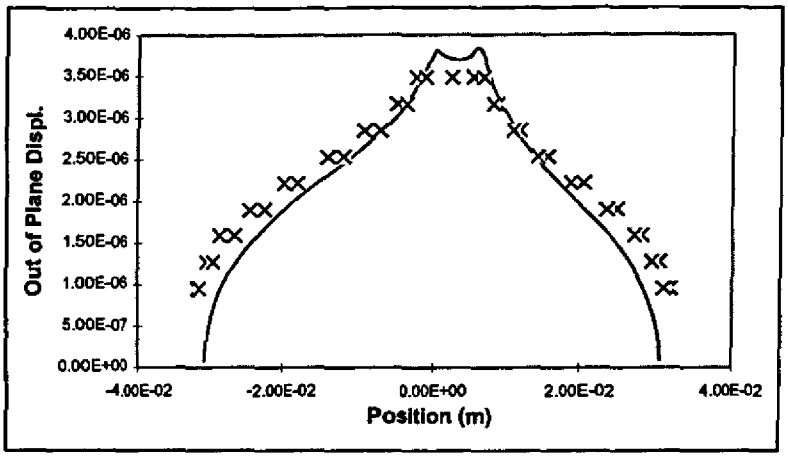

Figure 39 V-shaped crack at 90 psi

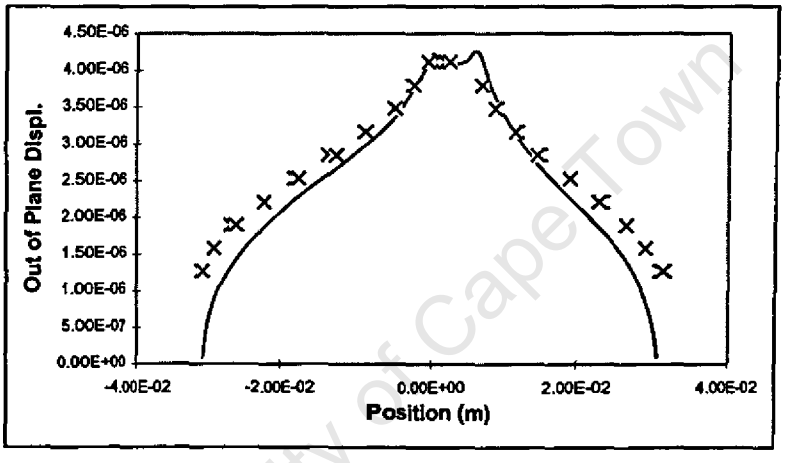

Figure 40 V-shaped crack at 100 psi

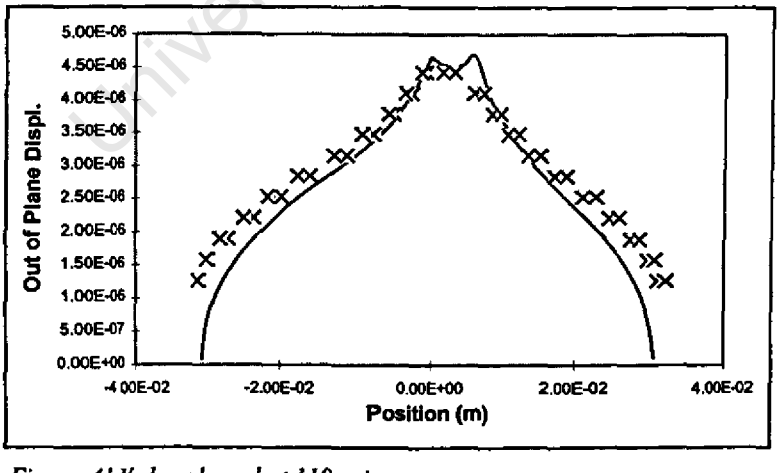

Figure 41 V-shaped crack at 110 psi

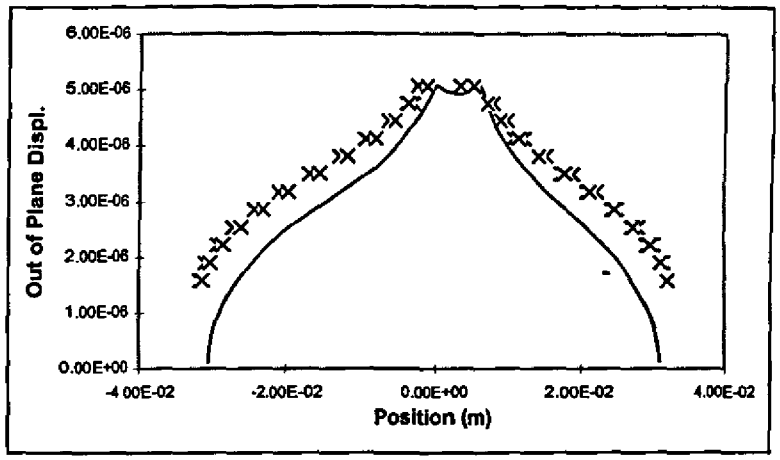

Figure 42 V-shaped crack at 120 psi